Analysis of Cool Season Lake-Related Mesoscale Phenomena Using Numerical Variational Analysis

Thomas H. Grayson

Techniques Development Laboratory
Systems Development Office
National Weather Service
National Oceanic and Atmospheric Administration
Department of Commerce
Silver Spring, Maryland 20910

December 1976

Final Report

Prepared for
U.S. Department of Commerce
National Oceanic and Atmospheric Administration
Great Lakes Environmental Research Laboratory
Ann Arbor, Michigan

ABSTRACT

ANALYSIS OF COOL SEASON LAKE-RELATED MESOSCALE PHENOMENA USING NUMERICAL VARIATIONAL ANALYSIS

by

Thomas Hilary Grayson

Chairman: Dennis G. Baker

An analysis model, based on Sasaki's variational technique, has been utilized to describe the fields of atmospheric motion, temperature and specific humidity over Lake Ontario at two times during the invasion of the lake by an Arctic air mass. The two times chosen were: (1) when the leading edge of the cold air mass was encroaching upon the lake and (2) fifteen hours later, when the air mass completely fills the lake basin. Special surface and upper-air data collected in conjunction with the International Field Year for the Great Lakes are interpolated to eleven σ surfaces extending from the earth's surface to 500 mb. The weak constraint variational formulation is used with variable weights assigned to the interpolated data.

The analyses show that the cold surge was accompanied by three lines of organized convective activity over the lake. Surface convergences of

greater than 4×10^{-4} s^{-1} were associated with the lead squall line while convergences of 2×10^{-4} s^{-1} were associated with the other areas of convective activity. Areas of upward motion coincided with the radar-echo line activity and exceeded 10×10^{-3} mb s^{-1}. Specific humidity showed a sharp increase at higher levels in the vicinity of the lead squall line. Cold air above 900 mb advanced ahead of the surface front and is believed responsible for the pre-frontal activity.

Fifteen hours after the cold frontal passage typical cool season lake-effect convective activity had organized over the southern and southeastern lake-shore. Ascending motion was induced over the lake from the surface to 700 mb except for a narrow strip (10-20 km) near the northwest shore. Upward velocity was at a maximum in the area of the convective activity with values greater than 10×10^{-3} mb s^{-1} occurring between 900-800 mb. Increased low level subsidence was in evidence windward of the lake. Surface sensible heat flux varied from 75 to 135 w m^{-2} over the lake; latent heat flux from 210 to 300 w m^{-2}.

ACKNOWLEDGMENTS

The author expresses his sincere appreciation to Professors Dennis Baker and John Lewis for the advice, valuable suggestions and encouragement which they offered throughout this study. The author is also grateful to Professors Vedat Arpaci, William Kuhn and Donald Portman for their interest in this work and their review of the manuscript.

Special thanks are extended to Drs. Bill Klein of the Systems Development Office, National Weather Service and Bob Glahn of the Techniques Development Laboratory, National Weather Service for their continued and unfaltering support without which this study would not have been possible.

The author also is indebted to Drs. Rasmusson and Almazan of the Center for Experiment Design and Data Analysis for their enthusiastic assistance in making available the edited IFYGL data, to the Great Lakes Environmental Research Laboratory for providing financial support, and to Mrs. Elizabeth Booth for her help in drafting the figures.

Finally thanks go to the author's mother, Lottie, for the care and patience she displayed in typing the manuscript.

TABLE OF CONTENTS

Page

CHAPTER

TABLE OF CONTENTS (continued)

LIST OF TABLES

Table Page

LIST OF FIGURES

LIST OF FIGURES (Continued)

LIST OF FIGURES (Continued)

LIST OF FIGURES (Continued)

LIST OF FIGURES (Continued)

LIST OF FIGURES (Continued)

LIST OF APPENDICES

DEFINITION OF SYMBOLS

C_D, C_E, C_H	transfer coefficients for momentum, water vapor and sensible heat
CEDDA	Center for Experiment Design and Data Analysis
c_p	specific heat at constant pressure
cm	centimeters
cP	continental polar
D	dynamical constraints
E	Euler-Lagrange or governing analysis equations
ESSA	Environmental Science Services Administration
EST	Eastern Standard Time
e	grid point values of meteorological elements
F_x	frictional force along X
F_y	frictional force along Y
f	coriolis parameter
GMT	Greenwich Mean Time
g	acceleration due to gravity; grams
H	approximate height at which surface stress vanishes (1000 m)
I	adjustment functional of variational formulation
i	unit vector in X-direction
IFYGL	International Field Year for the Great Lakes

DEFINITION OF SYMBOLS (continued)

J	joules
j	unit vector in Y-direction
K_M, K_q, K_H	eddy exchange coefficients for momentum, water vapor and sensible heat
K*	constant (10^5 cm^2 s^{-1})
kg	kilograms
km	kilometers
L	latent heat of vaporization
ly	langley (one calorie cm^{-2})
m	meters
mP	maritime polar
NVA	Numerical Variational Analysis
NWS	National Weather Service
P	pressure on a σ surface
P_o	1000 mb
P_s	surface pressure (at $\sigma = 1$)
P*	uppermost level of model (500 mb at $\sigma = 0$)
ΔP	difference in pressure between surfaces at $\sigma = 0$ and $\sigma = 1$
PPI	Plan Position Indicator
Q	sensible and latent heating rates
Q_S	sensible heating rate
Q_L	latent heating rate
q	specific humidity

DEFINITION OF SYMBOLS (continued)

q_s	saturation specific humidity
R	gas constant
S	two dimensional space; specific humidity generation
s	seconds
T	temperature (^oK)
t	time
u	horizontal velocity in X-direction
V	volume
$\overline{V}$	horizontal velocity
v	horizontal velocity in Y-direction
w	watts
x	spatial dimension; partial derivative in X-direction
y	spatial dimension; partial derivative in Y-direction
z	spatial dimension
α	weights assigned to terms in adjustment functional of variational formulation
δ	first variation of adjustment functional, I
γ	constant (10^4 cm $^oC^{-1}$)
μ	mean-square difference between NVA and interpolated values
ϕ	geopotential

DEFINITION OF SYMBOLS (continued)

ρ	density
σ	vertical coordinate $(P-P^*) / (P_S-P^*)$; partial derivative in σ - direction
$\dot{\sigma}$	vertical velocity in σ coordinate system
τ	surface stress
θ	potential temperature
∇	two dimensional gradient operator $\left(\frac{\partial}{\partial x} i + \frac{\partial}{\partial y} j\right)$
∇^2	two dimensional Laplacian operator $\left(\frac{\partial^2}{\partial x^2} + \frac{\partial^2}{\partial y^2}\right)$
$\sim$	tilde over a parameter indicates parameter is held fixed during variational process; over weight, α , indicates weight assigned based on reliability of observation

CHAPTER I

INTRODUCTION

GENERAL STATEMENT OF THE PROBLEM

When a cold, relatively dry air mass flows over a warm water surface the original air-mass properties are modified by the addition of heat and moisture from the underlying surface. Instability generated by the air-water temperature difference is responsible for large fluxes of heat and moisture from the water surface to the lowest atmospheric layers. Subsequently, the heat and moisture in these layers is transported to upper levels by eddy diffusion and larger scale circulations.

The Great Lakes basin is a region where this phenomenon is observed frequently in the fall and early winter (Phillips and McCulloch, 1972). During this period the Great Lakes still possess large amounts of thermal energy acquired during the summer months. Shallow layers of very cold and dry air of Arctic origin, produced by weeks of meager insolation or complete darkness and radiational cooling, coupled with upper-level subsidence, move south-eastward over the Canadian plains, undergoing little transformation prior to reaching the basin. Unfortunately all studies of the mesoscale activity associated with the modification of these air masses by the underlying lakes have been hampered by a lack of data.

The International Field Year for the Great Lakes (IFYGL) is a joint U.S.-Canadian experimental field program designed to improve knowledge of the limnology, hydrology and meteorology of Lake Ontario and the Ontario basin. During IFYGL a special meteorological observing network was established over and around Lake Ontario. The data collected from the network are of sufficient spatial and temporal density to provide insight into the winter lake-effect phenomenon.

The purpose of this investigation is to examine the evolutionary change of the three dimensional mesoscale motion, temperature and moisture structure of an air mass of Arctic origin during its passage over a relatively warm lake surface. To aid in this study a diagnostic numerical analysis model using the principles of the calculus of variations and employing appropriate physical constraints is developed and used to analyze a set of IFYGL data collected during an intensive cold air outbreak.

BACKGROUND

Air-mass modification studies until recently have primarily been of a qualitative nature, dealing generally with readily observable effects. Early studies attempting to quantify the modification process focused on the synoptic scale. Burke (1945) studied the transformation of cP to mP air off the east coast of North America. From his findings he was able to develop a method for forecasting the change of the surface air temperature at any phase of the transformation in terms of observable initial conditions and the distance the air had traveled over the sea. Klein (1946), who performed a similar study, concluded that a completely successful forecasting scheme had to await the solution of the problem of vertical motion associated with the transformation process. Manabe (1957) studied the modification of the northwest monsoon passing over the Japan Sea in winter and made quantitative estimates of the heat supply based on a heat and moisture budget analysis. He found that the amount of sensible heat supplied from the sea to the atmosphere was often as much as 1000 ly day^{-1} during the period of a typical outburst. This amount was much larger than the heat supplied by radiation or condensation. The amount of latent heat supplied through evaporation from the sea was estimated to reach about a half of the sensible heat supply.

Quantitative studies of the smaller scale activity associated with air-mass modification have not been possible until recently due to the lack of adequate data. Matsumoto et al. (1967 a,b) using special data obtained over the Japan Sea from the Heavy Snow Storm Project Observation in 1965 made detailed analyses of the three-dimensional structure of mesoscale disturbances observed in the vicinity of a cold vortex center and related the cumulus activity to the mesoscale convergence field. Their investigation revealed a characteristic wind field associated with the mesoscale convective activity. Convergence and cyclonic vorticity were observed in the lower part and divergence and anticyclonic vorticity in the upper part of the cold air. Their findings indicate that the cumulus activity is strongly controlled by the mesoscale convergence field with well developed cumuli existing only in the area of convergence of more than $10^{-4}\ s^{-1}$.

LAKE-EFFECT PHENOMENON

A spectacular consequence of the air-mass modification process in North America is the well-known lake-induced snowstorms generated over and to the lee of the Great Lakes. Under conducive conditions these squalls may persist for days and produce local accumulations of 30 inches or more per day (Wiggin, 1950; Sykes, 1966) and snowfall rates as large as 12 inches per hour (Davis et al., 1968). Normally these mesoscale storms begin several hours after the passage of a strong cold front.

In the literature there are numerous research papers pertaining to the lake-induced storms. Most earlier studies deal with storm effects and are of a qualitative nature (Dole, 1928; Remick, 1942 a,b: Wiggin, 1950; Lansing, 1965). Recent efforts have aimed at producing a complete description of the storms including the dynamics of their life cycle and their interaction with and dependency on the larger scales of atmospheric motion (McVehil and Peace, 1965, 1966; McVehil et al. 1967; McVehil et al. 1968; Davis et al., 1968; Rao, 1971; Lavoie, 1972). Lavoie (1968) provides an excellent review of the pertinent characteristics of lake-effect storms. The storms are intimately related to the configuration of the lake and the surrounding topography. Heavy precipitation is usually most pronounced just inland from the lee shore and the land-water boundary exerts a strong influence on the convective regime.

Even if heavy snowstorms fail to develop, the air-mass transformation process produces local effects in the neighborhood of the Great Lakes which are themselves of considerable importance. Harrison (1939) investigated conditions at Chicago and Cleveland airports. He observed a frontal effect at both stations which did not seem to move with the gradient wind, but rather appeared almost stationary. The front produced moderate snow and was characterized by a change in wind direction as well as in temperature and humidity. Baker (1976) observed a similar effect to the east and south of Lake Michigan. In this case a pseudo-front existed between the air that had a trajectory over the lake and the air to the south that did not.

Diagnostic studies to date that have addressed the many and variform features of the lake-effect phenomenon have all been impaired by a lack of sufficient observational data. This problem is especially evident in the recent studies that have attempted to quantify the governing dynamical processes. For example, Peace and Sykes (1966) performed extensive mesoscale analyses of the surface pressure and wind fields associated with a winter lake-snowstorm. Around the eastern end of Lake Ontario their analyses were based on data collected from a mesonetwork of recording stations. However along the western map boundary and crucially over the lake itself their analyses represent subjective interpolations drawn to agree with radar images of the storm location. Lenschow (1973) used aircraft measurements to examine the boundary layer structure over the Great Lakes in the late fall. In the two cases he considered, a flight over Lake Michigan and one over Lake Huron, cloud development was not sufficient for significant precipitation to occur. Because of the limited scope of his observations he was able to consider only the two-dimensional (vertical and along-wind), steady-state conditions of the air-mass modification process. Numerical models that have attempted to simulate the lake-effect, notably those of Lavoie (Lavoie et al., 1970) and Kaplan and Paine (1972) have all suffered from the lack of a complete observational set against which to check the model results. Finally, Rao (1971) attempted to investigate the initial mesoscale aspects of the three-dimensional motion, temperature and humidity fields of a snow squall situation over Lake Ontario. He succinctly sums up the difficulties he encountered in the conclusion of his paper:

> "A weakness of our study is that it is based on very few observations which are themselves subjectively analyzed."

His comment applies, generally, to all previous lake-effect studies.

OBSERVATIONAL BASE

As Rao (1971) noted, operational radiosonde data coverage of Lake Ontario is totally inadequate for any mesoscale study since the three relevant stations (Buffalo, Albany and Maniwaki) are separated from each other by more than 400 km. Additionally, surface reporting stations over and adjacent to the lake are practically non-existent.

One of the specific goals of the IFYGL program, according to Rasmusson (1974), is to investigate individual weather situations in detail to learn more about the life cycles and characteristics of lake related phenomena which are so important to users of the lake and residents of the area. To achieve this goal an

IFYGL observational network, shown in Fig. 1, was established. It consisted of special U.S. and Canadian meteorological observing buoys, over-water towers, land and island stations and rawinsonde stations. This network was operated from October 2, 1972 through December 10, 1972. During this period there were 3 separate intensive periods of data collection of 14-16 days each during which 8 soundings per day were scheduled from each of 6 rawinsonde stations located along the shore of the lake, with a routine 2 soundings per day schedule for the non-intensive days. Each of the rawinsonde stations was equipped with "LOCATE" wind finding systems that use re-transmitted LORAN-C signals for precise balloon tracking. In addition temperature, moisture, and wind data were recorded at 10 mb intervals.

Buoy and tower data over and adjacent to the lake also provide considerable information. The U.S. buoy instruments measured air temperature, dewpoint temperature, atmospheric pressure and wind speed and direction 3 meters above the lake surface and water temperature at various depths (Almazan, 1973). Offshore towers measured air temperature, dewpoint temperature and precipitation at the 3-meter level, wind speed and direction and atmospheric pressure at the 10-meter level

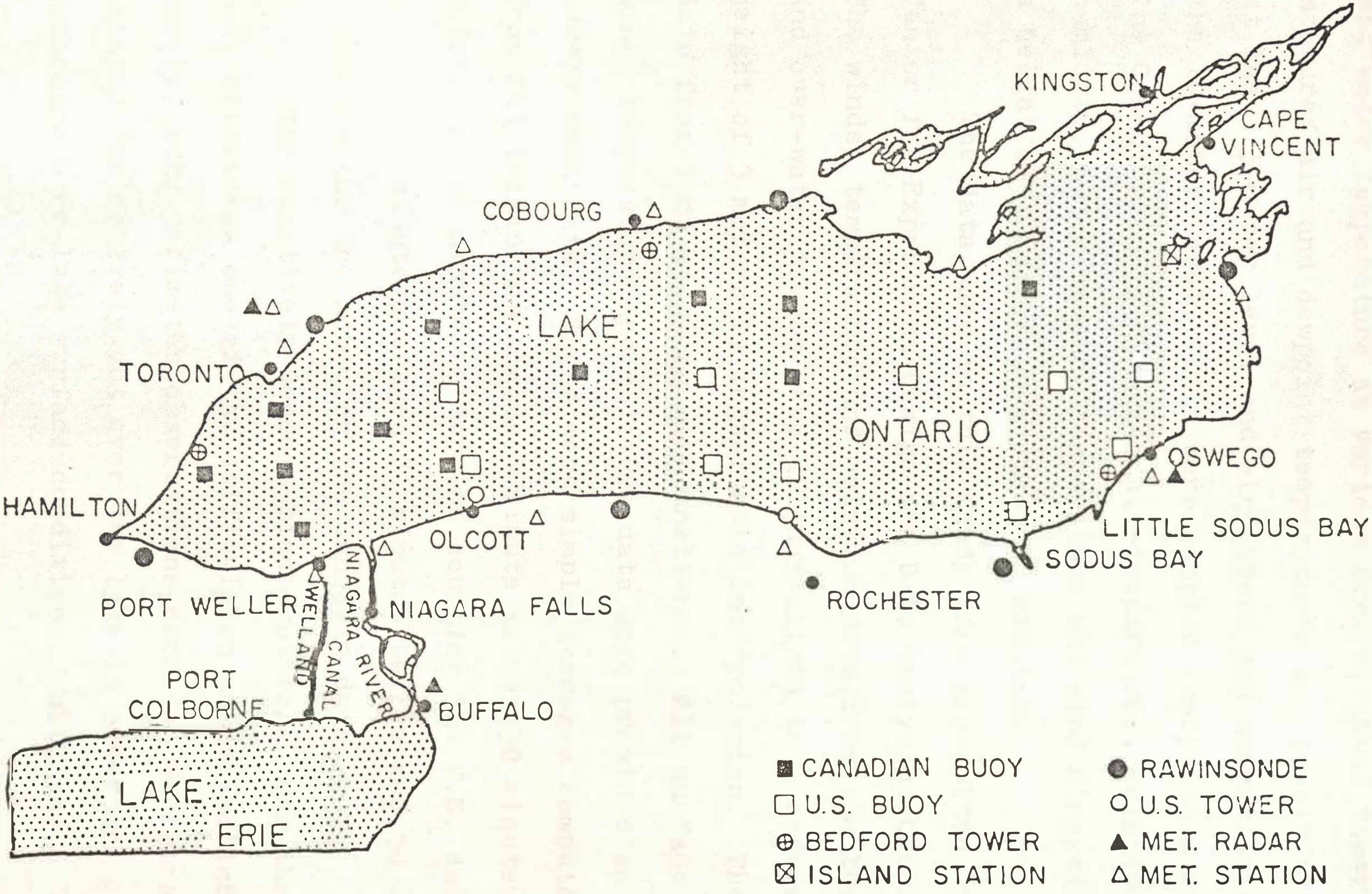

Fig. 1. International Field Year for the Great Lakes (IFYGL) observational network.

and water temperature at various depths. Land towers measured air and dewpoint temperatures and precipitation at the 1.5-meter level and wind speed and direction at the 10-meter level. Data were sampled every six minutes. The Canadian buoys measured air-temperature, relative humidity, water surface temperature and wind direction at a height of 4 meters once every 10 minutes.

The data used in this study were pre-edited by the Center for Experiment Design and Data Analysis (CEDDA). The winds, temperature and moisture data from the buoys and over-water towers were all normalized to a reference height of 3 meters by logarithmic interpolation. The data from land stations were unaltered. All surface wind, temperature and moisture data were provided as hourly mean data. These were simple averages computed from (1) the instantaneous 6 minute values 30 minutes before and 24 minutes after the hour for the U.S. data and (2) 10 minute averages 30 minutes before and 20 minutes after the hour for the Canadian data.

The relatively dense surface coverage over the lake alleviates one of the difficulties noted earlier, - namely, lake perimeter observations need not be extrapolated subjectively out over the lake in order to determine over-lake surface conditions. With the relatively high resolution rawinsonde flights, both in space and in time, the IFYGL observational data set provides an excellent opportunity to observe the mesoscale activity associated with the winter lake-effect phenomenon.

ANALYSIS TECHNIQUE

Since the purpose of this study is to describe the mesoscale features associated with the transformation of the three-dimensional temperature, wind and moisture fields of a cold air-mass modification situation, and, as noted in the previous section, since observations are available at frequent intervals only at the surface of the lake and in the upper air around the lake's perimeter, it is necessary to extrapolate the available information to the area above the lake-surface. Thus it would be desirable if the analysis method had the properties of (1) satisfying the observational information to within certain predetermined error tolerances and (2) extrapolating this information to areas devoid of data in a manner consistent with accepted physical relationships linking the variables.

Human subjective analysis and most objective analysis techniques do not satisfy these criteria (Haltiner, 1971). However, a diagnostic technique introduced by Sasaki (1958) does possess the above features. Additionally, the technique is capable of providing (1) dynamically consistent analyses in all areas of the analysis domain and (2) mutual adjustment among the meteorological parameters, thus allowing information about a particular variable to provide information on the other variables as well.

The application of this method requires two steps. First the meteorological observations are interpolated to grid points usually by a standard objective technique such as the successive corrections method, a scheme first introduced by Bergthórsson and Döös (1955) and later modified by Cressman (1959). These initial or "observational" fields are then adjusted by Sasaki's technique. Final meteorological analyses produced by this method have been shown to be physically more reasonable than the initial unadjusted fields (Lewis and Grayson, 1972; Lewis, 1972; Achtemier, 1975). Thus diagnostic calculations of vertical velocity and kinematic properties such as divergence and vorticity are also presumed to be more accurate.

In an extension of his earlier work Sasaki (1968) proposed using the technique to determine detailed three-dimensional patterns of temperature, wind, pressure and moisture in order to achieve useful and accurate local weather forecasts. He proposed generation of upper-air data by extrapolation of the dense surface data into the upper levels. In later papers Sasaki (1970 a,b,c) studied the theoretical aspects of the technique as a method of "four-dimensional analysis". He applied the method to the analysis of a severe storm gust over central Oklahoma (1970c) and with Lewis (Sasaki and Lewis, 1970) demonstrated another application using the method to analyze the planetary boundary layer in conjunction with a squall line formation. Lewis and Grayson (1972) used this approach to analyze surface wind and pressure on a global band extending from 40S to 60N in order to anchor the analysis to representative reports in data-rich regions while providing for dynamical adjustment between wind and pressure fields in data-poor areas. Lewis (1972) extended this work. He developed an upper air analysis model for the global band area that vertically extrapolated the adjusted surface fields through use of a generalized thermal wind formulation.

Sasaki's analysis procedure, referred to as numerical variational analysis (NVA), derives its properties by including in its formulation both the dynamical equations that describe the relationship between the variables being analyzed and the available observational information about these variables. The scheme, based on the calculus of variations, is briefly reviewed in the following chapter.

In this study the application of NVA is extended to the air-mass modification problem. This approach appears advantageous in view of the intent of this study to investigate over-lake mesoscale conditions of the atmosphere given the peripheral location of the IFYGL rawinsonde sites.

CHAPTER II

NUMERICAL VARIATIONAL ANALYSIS

GENERAL DISCUSSION OF VARIATIONAL METHOD

Sasaki (1970,a) discussed three possible basic formulations of NVA: (1) "timewise localized", (2) strong constraint and (3) weak constraint. The first and second formulations satisfy the governing dynamical equations exactly, within a certain numerical accuracy. Achtemier (197~~5~~2) describes the "timewise localized" method as a space filter and cautions that its use can violate quasi-geostrophic scale theory for a wide range of meteorological phenomena. The strong constraint formulation meanwhile is suited more for use in initialization of a numerical forecast model where model equations are considered rigorous mathematical analogs of the atmosphere.

Sasaki showed the third formulation to be the proper one to use when lack of knowledge about the phenomenon being investigated precludes a precise mathematical formulation of the process. He demonstrated the effectiveness of the weak constraint formulation in the mesoscale surface analysis of a severe storm gust. In this formulation the governing equations are only approximately satisfied. In the formulation of NVA for the air-mass modification problem, physical processes such as sensible and latent heat flux and momentum exchange with the lake-surface are not precisely known and have to be parameterized. Thus in this study this third formulation is adopted for the analysis of the IFYGL data.

REVIEW OF WEAK CONSTRAINT FORMULATION

The weak constraint NVA formulation may be briefly described as follows: an adjustment functional, I, is postulated so that

$$I = \iint\limits_{t\,V} \left\{ \sum_i \tilde{\alpha}_i (e_i - \tilde{e}_i)^2 + \sum_j \alpha_j \left[D_j(e_i(x,y,z,t)) \right]^2 \right\} dV dt \qquad (2.1)$$

where x,y,z are the three spatial dimensions, t is time, V represents volume, $\tilde{e}_i$ represent observed values of meteorological elements at a point, P(x,y,z,t), and e_i, the corresponding objectively analyzed values. $\tilde{\alpha}_i$ are weights chosen a priori and have the effect of forcing the e_i toward the $\tilde{e}_i$ in accord with the magnitude of the weights. In practice the $\tilde{e}_i$ are actually grid point values obtained from the observations by a previous interpolation or analysis step. Similarly, α_j are weights applied to the governing equations of the analysis model or, as they are commonly called, the equations of constraint, D_j.

To obtain the objectively modified meteorological elements the first variation of I is required to vanish. Expressed as

$$0 = \delta I = \delta \iiint_{t\,V} \left\{ \sum_i \tilde{\alpha}_i (e_i - \tilde{e}_i)^2 + \sum_j \alpha_j \left[D_j \left(e_i(x,y,z,t) \right) \right]^2 \right\} dV\,dt \qquad (2.2)$$

this is a necessary condition for obtaining a stationary value for a functional. Since the functional is composed of purely positive terms, the solution obtained by the requirement of stationarity automatically yields a solution which minimizes the integral (Lanczos, 1966). Using integration by parts and the commutative properties of the δ process, the functional takes the form

$$0 = \delta I = \iint_{t\,V} \sum_i E_i \, \delta e_i \, dV\,dt + \left\{ \begin{matrix} \text{boundary} \\ \text{terms} \end{matrix} \right\} \qquad (2.3)$$

Suitable choice of boundary conditions will result in the elimination of the boundary terms. Then solution of 2.3, because of the independence of the variations of e_i , is

$$E_1 = E_2 = E_3 = \cdots = E_i = 0 \tag{2.4}$$

The E_i are called the Euler or Euler-Lagrange equations and constitute the governing equations of the analysis. The simultaneous solution of the E_i provide the adjusted values of the e_i throughout the analysis region.

SOME ILLUSTRATIVE FORMULATIONS

Most published articles pertaining to NVA lack concise illustrations from which the reader is able to obtain a quick, clear understanding of the utility of the technique. In this section three simple examples are given to provide insight into the use of NVA for the lake-effect problem and to illustrate some of the important features of the method--namely, (1) the feedback mechanism between the meteorological parameters being analyzed, (2) satisfaction of observational information and (3) consistent extrapolation of this information into data deficient areas.

Fig. 2 presents the area and grid that is used throughout the study. The grid is oriented along 80°W, with the dimensions of (37,25) in the (X,Y) directions respectively. The image scale factor was assumed constant and used to compute a constant grid point distance of 10.77 km on the image plane. Similarly the Coriolis parameter, f, was chosen constant over the area at $1.0039\text{x}10^{-4}\ \text{s}^{-1}$.

In the examples to follow an analysis of horizontal wind and pressure fields at the earth's surface is sought. The governing dynamical relationships are specified as:

$$c_p \Theta \frac{\partial \pi}{\partial X} - fv - F_x = 0 \equiv D_1 \tag{2.5}$$

$$c_p \Theta \frac{\partial \pi}{\partial Y} + fu - F_y = 0 \equiv D_2 \tag{2.6}$$

where:

$\pi = \left[\frac{P}{P_o}\right]^{R/c_p}$

c_p = specific heat at constant pressure

R = gas constant

P = pressure of a σ surface

P_o = 1000 mb

θ = potential temperature (313^oK)

u = horizontal velocity along X

v = horizontal velocity along Y

F_x = frictional force along X

F_y = frictional force along Y

Eqs. 2.5 and 2.6 represent a balance between the pressure gradient, Coriolis and frictional forces on a horizontal surface. For the sake of clarity the terrain is considered uniformly flat. For convenience σ or terrain following coordinates are employed since this will be the system used in the development of the analysis model described later. Derivation of the complete horizontal equations of motion in the σ system is presented in Appendix A.

Eddy stresses are usually considered most important in the layer from the earth's surface up to 1000 meters, known as the planetary boundary layer (Haltiner, 1956). Following Lewis and Grayson (1972) the change of stress with height in this layer can be written as

$$\frac{1}{\rho}\frac{\partial \tau}{\partial z} = \frac{-\tau_s}{\bar{\rho} H} \tag{2.7}$$

where the eddy stress has vanished at the top of the layer of depth H=1000 meters, and $\bar{\rho}$ represents the mean density in this layer. Assuming the stress at the surface is proportional to the square of the wind speed yields

$$\frac{1}{\rho}\frac{\partial \tau}{\partial z} = -\frac{\rho C_D |\bar{V}| (ui+vj)}{\bar{\rho} H} \tag{2.8}$$

where $\bar{V}$ is horizontal velocity and C_D is the drag coefficient. Since $\rho/\bar{\rho} \simeq 1$, in the boundary layer the surface friction terms in 2.5 and 2.6 can be written

$$F_x = -\frac{C_D|\bar{V}|u}{H} \tag{2.9}$$

$$F_y = -\frac{C_D|\bar{V}|v}{H} \tag{2.10}$$

Roll (1965) provides a comprehensive and very useful compilation of surface drag coefficients determined by a large number of independent investigations. He cites the results of Wilson (1960) who determined that C_D increases between light and strong winds (5 m s^{-1} to 20 m s^{-1}) from about 1.5 to $2.4\text{x}10^{-3}$ with standard deviations of 0.83 to $0.56\text{x}10^{-3}$. Pond et al. (1971) analyzing data collected during the Barbados Oceanographic and Meteorological Experiment (BOMEX) and during a pre-BOMEX trial cruise near San Diego in February 1969 determined a C_D of $1.5\text{x}10^{-3}$ for winds about 7-8 m s^{-1}. Recent calculations of C_D by Smith (1974) for Lake Ontario agree with these findings. (In this study for grid points representing Lake Ontario C_D is uniformly set to $1.5\text{x}10^{-3}$.) ? Over land in accord with the hemispheric map of surface drag coefficient obtained by Cressman (1960) C_D is set to $1.8\text{x}10^{-3}$. These values

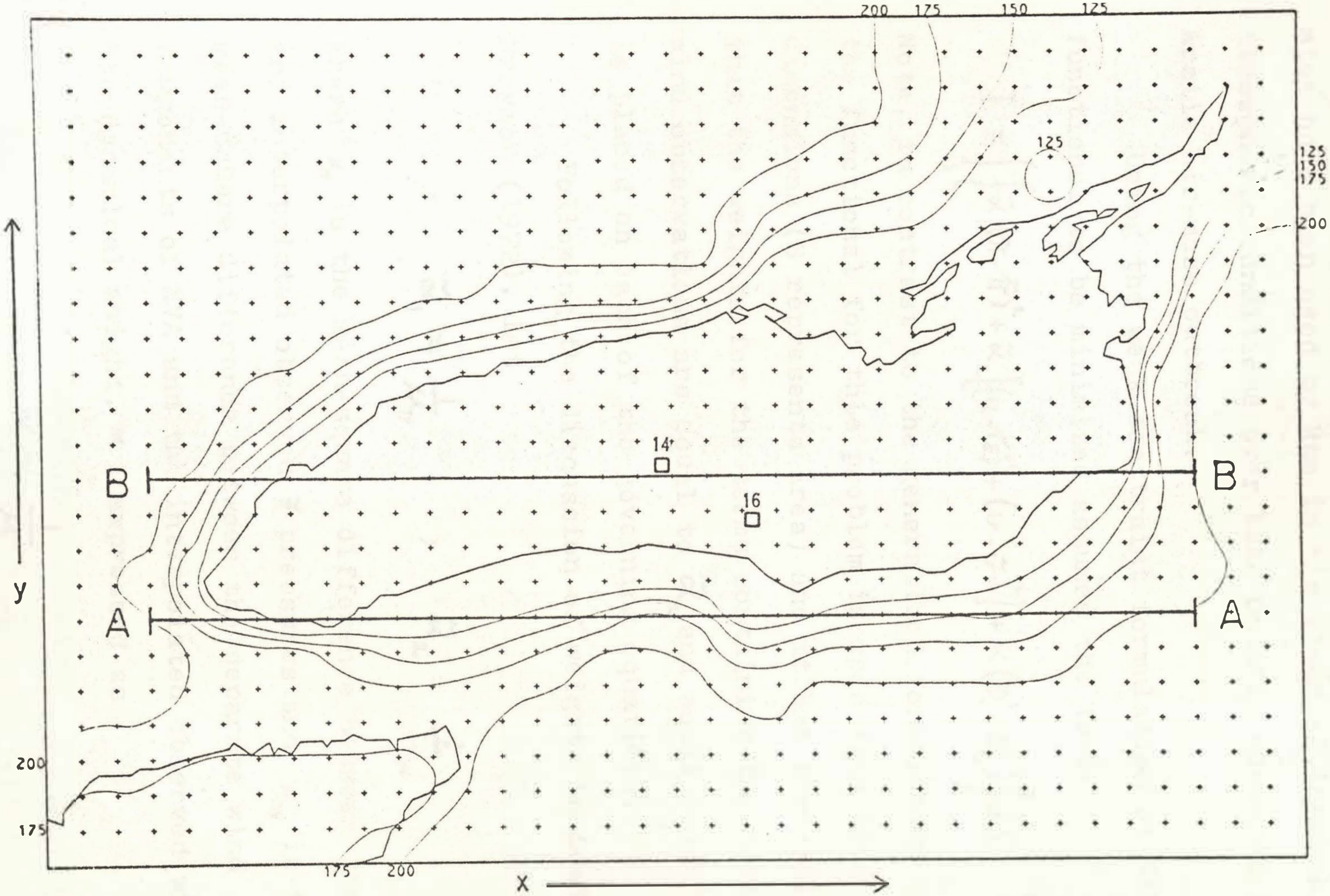

Fig. 2. Area over which NVA analyses are performed. Plus signs indicate location of interior grid points (mesh spacing = 10.77 km). Smoothed topography is shown in meters. Small squares show position of IFYGL observational buoys 14 and 16.

also have been used by Rao in his study of initial atmospheric conditions over Lake Ontario accompanying an Arctic air-mass outbreak.

Using the weak constraint formulation of NVA, the functional to be minimized assumes the form:

$$I = \iint_S \left\{ \tilde{\alpha}_1 (\pi - \tilde{\pi})^2 + \tilde{\alpha}_2 \left[(u - \tilde{u})^2 + (v - \tilde{v})^2 \right] + \alpha \left(D_1^2 + D_2^2 \right) \right\} dS \qquad (2.11)$$

Note, in contrast to the generalized formulation in 2.1, the functional for this problem is specified in only two dimensions (S represents area) and it has been assumed that the weights for the terms containing the horizontal wind observations are equal to $\tilde{\alpha}_2$ and equal weight, α , is placed on each of the governing equations.

Following the discussion of weights in Lewis and Grayson (1972), let

$$\tilde{\alpha}_1 = \frac{1}{\mu_\pi} \quad , \quad \tilde{\alpha}_2 = \frac{1}{\mu_w} \qquad (2.12)$$

where μ_π is the mean-square difference between the NVA and interpolated observed $\tilde{\pi}$ pressures and μ_W is the mean-square difference between the separate wind components of NVA and the interpolated observed winds. The dynamical weight, α , expressed as

$$\alpha = \frac{1}{\mu} \qquad (2.13)$$

may be thought of as a measure of the uncertainty in the constraints, D_j. Actually, however, as pointed out by Lewis (1972) it is only the ratios of the weights $\alpha/\tilde{\alpha}_1$ and $\alpha/\tilde{\alpha}_2$ that are important in the analysis equations.

Taking the first variation of 2.11 and requiring it to vanish yields

$$0 = \delta I = \iint_S \left[P\delta\pi + U\delta u + V\delta v \right] dS + \left\{ \begin{array}{c} \text{boundary} \\ \text{terms} \end{array} \right\} \qquad (2.14)$$

The boundary terms are expressions evaluated at the bounding sides of the domain.

Conditions necessary to cause these boundary terms to vanish are called the natural boundary conditions. A clear and instructive explanation of these terms can be found in books on variational calculus (see for example Lanczos, 1966). It has become customary when applying NVA to impose Dirichlet conditions at the boundary thus allowing no adjustment to occur there. These conditions force the boundary terms to vanish and from a practical standpoint are especially desirable when programming the numerical method. Dirichlet conditions, however, are just one of several possible conditions that can cause the boundary terms to vanish.

With the boundary terms eliminated and because of the independence of the variations of π, u and v, the solution of 2.14 is

$$P = U = V = 0 \tag{2.15}$$

where

$$P = \tilde{\alpha}_1(\pi - \tilde{\pi}) - \alpha\left\{ c_p\theta\nabla^2\pi + f\left(\frac{\partial u}{\partial y} - \frac{\partial v}{\partial x}\right) - \frac{\partial(C_D|\bar{V}|)u}{\partial x} - \frac{\partial(C_D|\bar{V}|)v}{\partial y} - C_D|\bar{V}|\left(\frac{\partial u}{\partial x} + \frac{\partial v}{\partial y}\right)\right\} = 0 \tag{2.16}$$

$$U = \tilde{\alpha}_2(u - \tilde{u}) - \alpha\left\{ C_D|\bar{V}|\left(c_p\theta\frac{\partial\pi}{\partial x} - fv - C_D|\bar{V}|u\right) - f\left(c_p\theta\frac{\partial\pi}{\partial y} + fu - C_D|\bar{V}|v\right)\right\} = 0 \tag{2.17}$$

$$V = \tilde{\alpha}_2(v - \tilde{v}) - \alpha\left\{ C_D|\bar{V}|\left(c_p\theta\frac{\partial\pi}{\partial y} + fu - C_D|\bar{V}|v\right) + f\left(c_p\theta\frac{\partial\pi}{\partial x} - fv - C_D|\bar{V}|u\right)\right\} = 0 \tag{2.18}$$

or

$$\pi = \tilde{\pi} + \frac{\alpha}{\tilde{\alpha}_1} \left\{ \text{bracketed terms in 2.16} \right\} \qquad (2.19)$$

$$u = \tilde{u} + \frac{\alpha}{\tilde{\alpha}_2} \left\{ \text{bracketed terms in 2.17} \right\} \qquad (2.20)$$

$$v = \tilde{v} + \frac{\alpha}{\tilde{\alpha}_2} \left\{ \text{bracketed terms in 2.18} \right\} \qquad (2.21)$$

where ∇^2 is the two-dimensional laplacian operator. Clearly, the solution for each variable is a weighted combination of the observational value and a dynamical relationship generated by the variational procedure. Simultaneous solution of 2.19-2.21 over the domain provides the analyzed fields. In this study the accelerated Liebmann relaxation procedure is used to solve 2.19-2.21 (Miyakoda, 1961).

In obtaining 2.16-2.18 the dynamical weight, α, is assumed to be invariant in space. It isn't necessary to apply this assumption to the observational weights, i.e., one area may have better data than another. Herein lies one of the special features of the variational method: by varying these observational weights over the domain the final analysis can be forced to "draw to" the observations in accord with their accuracy at that point while simultaneously extrapolating these data in accord with the specified dynamics.

Fig. 3 shows the initial or observational fields of wind and pressure for example 1. Super-imposed on an easterly zonal wind field of 13.84 m s^{-1} is a sinusoidal varying pressure field. Clearly, the initial conditions do not satisfy the analysis model's governing equations. The purpose of this example is to demonstrate the feedback mechanism acting through the dynamical terms in 2.19-2.21. The weights are chosen to express much greater confidence in the initial pressure field than the wind field. $\tilde{\alpha}_1$, and $\tilde{\alpha}_2$ are computed for mean differences of .01 mb for pressure and 2×10^3 cm s^{-1} for wind while, α, is calculated using $\mu^{\frac{1}{2}} = .1$ cm s^{-2}.

Fig. 4 shows the NVA analyzed wind and pressure fields; Fig. 5 the wind and isotach pattern. The cross-contour flow caused by the inclusion of friction is present and there is an increase of the wind velocity over the lake due to the differential drag coefficient. The adjusted wind velocity increased to values somewhat over 14 m s^{-1} caused by the generation of a v-component which was not present in the initial field.

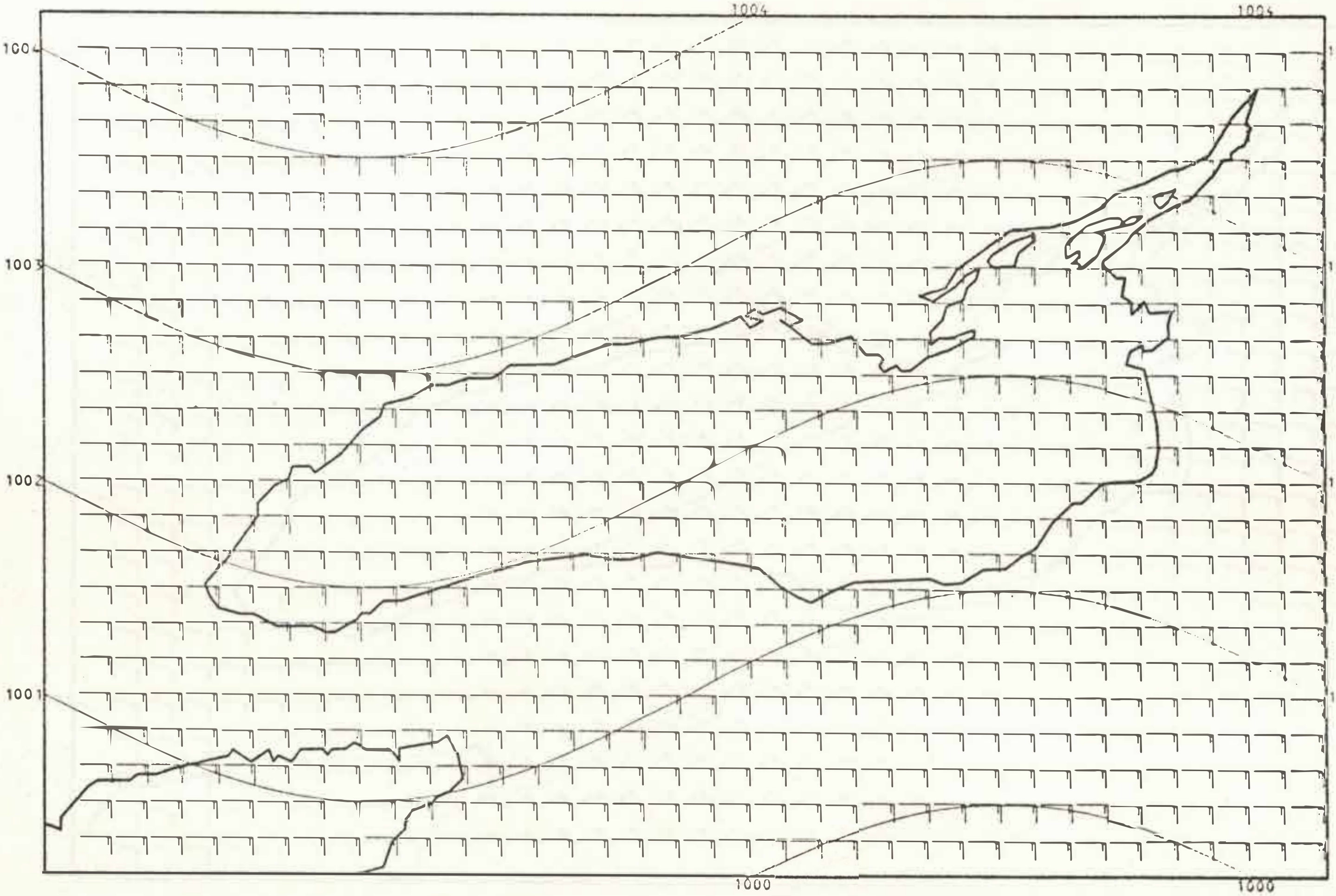

Fig. 3. Initial surface wind (full barb 10 m s^{-1}, half barbs 5 m s^{-1}) and pressure (mb) fields for example 1.

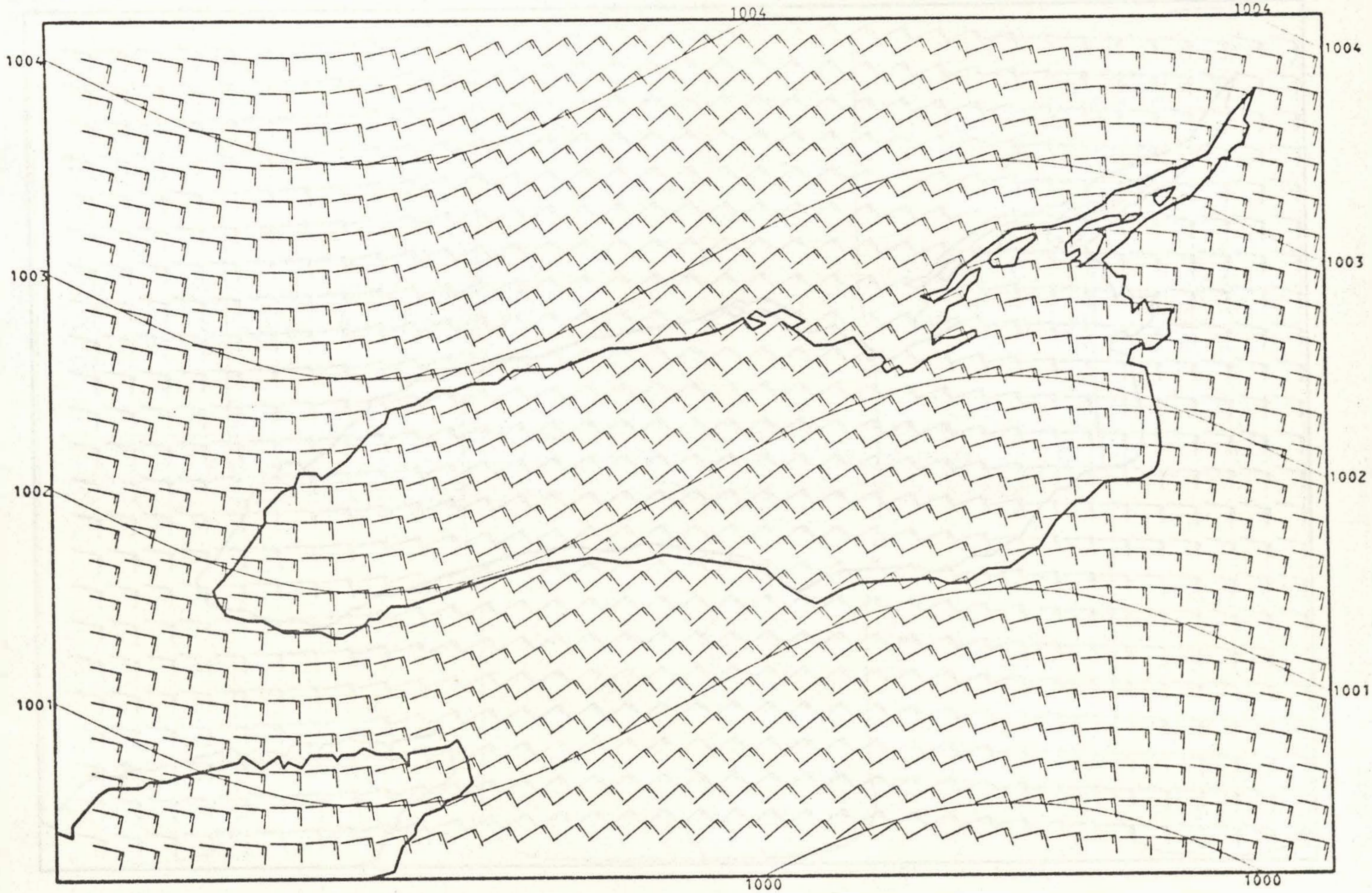

Fig. 4. Same as Fig. 3, except fields have now been adjusted by NVA.

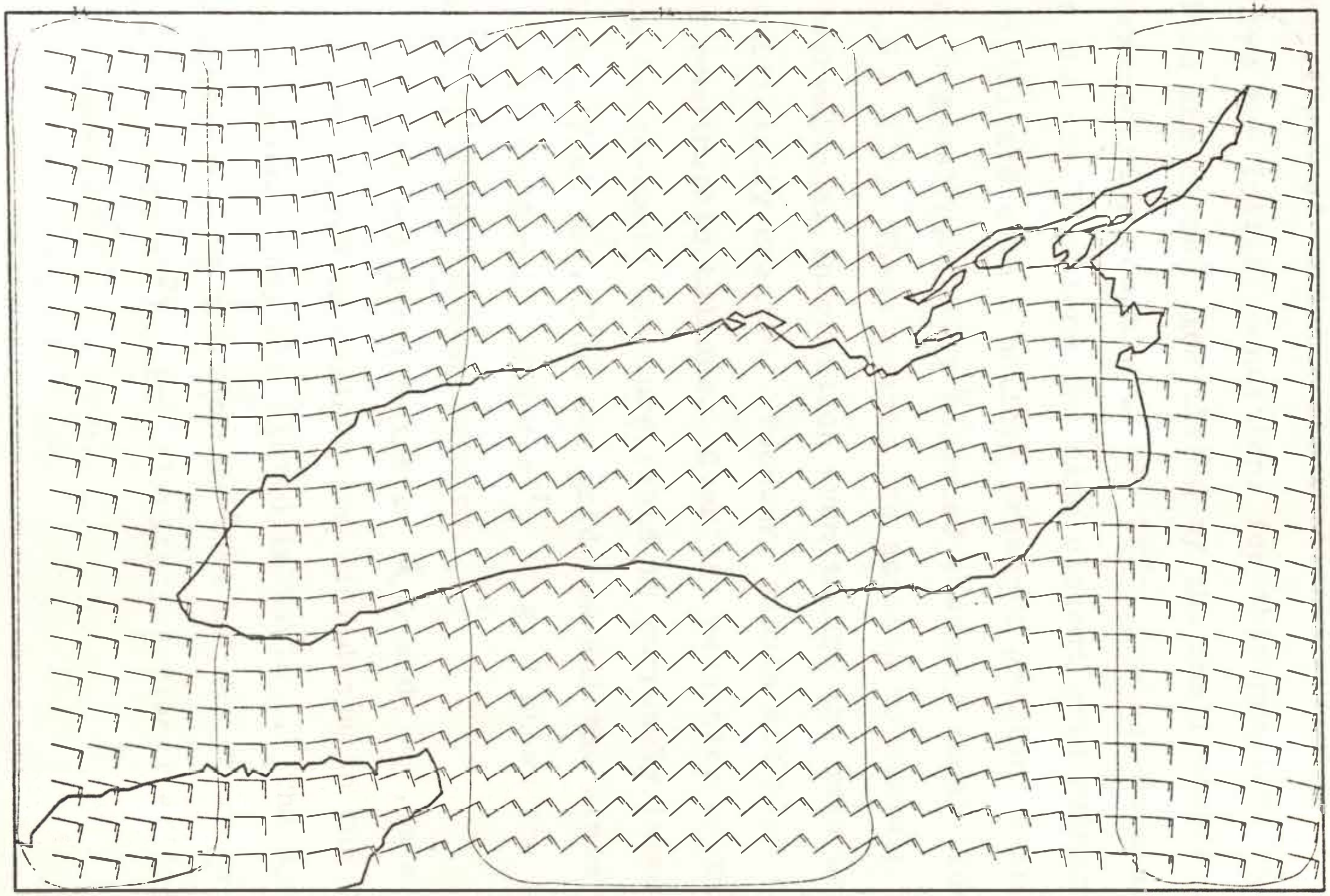

Fig. 5. Isotach pattern (m s^{-1}) of NVA adjusted surface wind for example 1. Surface wind barbs of Fig. 4 have been repeated.

The purpose of the second example is to illustrate the effect of variable observational weights. Fig. 6 shows the initial conditions for this problem. Here six sites are chosen, identified by the small squares, corresponding roughly to the IFYGL rawinsonde stations. At the six locations the nine closest grid points are initialized with a uniform pressure gradient calculated for a geostrophically balanced easterly zonal flow of 13.8 m s^{-1}. These points are assumed to contain reliable observational information even though the data were artificially created. Boundary values are also specified in geostrophic balance. Over the remainder of the area the north-south pressure field is purposely increased from .17 mb to .23 mb per grid row and the winds are reduced uniformly by 5 m s^{-1}. Fig. 7 shows the initial wind flow and isotach pattern.

Observational weights, $\tilde{\alpha}_1$, and $\tilde{\alpha}_2$, are variable and are chosen to reflect the confidence in the initial conditions. They are listed in Table 1. The dynamic weight, α , is the same as that of the previous example ($\mu^{\frac{1}{2}}$ = .1 cm s^{-2}). For clarity frictional effects are disregarded.

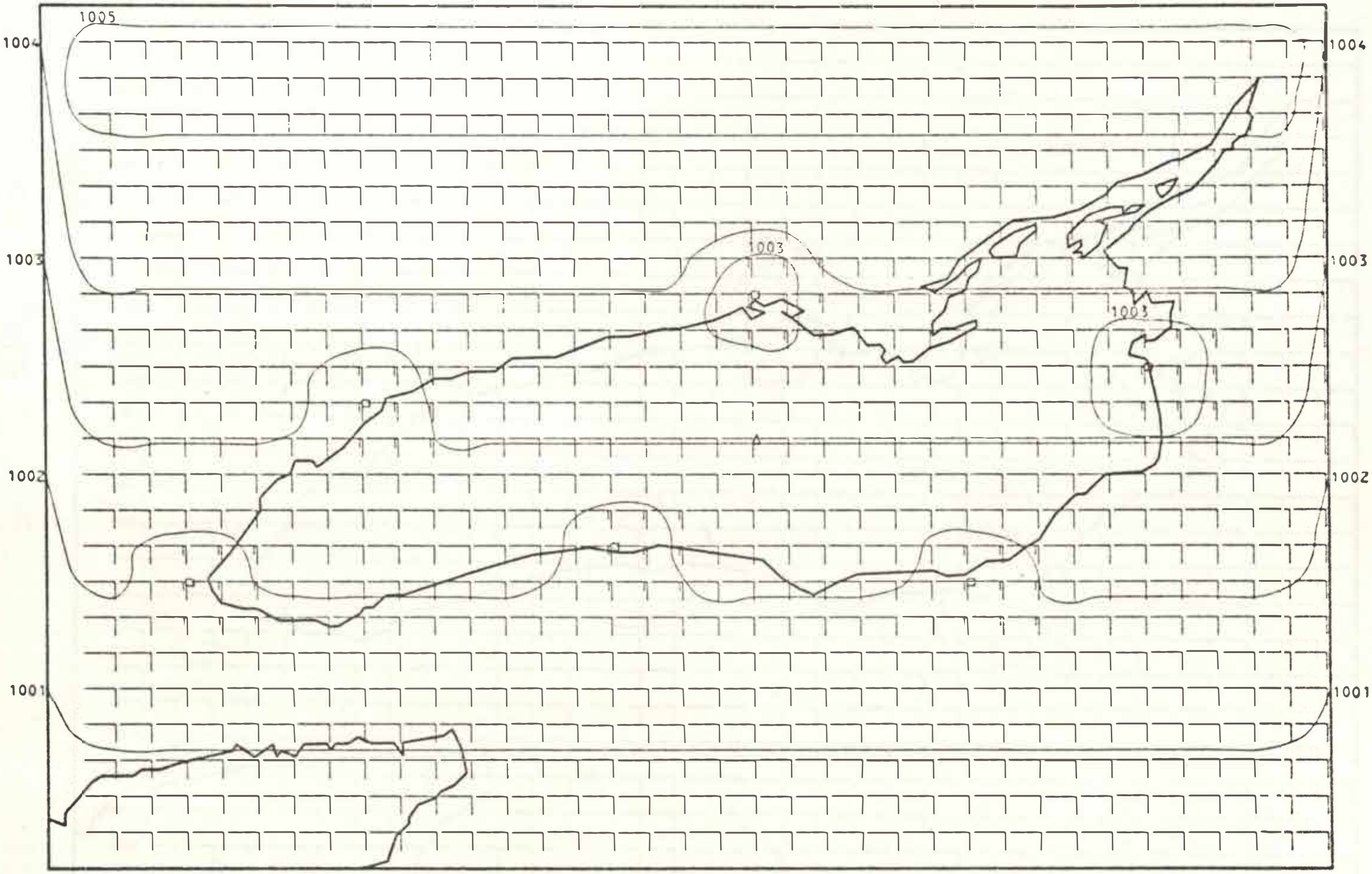

Fig. 6. Same as Fig. 3, except fields are for example 2.
Squares indicate location of simulated IFYGL rawinsondes.

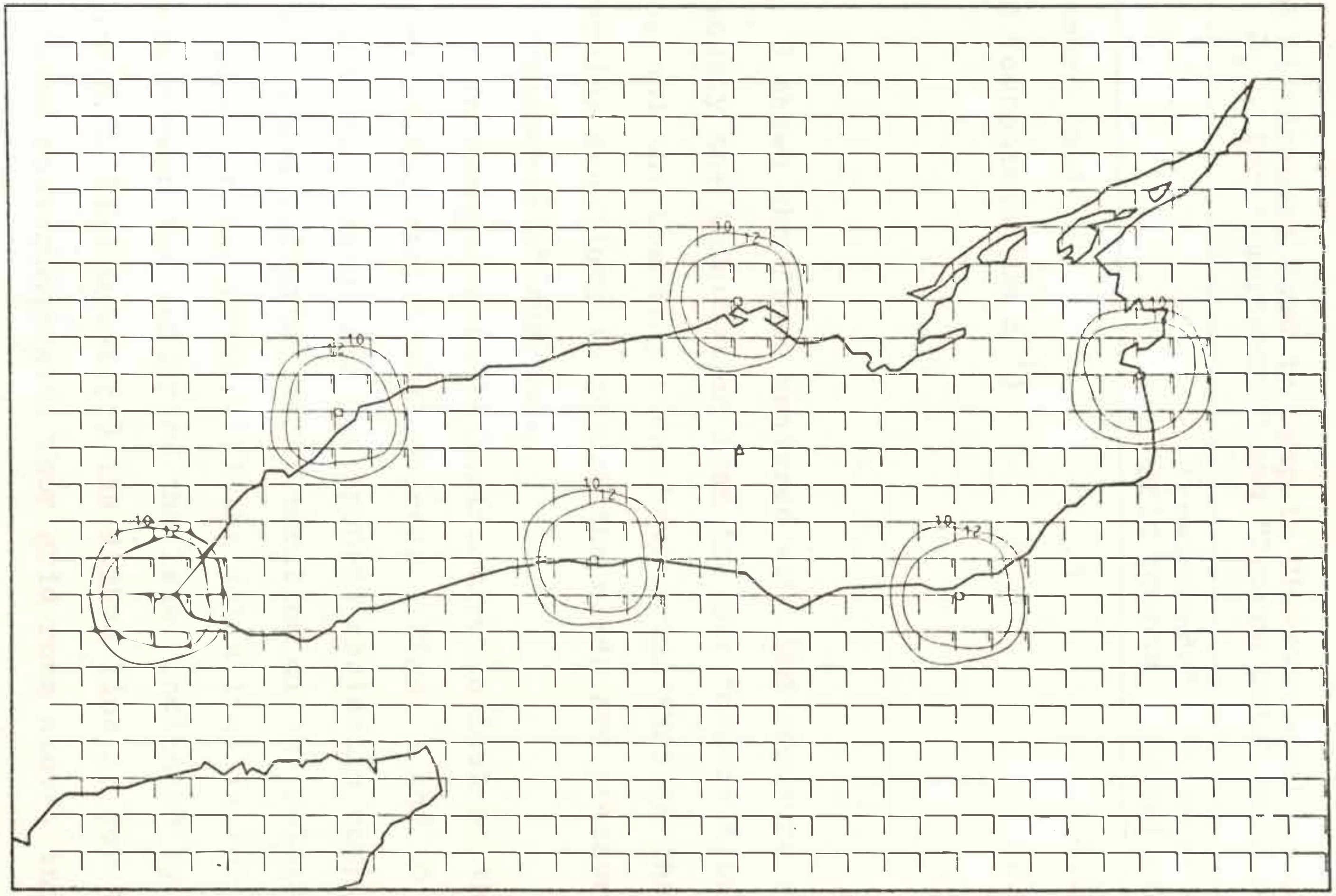

Fig. 7. Initial isotach pattern and surface wind barbs for example 2.

Table 1

Mean Differences Used to Compute Observational Weights $\tilde{\alpha}_1$, and $\tilde{\alpha}_2$, for "Rawinsonde" and "Sparse Data" grid points

	"rawinsonde" grid points	"sparse data" grid points
Pressure (mb)	.3	4.0
Wind Components (cm s^{-1})	40	800

Fig. 8 shows the final analyzed wind and pressure fields. Obviously the information from the six "observational" sites and the bounding sides have acted through the governing equations to adjust the winds and pressures in the "sparse-data" regions.

In example 2 it is instructive to look at the nature of the variational process. Figs. 9 and 10 contain respectively the u- and v-component residuals computed from 2.5 and 2.6 after each iteration of the relaxation procedure for two sites: (1) the solid line is for the location near the center of the lake, indicated by a triangle in Fig. 8 and (2) the dashed line is for the simulated rawinsonde site four grid rows above, indicated by the square.

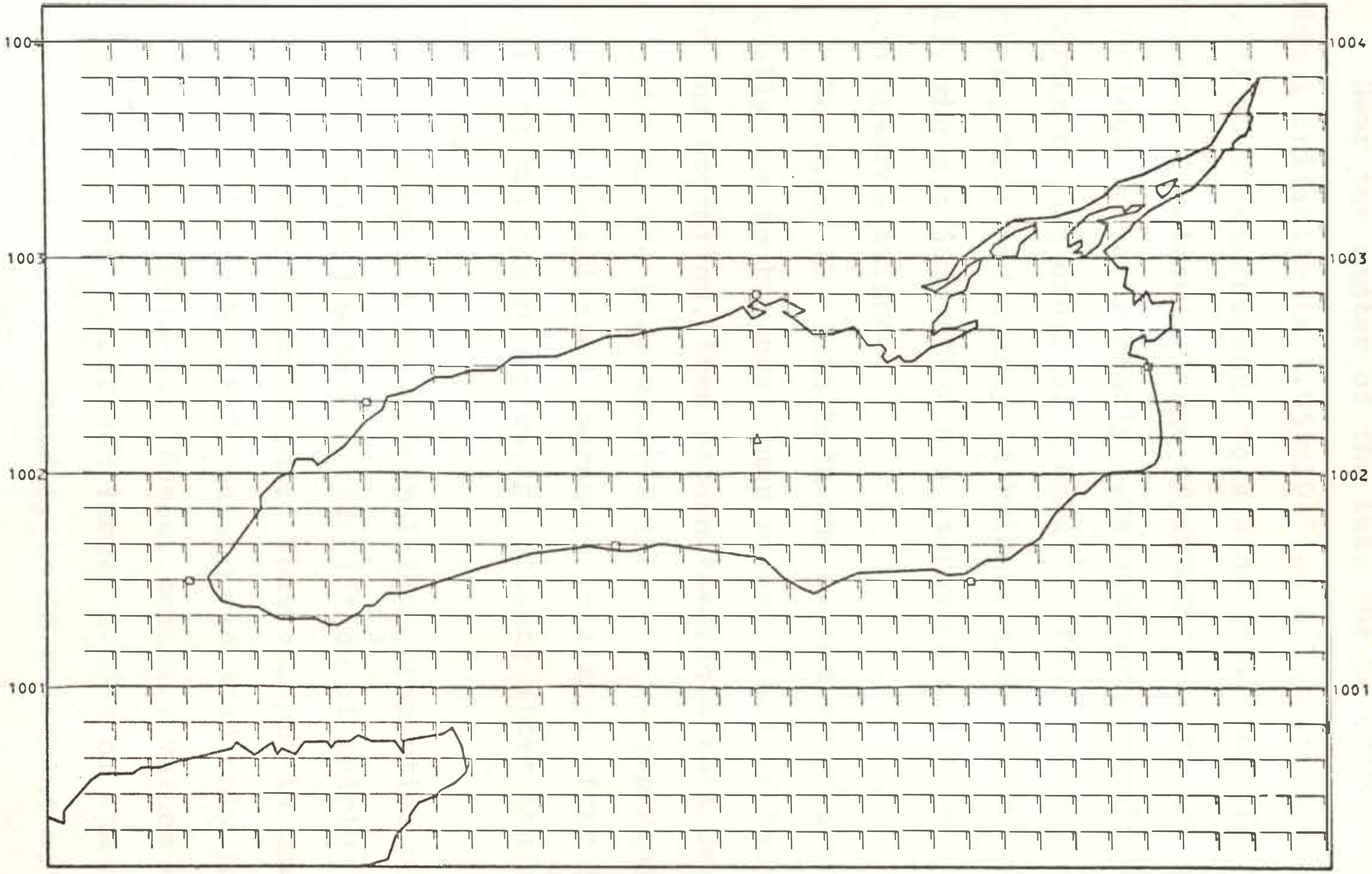

Fig. 8. Same as Fig. 4, except fields are NVA solution for example 2.

Near the center of the lake the u-component residual initially is 1.055×10^{-1} cm s^{-2} (not shown on Fig. 9) which corresponds to a wind imbalance of 10 m s^{-1}. After one iteration a large adjustment occurs and thence the residual remains nearly constant corresponding to an imbalance on the order of 1 cm s^{-1}. The v-component, initially zero and nearly in balance with the pressure field, shows a jump after one iteration and then a rapid return towards balance.

North of the lake both the u- and v-components initially are in balance, jump somewhat out of balance after one iteration, then return towards a balance of the same order as the over-water site. The v-component exhibits an unexplained increased imbalance after four iterations but again approaches balance after ten iterations.

In example 3 the extrapolation properties of NVA are again examined with the stipulation of poorly specified boundary conditions. This example is particularly relevant since the IFYGL data are located only in the vicinity of Lake Ontario. Hence, boundary values will have to be chosen to reflect larger scales of atmospheric motion and will not necessarily be in agreement with the smaller-scale motions discernible from the information

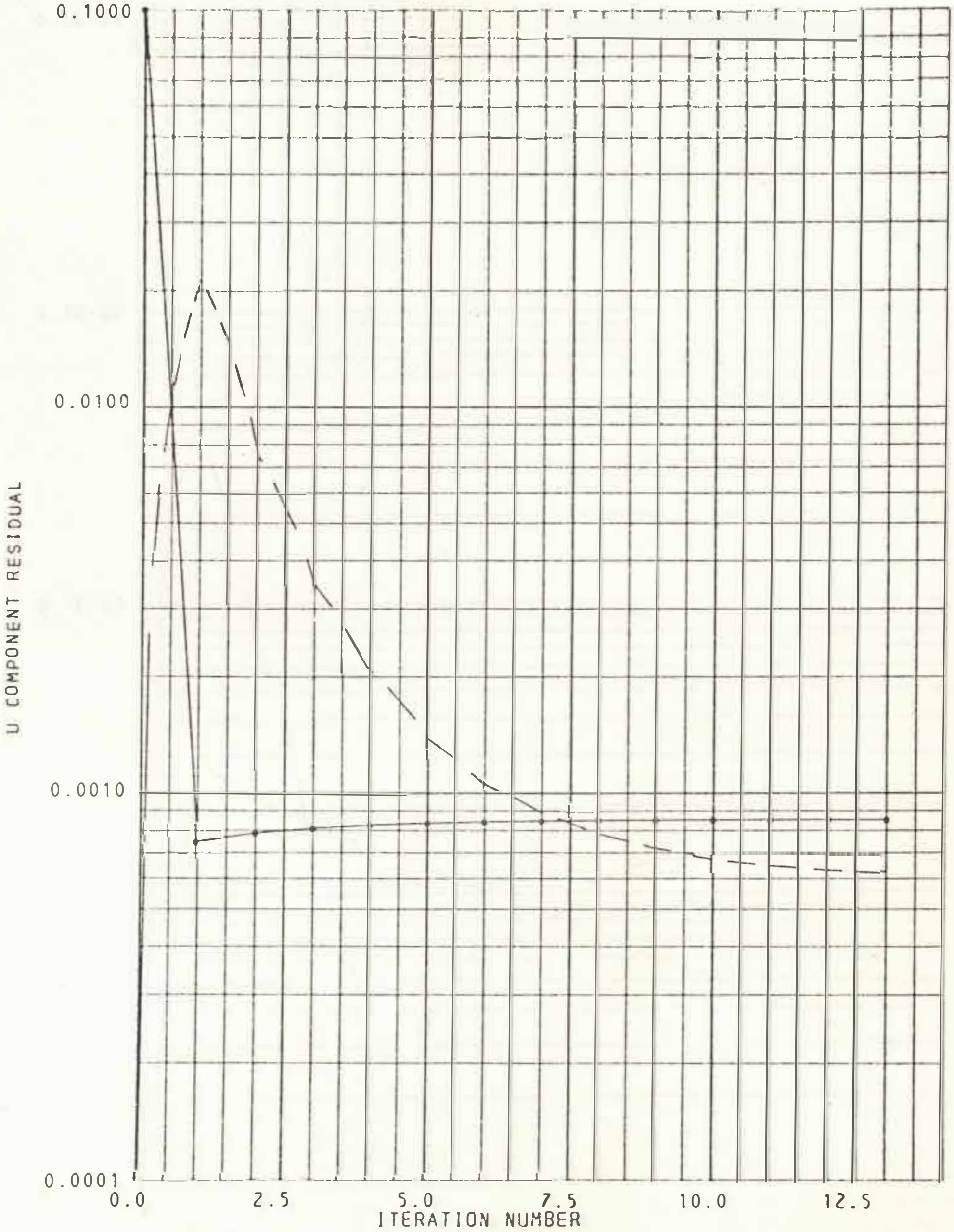

Fig. 9. Residuals computed at each iteration of relaxation procedure for u-component Eq. 2.6 at triangle over center of Lake Ontario (solid line) and at square four grid distances to the north (dashed line) of Fig. 7.

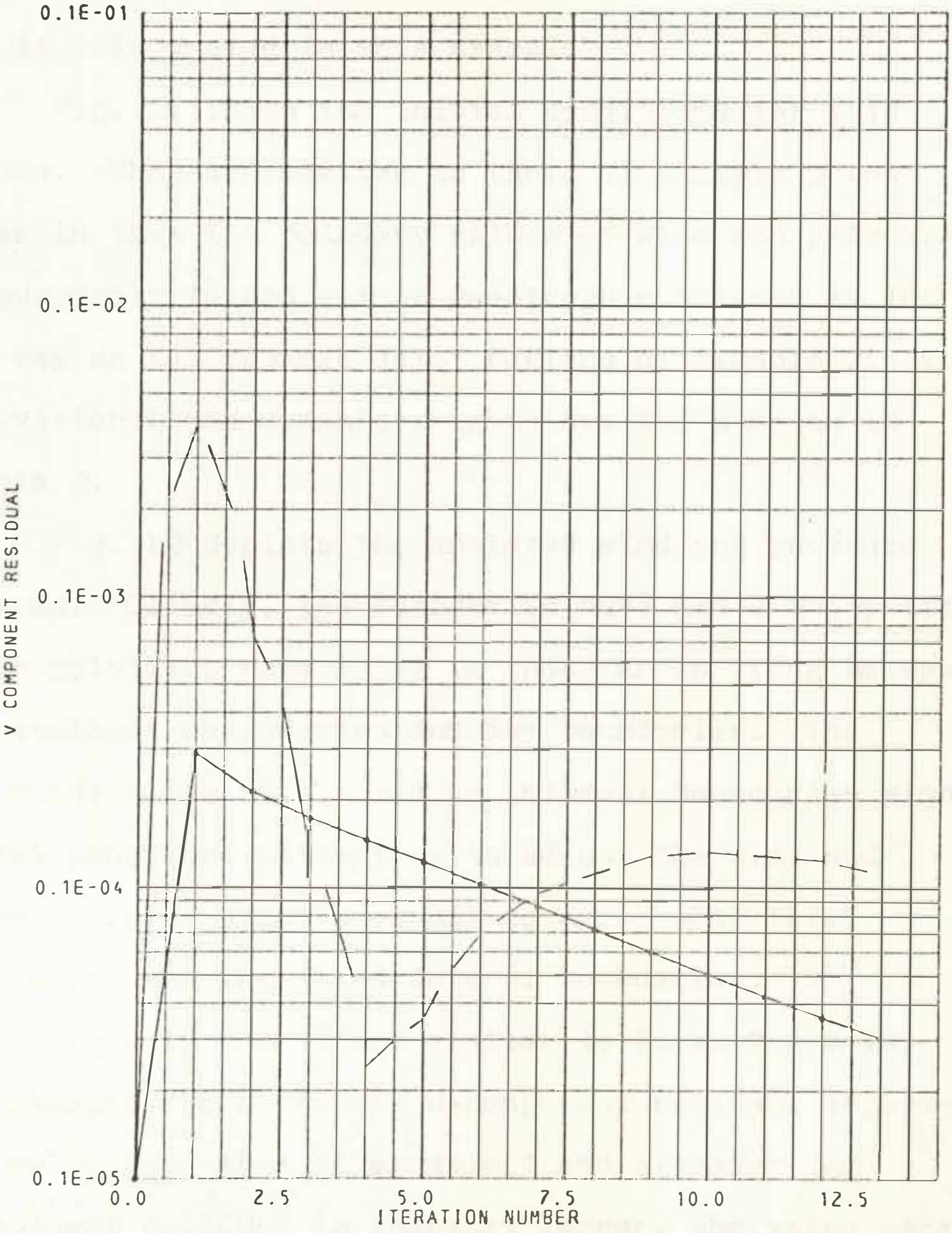

Fig. 10. Same as Fig. 9, except residual computed for v-component Eq. 2.5.

available near the lake. The effect this incompatibility has on the dynamical consistency of the analysis over the lake is illustrated in this example.

Fig. 11 shows the initial conditions for this problem. They are similar to those of example 2 but differ in that the boundary values of wind and pressure are purposely forced out of geostrophic balance in the same way as the "sparse data" regions of example 2. The observational and dynamic weights are the same as in example 2.

Fig. 12 depicts the analyzed wind and pressure patterns. Clearly, the boundaries have had a major effect on the solution, especially in those areas lying between the simulated rawinsondes and the boundaries. The rawinsonde sites have acted as internal boundaries with the NVA procedure attempting to adjust the wind and pressure fields simultaneously to agree with this information and the fixed lateral boundaries.

Figs. 13 and 14 are similar to Figs. 9 and 10. In this example the over-lake u-component residual adjusts to a value near that of example 2 and although the v-component residual is somewhat larger, the value here corresponds to an imbalance of less than 1 cm s^{-1}. Thus at this point over the lake the rawinsonde information

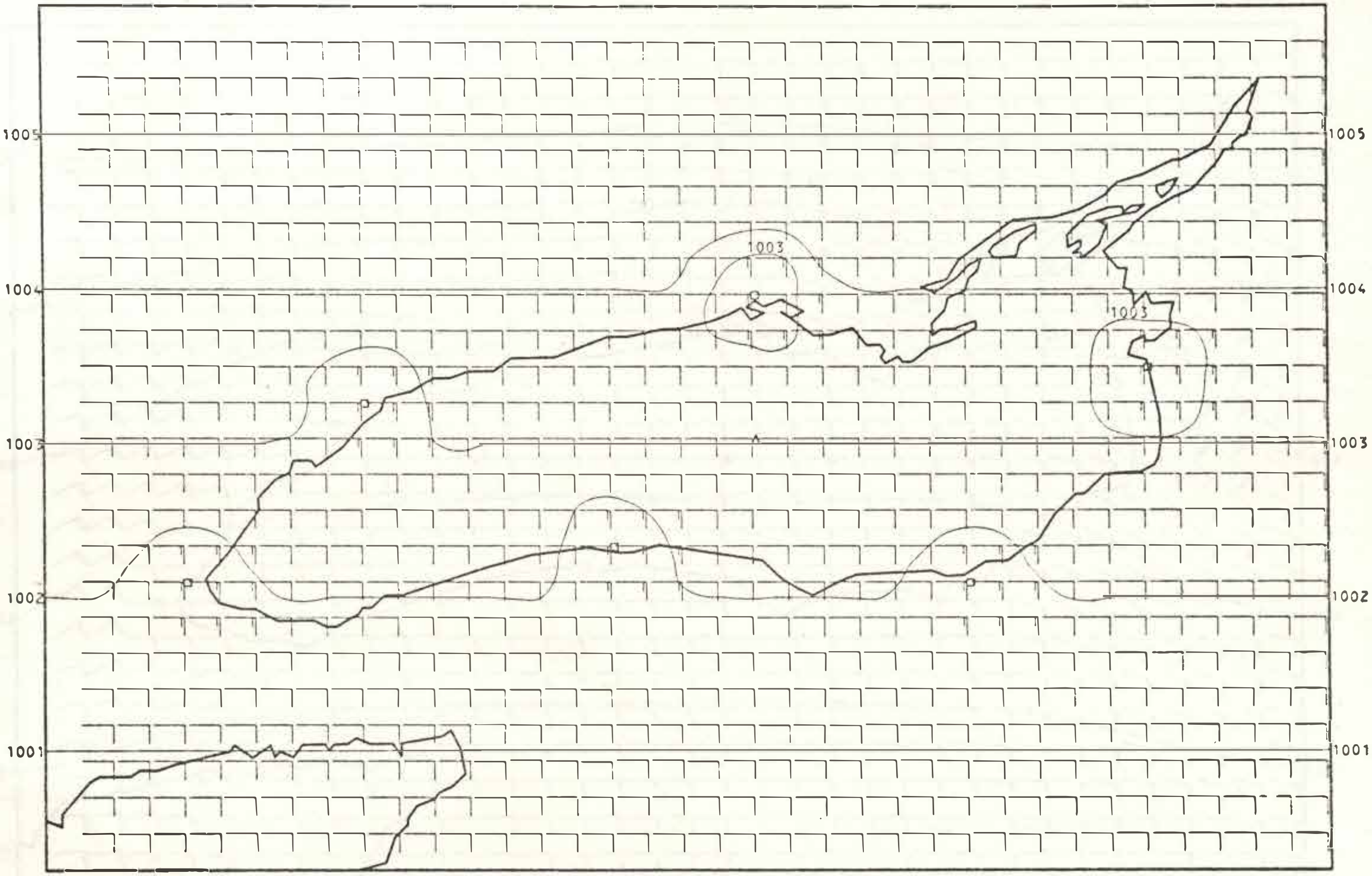

Fig. 11. Same as Fig. 7, except initial fields are for example 3.

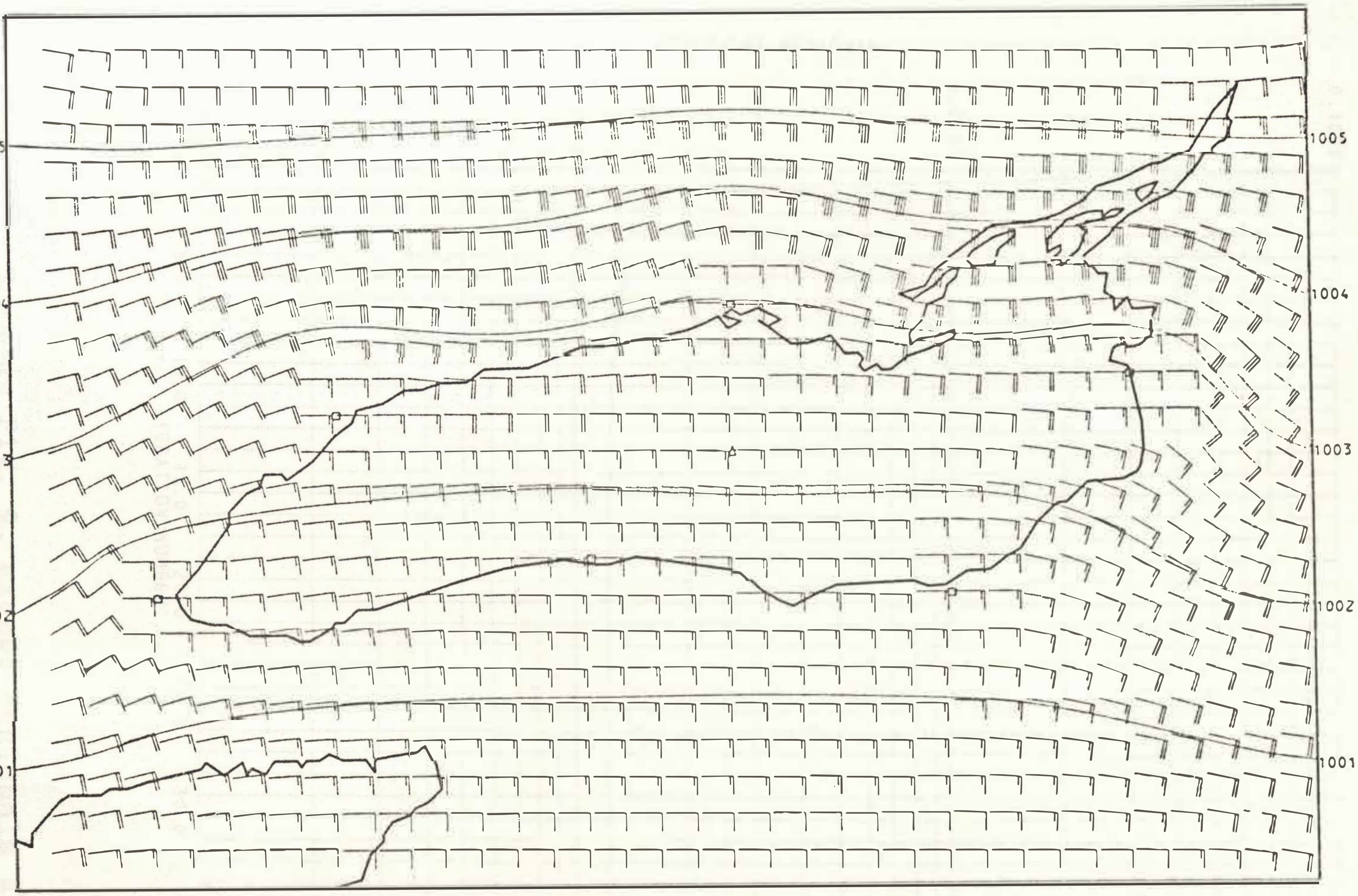

Fig. 12. Same as Fig. 4, except fields are NVA solution for example 3.

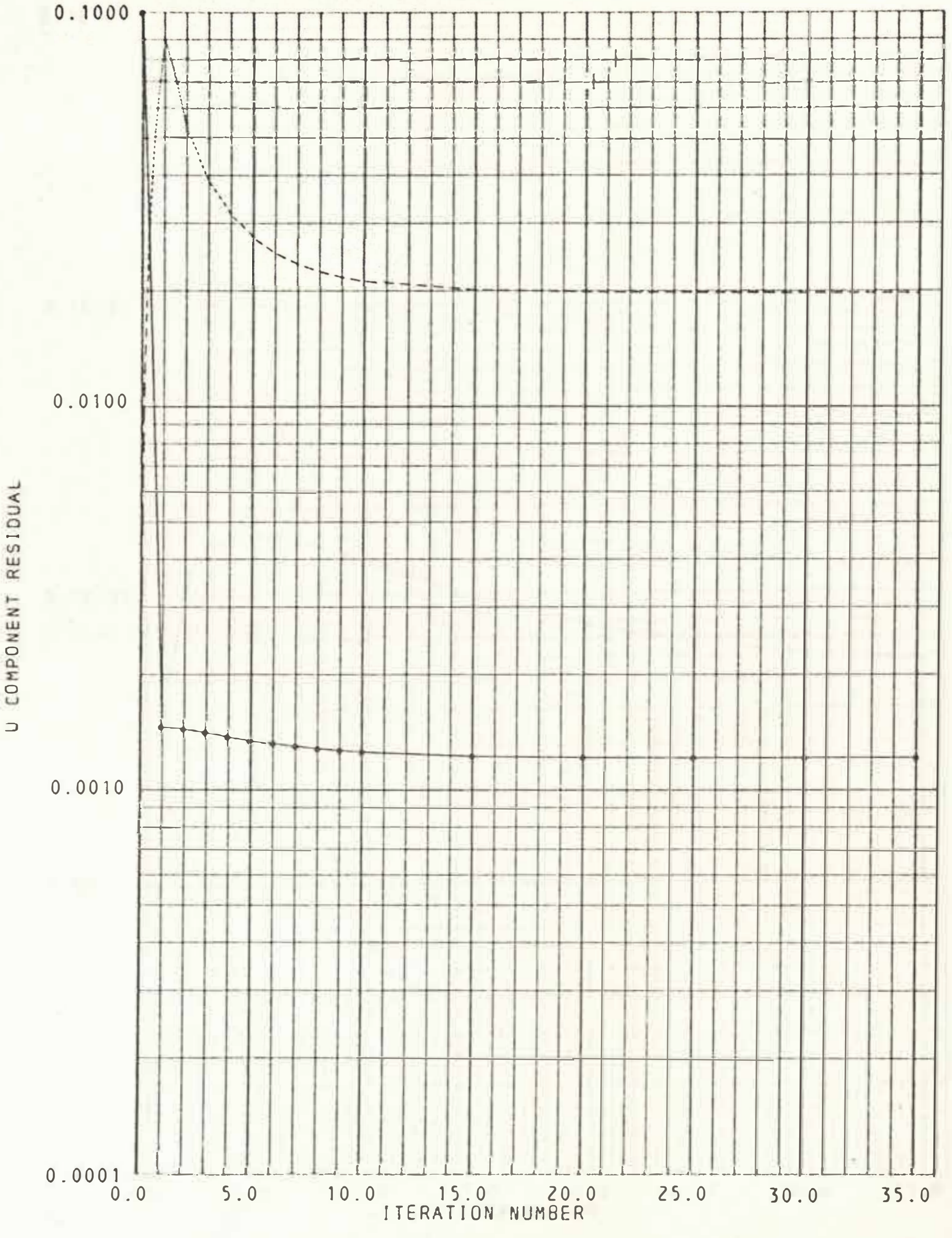

Fig. 13. Same as Fig. 9, except residuals are computed for example 3.

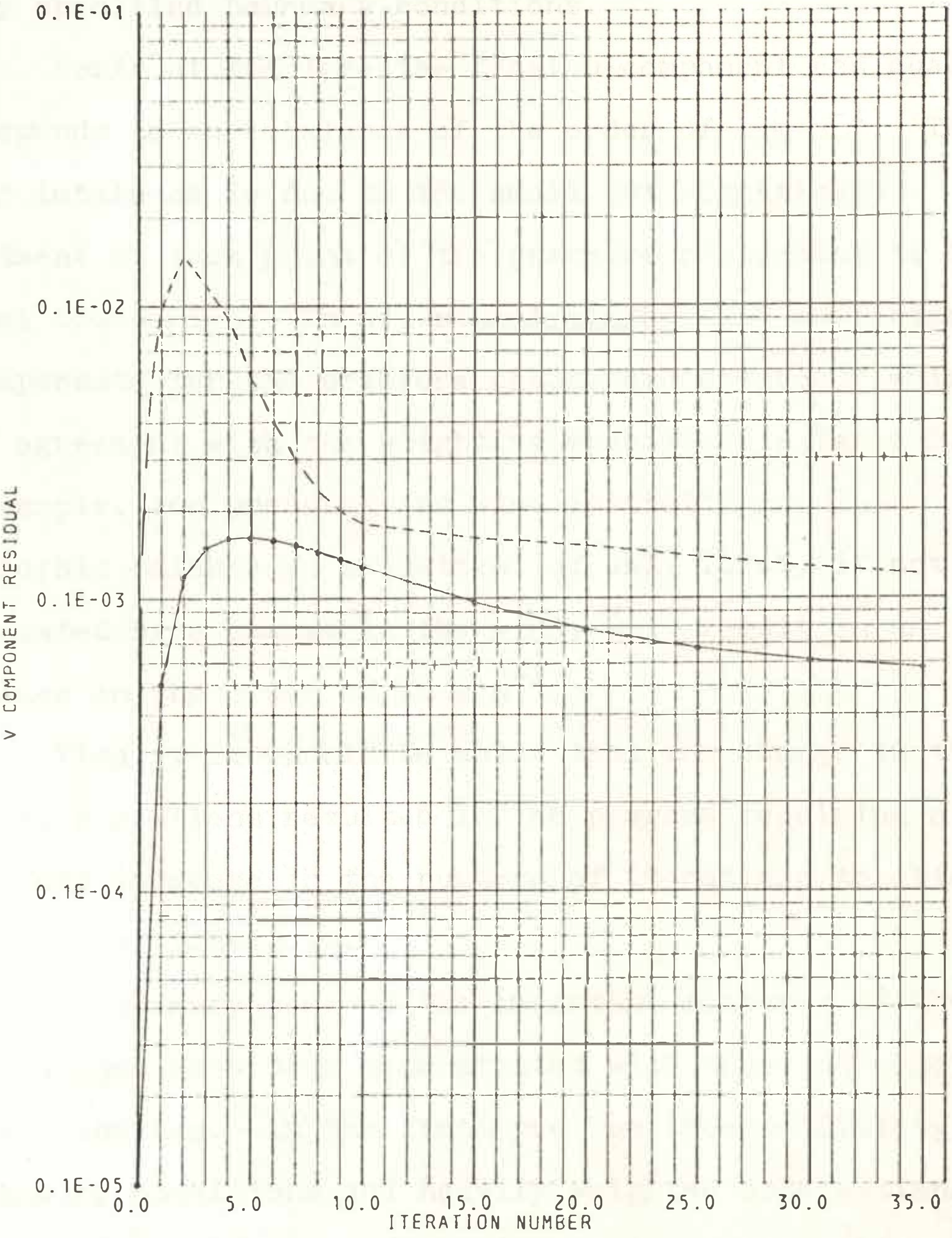

Fig. 14. Same as Fig. 10, except residuals are computed for example 3.

has been extrapolated quite successfully, even with very poorly specified boundary conditions.

North of the lake the final u-component residual corresponds to an imbalance of the order of 1 m s^{-1}. This larger imbalance is due to the small but significant adjustment at this point of the pressure responding to the lateral boundaries. An adjustment of the wind sufficient to compensate for the pressure change did not occur which is in agreement with the weighting specified in Table 1. For example, for pressure and wind initially in geostrophic balance an adjustment of only .1 mb, if not compensated by a change in the wind, will result in an imbalance on the order of 10 m s^{-1}.

Finally it should be noted that the change in the boundary conditions resulted in the program requiring a three-fold increase in the numbers of iterations to obtain a solution of 2.19-2.21.

In summary some of the important features of the NVA technique have been demonstrated with three straightforward examples. In the final problem incompatibility of boundary conditions and heavily weighted observational information results in major adjustments of the pressure and wind fields. Fortunately, that portion of the analysis domain located over the lake is mostly "shielded" from the poorly specified lateral boundaries. Although these examples employed dynamical constraints typical of large-scale flow the technique may be extended to the lake-effect phenomenon with attendant mesoscale motions by using appropriate and more complex constraints.

CHAPTER III

MODEL DEVELOPMENT

BACKGROUND

On the synoptic scale, in the free atmosphere, the atmospheric motion may be specified, to a good approximation, by a balance of the pressure gradient and Coriolis force. An NVA scheme developed to analyze wind and pressure on this scale might use the geostrophic condition as the equation to be applied as a weak constraint. Likewise, a general NVA scheme capable of depicting mesoscale features should have equations of constraint that embody those processes known to be of major importance on this scale. Sensible heat, moisture and momentum transfer with the earth's surface, horizontal and vertical advection, terrain effects and water vapor condensation should be included. In this chapter an NVA model is developed for application to analysis of mesoscale data and in particular to the lake-effect air-mass modification phenomenon.

Initially, numerical models previously developed to study the lake-effect phenomenon were scrutinized with the aim of using the governing equations of one of these models directly in this work. However, all models exhibited deficiencies of one kind or another that made them unsuitable for this study. Lavoie's model (1972), although quite useful for studying the general response of the atmosphere to various lake-related forcing, is limited in the detail it can represent by its vertical modelling assumptions. Kaplan and Paine's forecast model (1972) and Rao's analysis model (1971) are formulated in the p-coordinate system, thus the inclusion of important orographic and surface frictional effects must be handled somewhat artificially. A modification of Hovermale's cross-section model (1965), developed to study airflow over mountains was used by Lavoie et al. (1970) to study the effect of the vertical modelling assumptions of Lavoie's model. The physical response of the atmosphere to lateral inhomogenities is lost in a cross-section model such as this.

ANALYSIS EQUATIONS

Since the lake-effect phenomenon is closely linked to the configuration of the lake and its surrounding topography it is natural to formulate the analysis model in σ (terrain-following) coordinates (Phillips, 1957). The model equations in this system are derived in Appendix A and are presented here without detailed explanation. They are:

$$\sigma = \frac{P - P^*}{P_s - P^*} \tag{3.1}$$

$$\pi = \left[\frac{P}{P_0}\right]^{R/c_p} \tag{3.2}$$

$$\frac{\partial u}{\partial t} + u\frac{\partial u}{\partial x} + v\frac{\partial u}{\partial y} + \dot{\sigma}\frac{\partial u}{\partial \sigma} = -\frac{\partial \phi}{\partial x} - c_p\theta\frac{\partial \pi}{\partial x} + fv + F_x \equiv D_4 \tag{3.3}$$

$$\frac{\partial v}{\partial t} + u\frac{\partial v}{\partial x} + v\frac{\partial v}{\partial y} + \dot{\sigma}\frac{\partial v}{\partial \sigma} = -\frac{\partial \phi}{\partial y} - c_p\theta\frac{\partial \pi}{\partial y} - fu + F_y \equiv D_5 \tag{3.4}$$

$$\frac{\partial \phi}{\partial \sigma} = -c_p\theta\frac{\partial \pi}{\partial \sigma} \equiv D_1 \tag{3.5}$$

$$\frac{\partial \theta}{\partial t} + u\frac{\partial \theta}{\partial x} + v\frac{\partial \theta}{\partial y} + \dot{\sigma}\frac{\partial \theta}{\partial \sigma} = \frac{Q}{c_p\pi} \equiv D_2 \tag{3.6}$$

$$\frac{\partial q}{\partial t} + u\frac{\partial q}{\partial x} + v\frac{\partial q}{\partial y} + \dot{\sigma}\frac{\partial q}{\partial \sigma} = S \equiv D_3 \tag{3.7}$$

$$\dot{\sigma} = -\int_1^{\sigma}\left(\frac{\partial u}{\partial x} + \frac{\partial v}{\partial y}\right)d\sigma - \frac{1}{\Delta P}\left\{\frac{\partial P_s}{\partial x}\int_1^{\sigma} u\,d\sigma + \frac{\partial P_s}{\partial y}\int_1^{\sigma} v\,d\sigma\right\} + \frac{(1-\sigma)}{\Delta P}\frac{\partial P_s}{\partial t} \tag{3.8}$$

Eqs. 3.1 and 3.2 define σ and π respectively, 3.3 and 3.4 are the horizontal equations of motion, 3.5 is the hydrostatic equation, 3.6 and 3.7 the first law of thermodynamics and moisture conservation, respectively and 3.8 the vertical velocity equation.

Symbols in the above equations are defined as follows:

P = pressure on a σ surface

P_s = surface pressure (at $\sigma = 1$)

P^* = uppermost level of model (500 mb at $\sigma = 0$)

P_o = 1000 mb

R = gas constant

c_p = specific heat at constant pressure

u = horizontal velocity in X-direction

v = horizontal velocity in Y-direction

$\dot{\sigma}$ = vertical velocity

ϕ = geopotential

f = Coriolis parameter

θ = potential temperature

q = specific humidity

ΔP = difference in pressure between surfaces at $\sigma = 1$ and $\sigma = 0$

F_x = frictional force along X

F_y = frictional force along Y
Q = sensible and latent heating rates
S = rate of specific humidity generation

Determining the surface pressure, P_s, presented a special problem. The vertical coordinate, σ, and the vertical velocity, $\dot{\sigma}$, are functions of this variable. Unfortunately, even though all other parameters are well specified at the surface over and around the lake (Fig.1), the Canadian buoys were not equipped with pressure measuring equipment. Hence there is a gap in the surface pressure data over the northern portion of the lake.

To resolve this problem it was found necessary to perform the objective NVA in two parts: the first, performed at terrain level, provides an adjustment between the wind and pressure fields; the second provides the upper-air analysis over the lake. The first step serves to incorporate the more abundant wind information into the surface pressure field through the variational process. Because the dynamical constraints are posed in σ-coordinates the simultaneous adjustment of the surface pressure and wind fields in response to changes in terrain height is also inherent in this procedure. The adjusted surface pressure field then is used to specify the location of the upper air surfaces through 3.1.

As noted in Chapter II Sasaki (1970, c) has shown the weak constraint variational formulation to be the proper NVA formulation when the relationship linking the variables is not precisely known or is at best only an approximation or an empirical rule. He demonstrated the applicability of the analysis method by applying the empirical rule that certain meteorological systems move approximately with a prespecified velocity to reveal features of a severe storm gust. In this study the weak constraint formulation is adopted for developing the analysis model since it is necessary that the constraint equations 3.3-3.7 be approximated as noted below.

The formulations of the functionals for the two NVA problems assume the form:

$$I = \iint\limits_{t\,S} \left\{ \tilde{\alpha}_1 (\pi - \tilde{\pi})^2 + \tilde{\alpha}_2 \left[(u - \hat{u})^2 + (v - \tilde{v})^2 \right] + \alpha \left[D_1^2 + D_2^2 \right] \right\} dS\, dt \qquad (3.9)$$

here S signifies area and

$$I = \iint\limits_{t\,V}\Big\{\tilde{\alpha}_1(\phi-\tilde{\phi})^2+\tilde{\alpha}_2(\theta-\tilde{\theta})^2+\alpha_3(q-\tilde{q})^2+\tilde{\alpha}_4\left[(u-\tilde{u})^2+(v-\tilde{v})^2\right] \tag{3.10}$$

$$+\alpha_1 D_1^2+\alpha_2 D_2^2+\alpha_3 D_3^2+\alpha_4\left[D_4^2+D_5^2\right]\Big\}\,dV\,dt$$

In 3.9 the variables to be solved for to minimize the functional, I, are the surface wind and pressure (represented by π). F_x and F_y in D_4 and D_5 in 3.9 are approximated by 2.9 and 2.10 respectively. These are reasonable formulations in light of recent experimental results cited earlier specifying the drag coefficient. D_4 and D_5 are further approximated by presetting the horizontal advection terms. Thus these terms are not varied and $V\cdot\nabla(u, v)$ become $\tilde{V}\cdot\nabla(\tilde{u}, \tilde{v})$, where the tilde indicates these terms have been approximated using initial unadjusted variables. As noted by Lewis (1972) this approximation results in simplification of the Euler equations and the guarantee of an elliptic differential equation system. Admittedly this approximation will produce less than satisfactory results where the initial unadjusted wind fields are poorly specified. Fortunately for the cases the model is to be applied to in this study the initial winds were well specified by the abundant IFYGL data. Also an iterative procedure, described below, was used to obtain improved estimates of these non-linear terms.

Following the formal procedure of the variational process outlined in Chapter II, the analysis equations resulting from 3.9 are:

$$\begin{aligned}\pi = \tilde{\pi} - \frac{\alpha}{\tilde{\alpha}_1}\Big\{ & c_p\theta\left(u_{tx} + \tilde{A}_x + c_p\tilde{\theta}_x\pi_x + c_p\tilde{\theta}\pi_{xx} - fv_x - (C_D|\tilde{V}|)_x u - C_D|\tilde{V}|u_x\right) \\ & + c_p\tilde{\theta}_x\left(u_t + \hat{A} + c_p\tilde{\theta}\pi_x - fv - C_D|\tilde{V}|u\right) \\ & + c_p\tilde{\theta}\left(v_{ty} + \tilde{B}_y + c_p\tilde{\theta}_y\pi_y + c_p\tilde{\theta}\pi_{yy} + fu_y - (C_D|\tilde{V}|)_y v - C_D|\tilde{V}|v_y\right) \\ & + c_p\tilde{\theta}_y\left(v_t + \tilde{B} + c_p\tilde{\theta}\pi_y + fu - C_D|\tilde{V}|v\right)\Big\}\end{aligned} \tag{3.11}$$

$$\begin{aligned}u = \tilde{u} - \frac{\alpha}{\tilde{\alpha}_2}\Big\{ & u_{tt} + \tilde{A}_t + c_p\tilde{\theta}_t\pi_x + c_p\hat{\theta}\pi_{xt} - fv_t - (C_D|\tilde{V}|)_t u - C_D|\tilde{V}|u_t \\ & + C_D|\tilde{V}|\left[u_t + \tilde{A} + c_p\tilde{\theta}\pi_x - fv - C_D|\tilde{V}|u\right] \\ & - f\left[v_t + \hat{B} + c_p\tilde{\theta}\hat{\pi}_y + fu - C_D|\tilde{V}|v\right]\Big\}\end{aligned} \tag{3.12}$$

$$v = \tilde{v} - \frac{\alpha}{\tilde{\alpha}_2}\Big\{ v_{tt} + \tilde{B}_t + c_p\tilde{\Theta}_t\pi_y + c_p\tilde{\Theta}\pi_{yy} + fu_t - (c_D|\tilde{V}|_t v - c_D|\tilde{V}|v_t \tag{3.13}$$

$$+ c_D|\tilde{V}|\left[v_t + \tilde{B} + c_D\tilde{\Theta}\pi_y + fu - c_D|\tilde{V}|v\right]$$

$$+ f\left[u_t + \tilde{A} + c_p\tilde{\Theta}\pi_x - fv - c_D|\tilde{V}|u\right]\Big\}$$

where $$(\tilde{A},\tilde{B}) = \tilde{V}\cdot\nabla(\tilde{u},\tilde{v}) + (\phi_x,\phi_y)$$

and where subscripts x, y, and t denote the partial derivative operator for the respective dimensions.

In the second NVA problem, posed by the functional in 3.10, a solution is sought for the three dimensional structure of the geopotential height, potential temperature, moisture and the two components of the wind. In D_2, the heating rate is specified as having a sensible and latent heat component

$$Q = Q_S + Q_L \tag{3.14}$$

that are parameterized

$$Q_s = K_H \frac{\tilde{\rho}^2 g^2}{\Delta P^2}\frac{\partial^2\tilde{\Theta}}{\partial\sigma^2} \tag{3.15}$$

and

$$Q_L = -\dot{\sigma} L \frac{\partial\tilde{q}_s}{\partial\sigma} \tag{3.16}$$

Q_s represents the vertical diffusion of sensible heat and Q_L is the latent heat made available when saturated ascent occurs. Rao (1971) included a Q_L of this form and found that vertical ascent rates were increased by as much as 60%.

In D_3, the rate of specific humidity generation is given by

$$S = K_q \frac{\tilde{\rho}^2 g^2}{\Delta P^2} \frac{\partial^2 \tilde{q}}{\partial \sigma^2} \qquad (3.17)$$

Tilde over the variable indicates these terms are evaluated using the initial unadjusted fields. K_H and K_q denote the eddy exchange coefficients for sensible heat and water vapor and here are assumed equal and invariant with height. Experimental evidence presented by Roll (1965) indicates that the difference between K_H and K_q is quite small. Roll also provides profiles of K_q over the sea for various atmospheric stabilities with the range of K_q from strong stability to very strong instability being 10^3 to $5x10^5$ cm^2 s^{-1}. For very strong instability K_q varied from 5 to $1x10^5$ cm^2 s^{-1} for a range of height of 200 to 5000 meters. In this study a stability dependent formulation for K_H and K_q, introduced by Asai (1965) in a theoretical study of air-mass modification over the Sea of Japan, is adopted.

$$K_H = \frac{K^*}{\left[1 + \gamma\left(-\frac{\tilde{\rho} g}{\Delta p}\frac{\partial \tilde{\theta}}{\partial \sigma}\right)\right]} \qquad (3.18)$$

where $K^* = 10^5 \text{ cm}^2 \text{ s}^{-1}$

$\gamma = 10^4 \text{ cm } {}^{o}\text{C}^{-1}$

This formulation implies that K_H increases with decreasing stability and decreases with increasing stability, while K* is the exchange coefficient which might be expected under adiabatic conditions. For the range of stabilities (weak to strong instability) and the resolution of scale considered in this study Asai's formulation seems quite appropriate.

In D_4 and D_5 frictional terms are specified as

$$F_x = -K_M \frac{\tilde{\rho}^2 g^2}{\Delta p^2}\frac{\partial^2 \tilde{u}}{\partial \sigma^2} \qquad (3.19)$$

$$F_y = -K_M \frac{\tilde{\rho}^2 g^2}{\Delta p^2}\frac{\partial^2 \tilde{v}}{\partial \sigma^2} \qquad (3.20)$$

Again, these terms are evaluated using initial unadjusted fields. K_M, the exchange coefficient for momentum, is set at 10^4 cm^2 s^{-1}. This value was chosen principally because it has been used in other numerical models designed to simulate mesoscale phenomena (Rao, 1971; Sasaki and Lewis, 1970). K_M was not set equal to K_H, even though this assumption is frequently made, since experimental evidence presented by Lumley and Panofsky (1964) indicate the ratio K_H/K_M, near unity in neutral air, increases with decreasing stability. This is physically understandable since the momentum exchange is influenced by pressure forces on eddies while the heat exchange is affected by buoyancy processes.

Boundary conditions at the surface formulated to account for heat, water vapor and momentum fluxes are,

$$F_H = \tilde{\rho} c_p C_H |\tilde{v}| (T_L - T_A) \tag{3.21}$$

$$F_q = \tilde{\rho} C_E |\tilde{v}| (q_L - q_A) \tag{3.22}$$

$$F_x = \hat{\rho} C_D |\tilde{v}| \tilde{u} \tag{3.23}$$

$$F_y = \hat{\rho} C_D |\hat{v}| \tilde{v} \tag{3.24}$$

where T_L, q_L denote lake surface temperature and saturation specific humidity corresponding to the surface water temperature, T_A, q_A, u and v denote the temperature of the air, specific humidity and wind components at 3 meters, and C_H and C_E are transfer coefficients and C_D the drag coefficient. 3.21-3.24 are known as the bulk transfer equations (Roll, 1965). Determination of the transfer coefficients have been the objective of numerous studies (e.g. Kondo, 1975; Pond et al., 1971). Generally experimental results show all three coefficients to be very nearly equal, with some indications that C_H and C_E may be somewhat smaller than C_D although this is still open to question. Here C_H and C_E are assumed equal to C_D over water with C_D assigned the values of $1.5\text{x}10^{-3}$ over water and $1.8\text{x}10^{-3}$ over land (see Chapter II).

Again following the formal procedure of the variational process the analysis equations resulting from 3.10 are:

$$\phi = \tilde{\phi} - \frac{\alpha_1}{\tilde{\alpha}_1}\left\{\phi_{\sigma\sigma} + c_p(\theta\hat{\pi}_{\sigma\sigma} + \theta_\sigma \hat{\pi}_\sigma)\right\} - \frac{\alpha}{\tilde{\alpha}}\left\{u_{tx} + \tilde{A}_x + \phi_{xx}\right. \tag{3.25}$$

$$\left. + c_p\theta_x\pi_x + c_p\theta\hat{\pi}_{xx} - fv_x + \tilde{\rho}^2 g^2 K_M \frac{1}{\Delta P^2}\tilde{u}_{\sigma\sigma x}\right\}$$

$$- \frac{\alpha_5}{\tilde{\alpha}_1}\left\{v_{ty} + \tilde{B}_y + \phi_{yy} + c_p\theta_y\pi_y + c_p\theta\hat{\pi}_{yy} + fu_y + \tilde{\rho}^2 g^2 K_M \frac{1}{\Delta P^2}\tilde{v}_{\sigma\sigma y}\right\}$$

$$\begin{aligned}\Theta = \tilde{\Theta} &+ \frac{\alpha_1}{\tilde{\alpha}_2} c_p \pi_\sigma \left\{ \phi_\sigma + c_p \Theta \pi_\sigma \right\} - \frac{\alpha_2}{\tilde{\alpha}_2} \left\{ \Theta_{tt} + \tilde{C}_t - \frac{1}{c_p} \left(\frac{\tilde{Q}}{\pi} \right)_t \right\} \\ &+ \frac{\alpha_4}{\tilde{\alpha}_2} c_p \pi_x \left\{ u_t + \tilde{A} + \phi_x + c_p \Theta \pi_x - f v + \tilde{\rho}^2 g^2 K_M \frac{1}{\Delta P^2} \tilde{u}_{\sigma\sigma} \right\} \\ &+ \frac{\alpha_5}{\tilde{\alpha}_2} c_p \pi_y \left\{ v_t + \tilde{B} + \phi_y + c_p \Theta \pi_y + f u + \tilde{\rho}^2 g^2 K_M \frac{1}{\Delta P^2} \tilde{v}_{\sigma\sigma} \right\}\end{aligned} \tag{3.26}$$

$$q = \tilde{q} - \frac{\alpha_3}{\tilde{\alpha}_3} \left\{ q_{tt} + \tilde{D}_t - \tilde{S}_t \right\} \tag{3.27}$$

$$\begin{aligned}u = \tilde{u} &- \frac{\alpha_4}{\tilde{\alpha}_4} \left\{ u_{tt} + \tilde{A}_t + \phi_{xt} + c_p \Theta_t \pi_x + c_p \Theta \pi_{xt} - f v_t \right. \\ &\qquad \left. + \tilde{\rho}^2 g^2 K_M \frac{1}{\Delta P^2} \tilde{u}_{\sigma\sigma t} \right\} \\ &+ \frac{\alpha_4}{\tilde{\alpha}_4} f \left\{ v_t + \tilde{B} + \phi_y + c_p \Theta \pi_y + f u + \tilde{\rho}^2 g^2 K_M \frac{1}{\Delta P^2} \tilde{v}_{\sigma\sigma} \right\}\end{aligned} \tag{3.28}$$

$$v = \tilde{v} - \frac{\alpha_4}{\tilde{\alpha}_4}\Big\{v_{tt} + \tilde{B}_t + \phi_{yt} + c_p\Theta_t\pi_y + c_p\Theta\pi_{yt} + fu_t + \tilde{\rho}^2 g^2 K_M \frac{1}{\Delta P^2}\tilde{v}_{\sigma\sigma t}\Big\} - \frac{\alpha_4}{\tilde{\alpha}_4} f\Big\{u_t + \hat{A} + \phi_x + c_p\Theta\pi_x - fv + \tilde{\rho}^2 g^2 K_M \frac{1}{\Delta P^2}\hat{u}_{\sigma\sigma}\Big\} \tag{3.29}$$

where

$$(\tilde{A},\tilde{B},\tilde{C},\tilde{D}) = \hat{u}(\tilde{u},\tilde{v},\tilde{\theta},\tilde{q})_x + \tilde{v}(\tilde{u},\hat{v},\tilde{\theta},\hat{q})_y + \dot{\sigma}(\tilde{u},\tilde{v},\hat{\theta},\hat{q})_\sigma$$

GRID DOMAIN, VERTICAL AND HORIZONTAL RESOLUTION, AND TOPOGRAPHY

The analysis equations 3.11-3.13, and 3.25-3.29, are applied over the area depicted in Fig. 2. Surface fluxes of sensible heat and moisture are calculated for only those grid points representing Lake Ontario. Over land these fluxes are considered negligible. Mesh distance is constant at 10.77 km and hence is capable of depicting scales as small as 20 km. Thus no attempt is made to depict individual convective cells. This is consistent with the use of the hydrostatic assumption, 3.5. The Coriolis parameter varies inconsequently over the area and for this study is chosen as noted above (see Chapter II).

Surface topography (Fig. 2) was obtained by filtering grid-point elevations taken from a detailed topographic chart. The filtering process suppressed all wavelengths of two grid increments and decreasingly damped larger wavelengths. This had the effect of specifying the topography in a manner reasonably consistent with the scale of atmospheric motions being studied.

Lavoie et al. (1970) through a series of experiments found that for studying the lake-effect phenomenon 500 mb was a sufficiently high model upper-level. They found that changing the upper-level from 200 mb to 500 mb resulted in no important changes in the flow over the lake. This result seems reasonable since observational evidence indicates the lake effect seldom extends above 700 mb. Also, between 500 mb and the surface they found that 10 prediction levels yield solutions within a few percent of solutions obtained with 20 levels. For these reasons, in this study the analysis equations 3.25-3.29 are solved on the eleven surfaces extending from the surface to 500 mb depicted in Fig. 15.

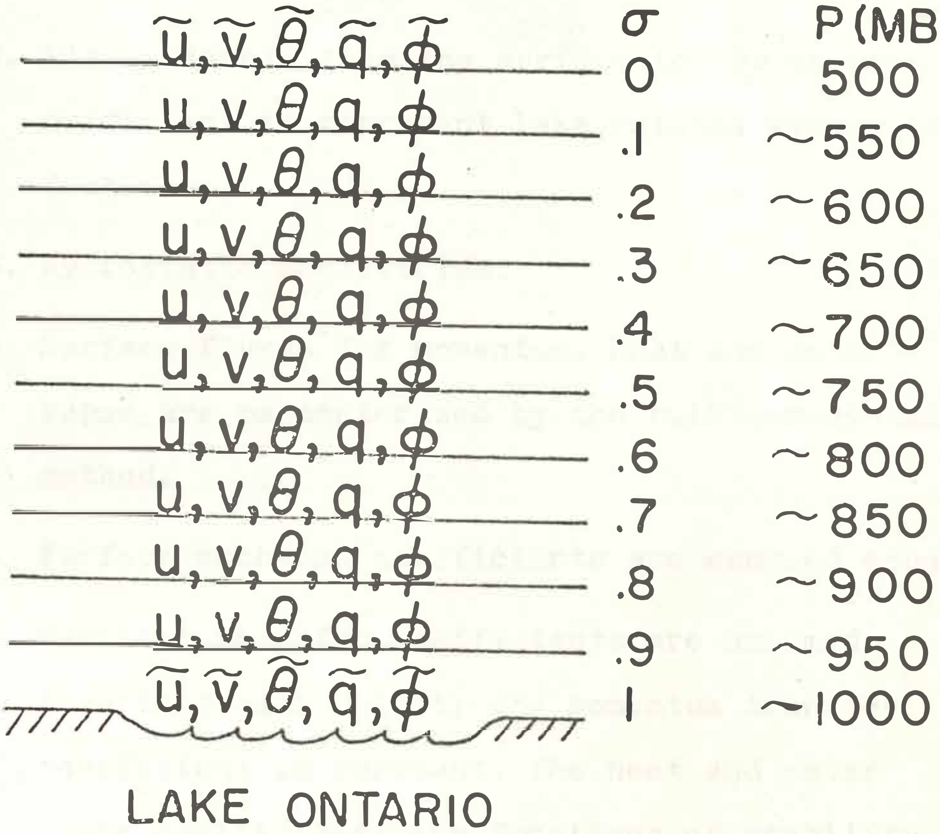

Fig. 15. Terrain or σ-coordinate surfaces used in NVA model. Variables undergoing NVA adjustment at each level are shown (tilde indicates fixed boundary values).

MAJOR MODELLING ASSUMPTIONS

1. Horizontal advection, source and sink terms in the constraint equations are approximated by the initial unadjusted fields.
2. Eleven levels from the surface to 500 mb are sufficient to represent lake related mesoscale features.
3. Hydrostatic equilibrium.
4. Surface fluxes for momentum, heat and water vapor are parameterized by the bulk aerodynamic method.
5. Surface exchange coefficients are assumed equal.
6. Vertical transfer coefficients are assumed invariant with height; the momentum transfer coefficient is constant, the heat and water vapor coefficients are functions of stability.

Small scale features such as the lake breeze cannot be adequately represented by the analysis model described here. Finer vertical resolution, especially in the lower layers and inclusion of more sophisticated representations for surface fluxes and vertical eddy diffusion are refinements necessary to make the model more general. However, assumptions 2-6 are believed reasonable for a model intended to represent the mesoscale phenomenon related to the cool season lake effect. In fact Lavoie (1968) was able to simulate some of the gross features of the winter lake-effect phenomenon with a numerical model that incorporated physical assumptions much more restrictive than those applied here.

Assumption 1 is necessary in order to make the NVA scheme mathematically tractable and is justified on the basis of the excellent IFYGL observations. If the NVA fields are thought of as adjustments to the initial fields then this assumption has the effect of neglecting these adjustments in the calculation of the horizontal advection, source and sink terms. Thus the model described here is restricted in its application to those cases where the initial approximation of these terms is reasonably well specified. The error caused by neglecting the contribution to these terms by the adjustments is considered to be of low order. Also, in this study an iterative procedure has been introduced to help ameliorate the effects of assumption 1. In step 1 of the procedure the Euler equations are solved to obtain a new estimate of the dependent variables that differ from the initial unadjusted values. These new values are then used to re-estimate the horizontal advection, source and sink terms and a new solution to the Euler equations is sought. This recycling procedure is carried out until two successive solutions differ insignificantly. Effectively, several sets of linear equations are solved to obtain the approximate solution to the non-linear system. Although no formal proof of convergence of the system is offered, for the cases described in the following Chapter, convergence occurred after a small number of iterations. Remson et al. (1971, pp. 336) provide an example of one possible way to treat a non-linear variational problem by using an iterative process similar in many respects to the above procedure.

TECHNIQUE OF SOLUTION

For clarity 3.11-3.13 may be rewritten

$$\frac{\tilde{\alpha}_1}{\alpha}\pi - c_p^2\left[2\tilde{\theta}(\tilde{\theta}_x\pi_x + \tilde{\theta}_y\pi_y) + \tilde{\theta}^2\nabla^2\pi\right] = \frac{\tilde{\alpha}_1}{\alpha}F_1 + G_1 \qquad (3.30)$$

where $$F_1 = \tilde{\pi} + \frac{\alpha}{\tilde{\alpha}_1}\left\{ c_p\tilde{\Theta}\tilde{A}_x + c_p\tilde{\Theta}\tilde{B}_y + c_p\tilde{\Theta}_x\tilde{A} + c_p\tilde{\Theta}_y\tilde{B} + c_p\left[\tilde{\Theta}(u_{tx} + v_{ty}) + \tilde{\Theta}_x u_t + \tilde{\Theta}_y v_t\right]\right\}$$

$$G_1 = c_p\left(\tilde{\Theta}\left[-f(v_x - u_y) - k(u_x + v_y) - u k_x - v k_y\right] + \tilde{\Theta}_x(-fv - ku) + \tilde{\Theta}_y(ku - kv)\right\}$$

$$\frac{\tilde{\alpha}_2}{\alpha}u - u_{tt} + u(f^2 + k^2 + k_t) = \frac{\tilde{\alpha}_2}{\alpha}F_2 + G_2 \qquad (3.31)$$

where $$F_2 = \tilde{u} + \frac{\alpha}{\tilde{\alpha}_2}\left\{\tilde{A}_t + k\tilde{A} + f(-\tilde{B} - 2v_t) + c_p\tilde{\Theta}\tilde{\pi}_{xt}\right\}$$

$$G_2 = c_p(\tilde{\Theta}_t\pi_x + k\tilde{\Theta}\pi_x - f\tilde{\Theta}\pi_y)$$

$$\frac{\tilde{\alpha}_2}{\alpha}v - v_{tt} + v(f^2 + k^2 + k_t) = \frac{\tilde{\alpha}_2}{\alpha}F_3 + G_3 \qquad (3.32)$$

where $$F_3 = \tilde{v} + \frac{\alpha}{\tilde{\alpha}_2}\left\{\tilde{B}_t + k\tilde{B} + f(\tilde{A} + 2u_t) + c_p\tilde{\Theta}\pi_{yt}\right\}$$

$$G_3 = c_p(\Theta_t\pi_y + k\tilde{\Theta}\pi_y + f\tilde{\Theta}\pi_x)$$

In each of these equations the dependent variables have been moved to the left side with known or constant quantities on the right side. ∇^2 denotes the two dimensional Laplacian operator and for convenience $C_D|\tilde{V}|$ has been replaced by the letter k.

With the observational and dynamical weights specified, finite difference analogs of 3.30-3.32 may be solved by the iterative accelerated Liebmann relaxation technique. Tendency terms are evaluated using hourly distributions of the variables calculated by the successive corrections method, e.g., an analysis at $t = 0$ uses tendencies from $t = -1$ to $t = +1$ hr. Table 2 specifies the mean differences used to compute observational weights. If the constraint equations are scaled using scaling parameters characteristic of mesoscale systems (Hart, 1967) then the tendency, horizontal advection, pressure gradient and Coriolis terms are found to be of the same order of magnitude, 0.1 cm s^{-2}. Thus, the dynamical weight is calculated using $\mu^{\frac{1}{2}} = 0.1$ cm s^{-2}. Two sets of observational weights were employed to express the varying confidence in the initial interpolated fields. All grid-points within a radius of one mesh distance from an observation were assigned the larger weight (designated "Observations" in Table 2) while those grid-points outside this distance were considered less reliable and were accordingly assigned a lower weight (designated "No Observations" in Table 2).

Table 2

Mean Differences Used to Compute Observational Weights for Surface Adjustment of Wind and Pressure

	Observations	No Observations
Pressure (mb)	.1	5.0
Wind Components (cm s^{-1})	50	250

The analysis equations for the upper air NVA, 3.25-3.29, are written:

$$\phi - \frac{\alpha_1}{\tilde{\alpha}_1}\phi_{\sigma\sigma} - \frac{\alpha_1}{\tilde{\alpha}_1}K_1 - \frac{\alpha_4}{\tilde{\alpha}_1}K_2 - \frac{\alpha_4}{\tilde{\alpha}_1}\nabla^2\phi = \tilde{\phi} + \frac{\alpha_4}{\tilde{\alpha}_1}K_3 \qquad (3.33)$$

where

$$K_1 = c_p(\theta\pi_{\sigma\sigma} + \theta_\sigma\pi_\sigma)$$

$$K_2 = u_{tx} + v_{ty} + c_p(\theta_x\pi_x + \theta\pi_{xx} + \theta_y\pi_y + \theta\pi_{yy}) + f(u_y - v_x)$$

$$K_3 = \hat{A}_x + \tilde{B}_y + \tilde{\rho}^2 g^2 K_M \frac{1}{\Delta P^2}(\tilde{u}_{\sigma\sigma x} + \hat{v}_{\sigma\sigma y})$$

$$\theta + \frac{\alpha_1}{\tilde{\alpha}_2}c_p^2\pi_\sigma^2\theta - \frac{\alpha_2}{\tilde{\alpha}_2}\theta_{tt} + \frac{\alpha_4}{\tilde{\alpha}_2}c_p^2(\pi_x^2\theta + \pi_y^2\theta) = \qquad (3.34)$$

$$\tilde{\theta} + \frac{\alpha_2}{\tilde{\alpha}_2}K_4 - \frac{\alpha_4}{\tilde{\alpha}_2}K_5 - \frac{\alpha_1}{\tilde{\alpha}_2}K_6 - \frac{\alpha_4}{\tilde{\alpha}_2}K_7$$

where

$$K_4 = \tilde{C}_t - \frac{1}{c_p}\left(\frac{\tilde{Q}}{\pi}\right)_t$$

$$K_5 = c_p\left(\pi_x\hat{A} + \pi_y\tilde{B} + \tilde{\rho}^2 g^2 K_M \frac{1}{\Delta P^2}(\pi_x\tilde{u}_{\sigma\sigma} + \pi_y\tilde{v}_{\sigma\sigma})\right)$$

$$K_6 = c_p\pi_\sigma\phi_\sigma$$

$$K_7 = c_p\left(\pi_x[u_t + \phi_x - fv] + \pi_y[v_t + \phi_y + fu]\right)$$

$$q - \frac{\alpha_3}{\tilde{\alpha}_3}\{q_{tt}\} = \tilde{q} + \frac{\alpha_3}{\tilde{\alpha}_3}(\tilde{D}_t - \tilde{S}_t) \qquad (3.35)$$

$$u - \frac{\alpha_4}{\tilde{\alpha}_4} u_{tt} - \frac{\alpha_4}{\tilde{\alpha}_4} K_8 + \frac{\alpha_4}{\tilde{\alpha}_4} K_9 = \tilde{u} + \frac{\alpha_4}{\tilde{\alpha}_4} K_{10} \qquad (3.36)$$

where

$$K_8 = c_p(\theta_t \hat{\pi}_x + \theta \hat{\pi}_{xt}) - f v_t$$

$$K_9 = f(v_t + \phi_y + c_p \theta \hat{\pi}_y + f u)$$

$$K_{10} = \tilde{A}_t + \phi_{xt} + \tilde{\rho}^2 g^2 K_M \frac{1}{\Delta P^2} \tilde{u}_{\sigma\sigma t} - f\left(\tilde{B} + \tilde{\rho}^2 g^2 K_M \frac{1}{\Delta P^2} \tilde{v}_{\sigma\sigma}\right)$$

$$v - \frac{\alpha_4}{\tilde{\alpha}_4} v_{tt} - \frac{\alpha_4}{\tilde{\alpha}_4} K_{11} - \frac{\alpha_4}{\tilde{\alpha}_4} K_{12} = \tilde{v} + \frac{\alpha_4}{\tilde{\alpha}_4} K_{13} \qquad (3.37)$$

where

$$K_{11} = c_p(\theta_t \hat{\pi}_y + \theta \hat{\pi}_{yt}) + f u_t$$

$$K_{12} = f(u_t + \phi_x + c_p \theta \hat{\pi}_x - f v)$$

$$K_{13} = \tilde{B}_t + \phi_{yt} + \tilde{\rho}^2 g^2 K_M \frac{1}{\Delta P^2} \tilde{v}_{\sigma\sigma t} + f\left(\tilde{A} + \tilde{\rho}^2 g^2 K_M \frac{1}{\Delta P^2} \tilde{u}_{\sigma\sigma}\right)$$

The observational weights assigned in this problem are given in Table 3 below.

Table 3

Mean Differences Used to Compute Observational Weights for Upper Air Adjustment

	Observations	No Observations
Geopotential Height (cm)	10^3	$5\text{x}10^3$
Potential Temperature (^{o}C)	.5	2
Specific Humidity (g kg^{-1})	.5	2
Wind Components (cm s^{-1})	$2.5\text{x}10^2$	$2.5\text{x}10^2$

Dynamical weights $\alpha_1 - \alpha_4$ of 3.10 are computed respectively from:

$$\mu_1^{\frac{1}{2}} = 4.9\text{x}10^8 \text{ cm}^2 \text{ s}^{-2}$$

$$\mu_2^{\frac{1}{2}} = 1.0\text{x}10^{-3} \ ^o\text{C s}^{-1}$$

$$\mu_3^{\frac{1}{2}} = 1.0\text{x}10^{-6} \text{ s}^{-1}$$

$$\mu_4^{\frac{1}{2}} = 5.0\text{x}10^{-1} \text{ cm s}^{-2}$$

As in the surface NVA problem, these weights were chosen to reflect the mesoscale motions associated with the lake-effect phenomenon.

The method followed to solve this set of equations is as follows:

(1) Initially the vertical velocity, $\dot{\sigma}$, is set equal to zero.

(2) Eq. 3.33 is solved for ϕ.

(3) Eqs. 3.34-3.37 are solved for θ, q, u and v.

(4) The vertical velocity equation, 3.8, is solved.

Tendency terms are evaluated using 3-hourly distributions derived from the rawinsondes at these times by the successive corrections method.

(5) Steps (1)-(4) are repeated until a solution is obtained.

(6) Using the newly calculated values of the parameters, the non-linear terms and source and sink terms, approximated originally by the initial parameter distributions are re-evaluated and steps (2)-(5) are repeated. In the applications to be discussed in Chapter IV it was found necessary to repeat this cyclic procedure only once since the solutions obtained after the second cycle did not vary significantly from those of the first.

In summary (1) a variational analysis model has been developed to study mesoscale lake-effect phenomena, (2) all processes thought to have a major role in these phenomena have been included in the model's equations of constraint, and (3) the procedure of analysis is specified as a two part NVA problem.

PREPARATION OF INITIAL INTERPOLATED FIELDS

In the following chapter the analysis model described in this chapter is utilized to describe the motion, temperature and moisture fields for two cases of cool season mesoscale phenomena related to Lake Ontario. Prior to discussing that part of this study it is necessary to explain briefly the procedure used to obtain the initial or observed fields, denoted by the tilde in the analysis equations 3.11-3.13 and 3.25-3.29.

As was noted earlier, it was necessary to perform an initial variational adjustment of surface wind and pressure, to obtain a surface pressure field consistent with the wind field and model constraints. After the surface pressure field was found, the σ surface pressures were determined through use of 3.1. It was then possible to interpolate the rawinsonde data, which had a vertical resolution of 10 mb, to the σ surfaces.

Knowledge of the precise location of the rawinsonde in its flight was necessary since the pressure of the surfaces varied in much the same manner as the surface pressure field.

Care had to be exercised in determining the initial fields on the σ surfaces from the interpolated observations. The successive corrections method was used for this purpose. This scheme does best when the surface that the interpolation is performed over is horizontal. Since this was not the case here, the scheme was applied in the following manner: all observations of a parameter at a particular time interpolated to a surface were averaged to obtain a mean or larger scale first approximation which was then modified using three scans through the data with successively smaller influence radii. In this procedure each observation was permitted to affect only a small area in its immediate vicinity and the difference between the final initial fields and interpolated observations was required to be small.

A special problem was encountered in obtaining the initial surface pressure fields. A first approximation constructed as the mean of the surface pressure observations would have been useless, since the surface pressure is a strong function of the terrain height. Here a mean lake-surface pressure was calculated using only over-lake observations. Then using the hypsometric formula, with a virtual temperature at each grid point, a first approximation surface pressure field for the area was calculated. Surface pressure observations were then employed as described above. Fig. 16 illustrates an initial surface pressure field arrived at by this method.

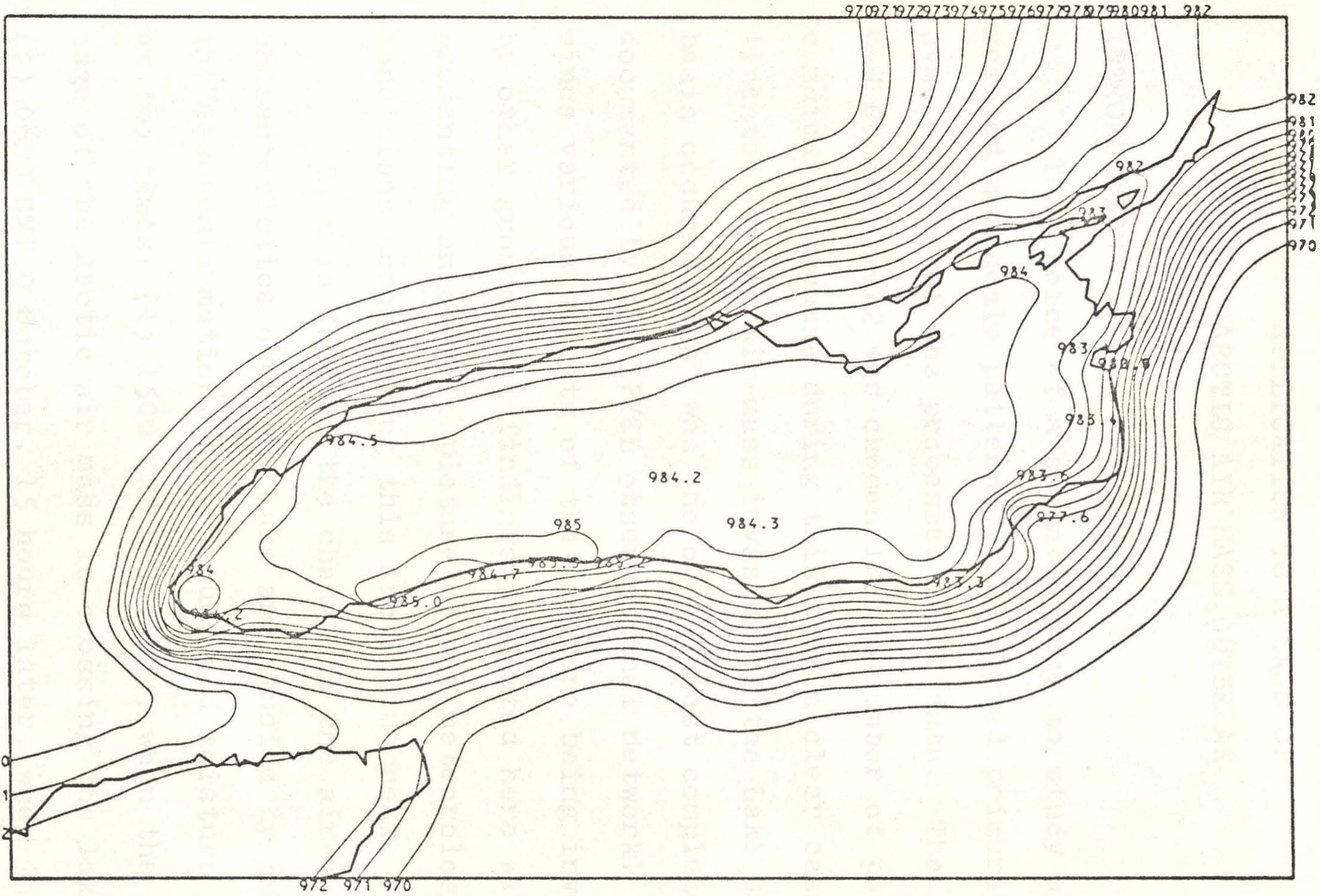

Fig. 16. Sample of initial interpolated surface pressure field (1500 GMT October 8, 1972). Surface pressure observations are superimposed. (The tight gradient west of Lake Ontario has caused the computer contouring program to erroneously overlap isobars).

CHAPTER IV

APPLICATION TO A CASE OF ARCTIC AIR-MASS OUTBREAK

INTRODUCTION

The choice of a suitable case to study winter lake related mesoscale patterns was dictated primarily by the availability of the processed IFYGL data. The period of 8-9 October 1972 was chosen from a number of possible candidates because during this time a clear case of continental Arctic air-mass invasion of the Lake Ontario basin occurred that was one of the most completely documented by the IFYGL observational network. Also, since various aspects of the case are being investigated by other groups, the findings presented here will aid in presenting an overall picture of the meteorological conditions accompanying this Arctic outbreak.

In this Chapter the change in the air-mass characteristics over the lake are studied by analyzing the mesoscale motion, temperature and moisture features at two times: (1) 1500 GMT 8 October, when the leading edge of the Arctic air mass is crossing the lake and (2) 0600 GMT 9 October, 15 hours later, when the air mass completely fills the Lake Ontario basin. The NVA model described in Chapter III is applied at these times to aid in obtaining the over-lake atmospheric structure. Subjective verification of results with radar and satellite data, contrasts in air-mass characteristics between the two times, physical processes and comparison of findings with other investigations are discussed. Furthermore a presentation and discussion of representative illustrations of the adjustment of the initial interpolated fields by the NVA procedure is contained in Appendix B.

MACROSCALE SITUATION

At 1500 GMT (1000 EST) 8 October 1972 the synoptic surface analysis of the National Weather Service showed the leading edge of a cold front positioned on the western edge of Lake Ontario (Fig. 17) and extending northward to a deep low (980 mb) east of James Bay. The center of the cold air mass was over the Canadian plains west of Lake Winnipeg. Upper air analyses, 3 hours before, at 1200 GMT, showed a 700 mb trough extending southwestward from the low center over James Bay with maximum winds from west-northwest reported at Flint, Michigan. Typically, at 500 mb the low center and trough were positioned westward of the 700 mb locations with a maximum wind of 100 knots from west-northwest reported at Green Bay (Figs. 18 and 19). By 1800 GMT

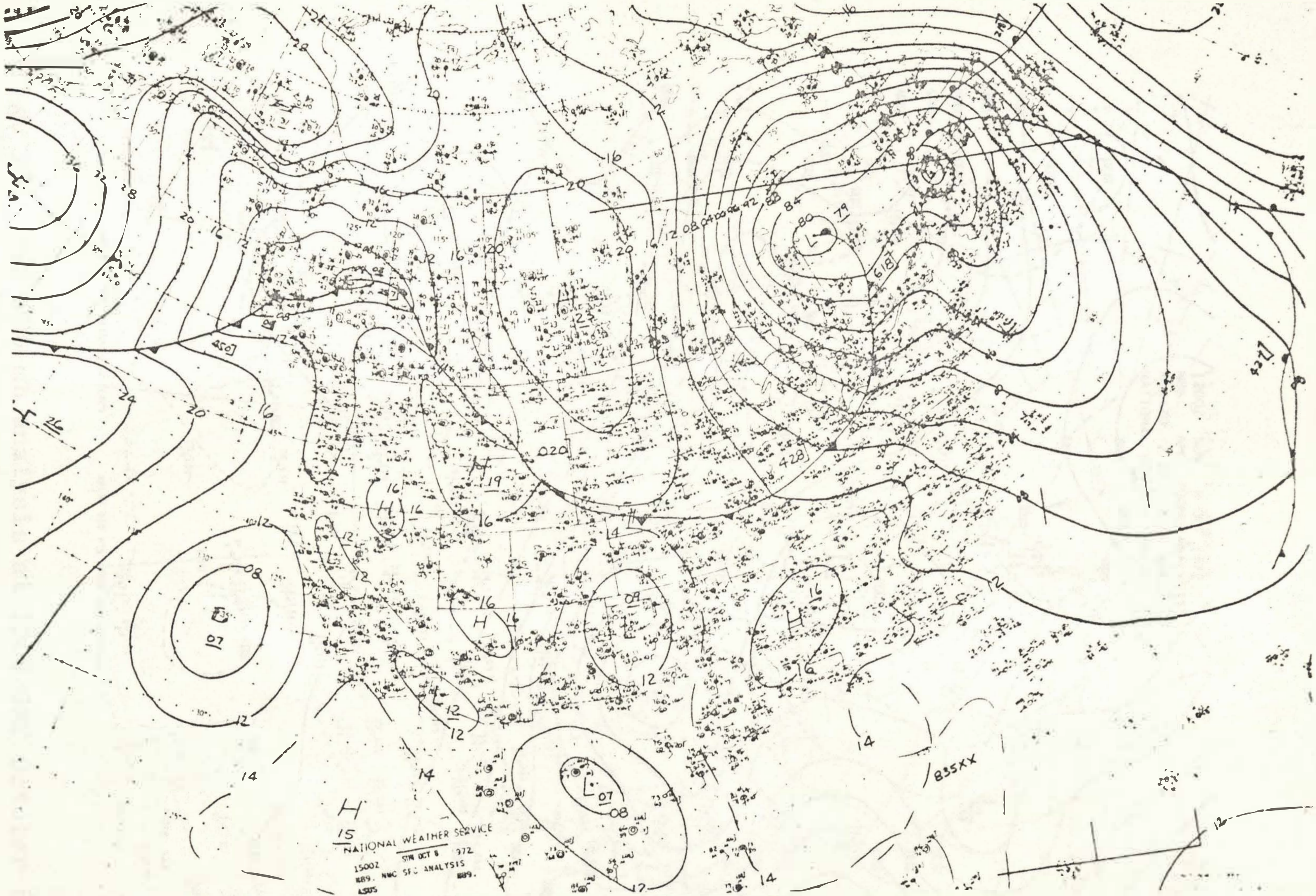

Fig. 17. National Weather Service (NWS) surface analysis at 1500 GMT October 8, 1972. Note cold front at western edge of Lake Ontario.

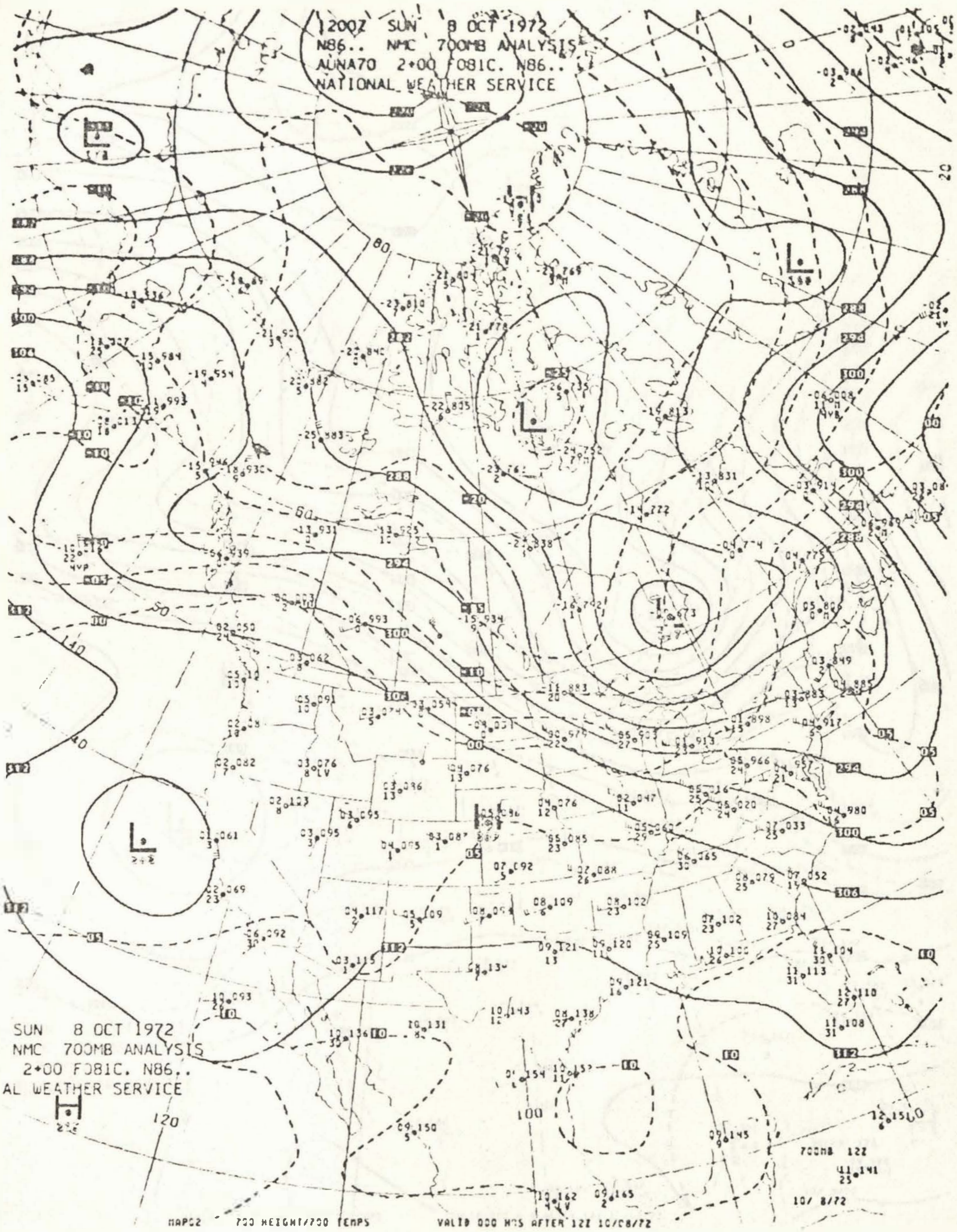

Fig. 18. NWS 700 mb analysis at 1200 GMT October 8, 1972.

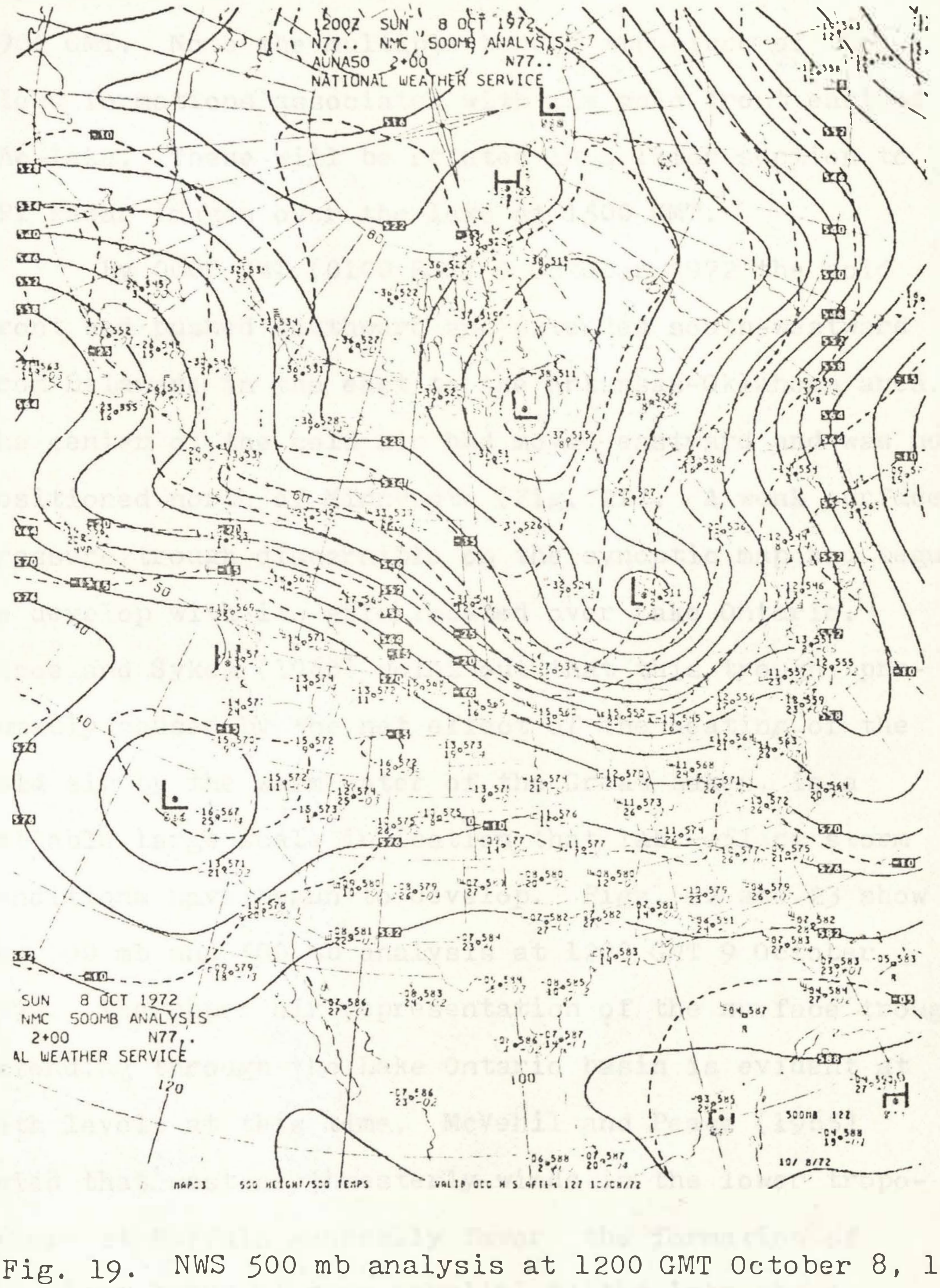

Fig. 19. NWS 500 mb analysis at 1200 GMT October 8, 1972.

the surface front had completely traversed the lake. Fig. 20 is a satellite photo taken from ESSA 9 at 1902 GMT. Note the multiple banded structure of the cloud formations associated with the cold front east of the lake. These will be related in a later section to PPI radar images over the lake at 1500 GMT.

By 0600 GMT (0100 EST) 9 October 1972 the cold front had pushed southward and extended south-westward from Delaware in the east to the Arkansas-Oklahoma area. The center of the cold air had moved eastward and was now positioned north of Minnesota (Fig. 21). A weak surface pressure trough discernible on the synoptic map had begun to develop with its axis located over Lake Ontario. Peace and Sykes (1966) point out that this trough, presumably caused by the net effect of the heating of the cold air by the warm water of the Great Lakes, is a reliable large scale indication that lake-effect storm conditions have begun to develop. Figs. 22 and 23 show the 700 mb and 500 mb analysis at 1200 GMT 9 October 1972. The upper air representation of the surface trough extending through the Lake Ontario basin is evident at both levels at this time. McVehil and Peace (1965) noted that west-northwesterly winds in the lower troposphere at Buffalo generally favor the formation of shoreline bands of snow parallel to the lake shore.

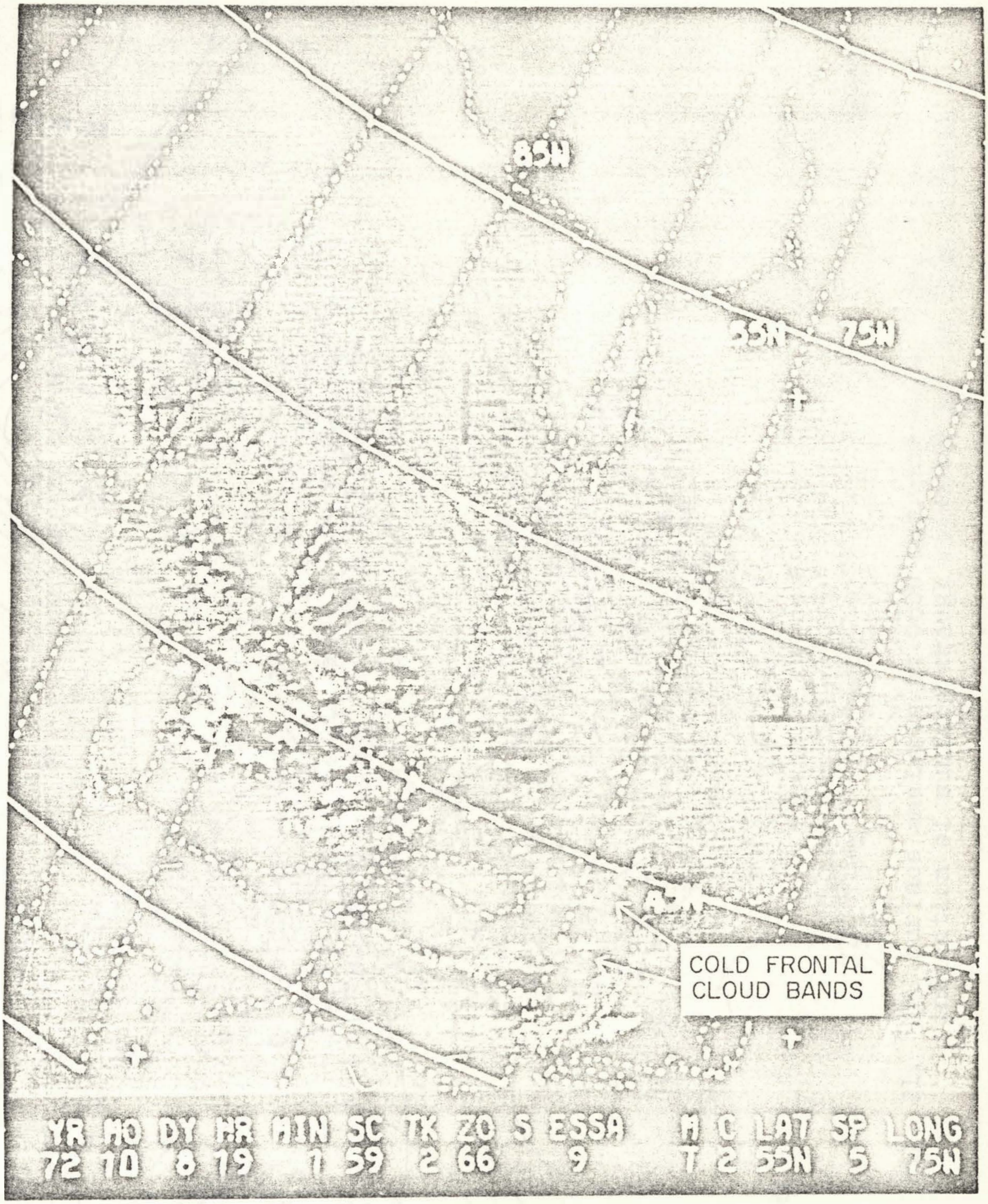

Fig. 20. ESSA 9 satellite photograph taken at 1902 GMT October 8, 1972. Cold front location east of Lake Ontario is depicted.

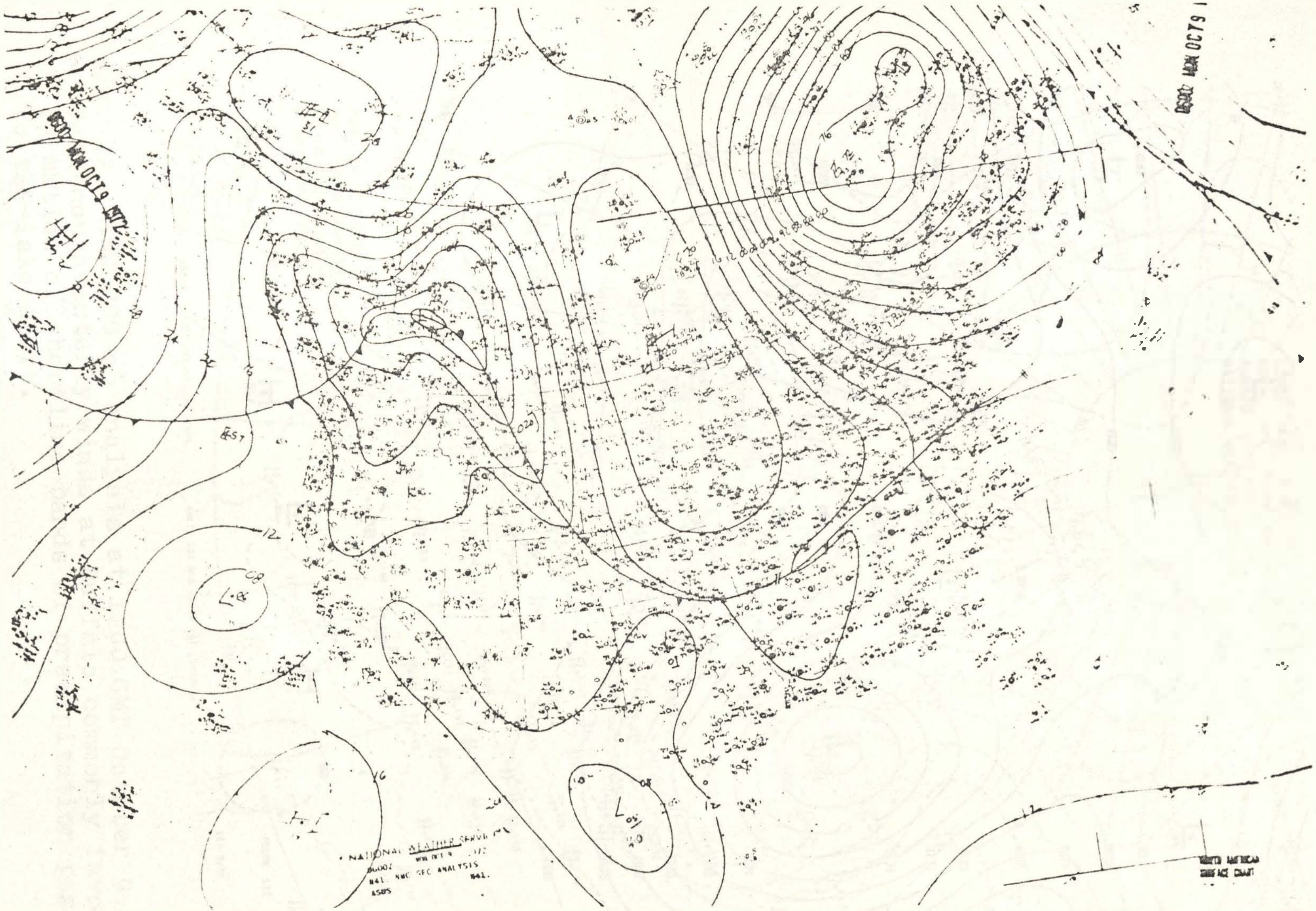

Fig. 21. NWS surface analysis at 0600 GMT October 9, 1972. Note indication of surface trough oriented across Lake Ontario.

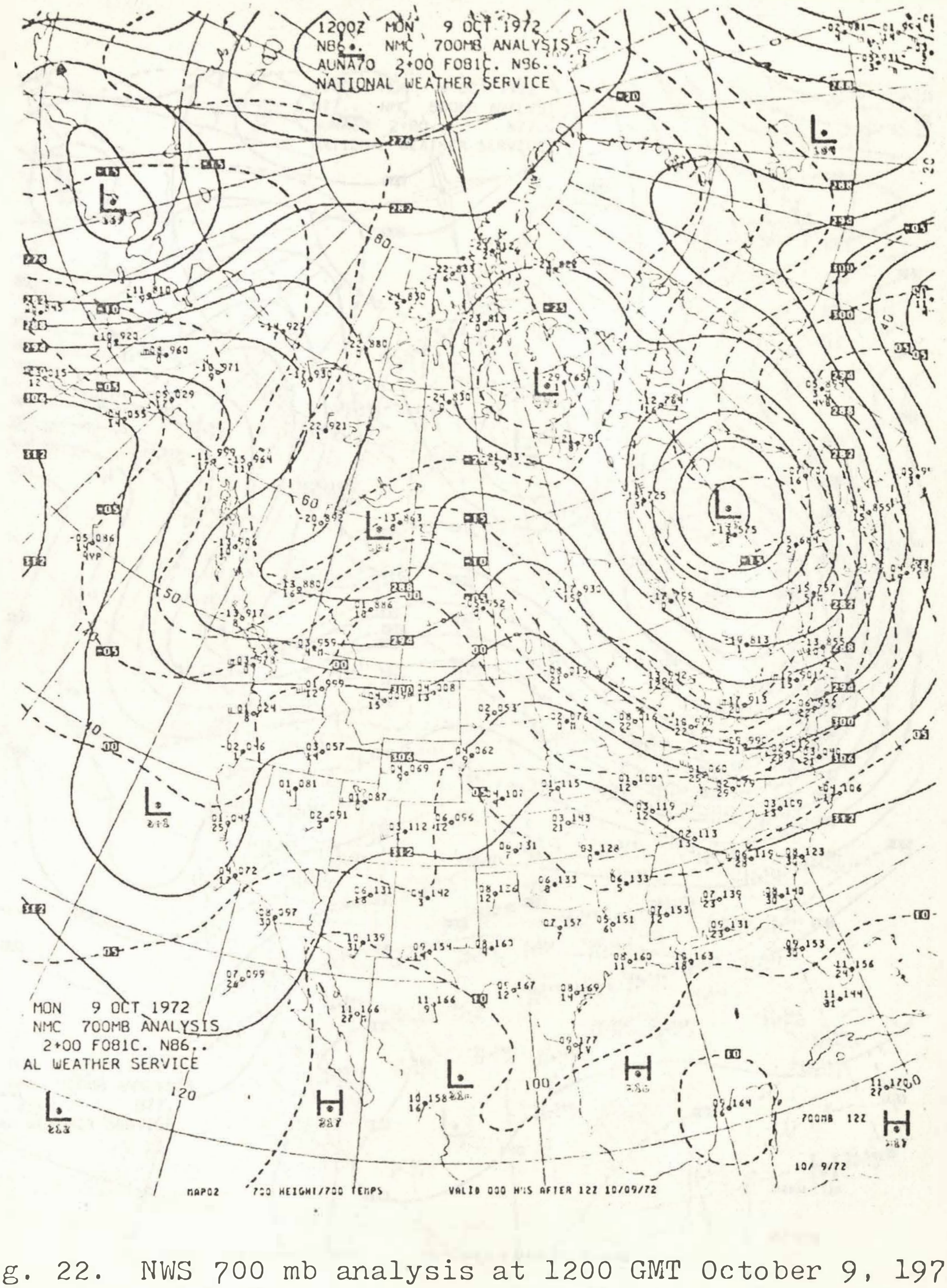

Fig. 22. NWS 700 mb analysis at 1200 GMT October 9, 1972. West-northwesterly winds at Buffalo commonly favors the formation of shoreline bands of precipitation parallel to the lake shore.

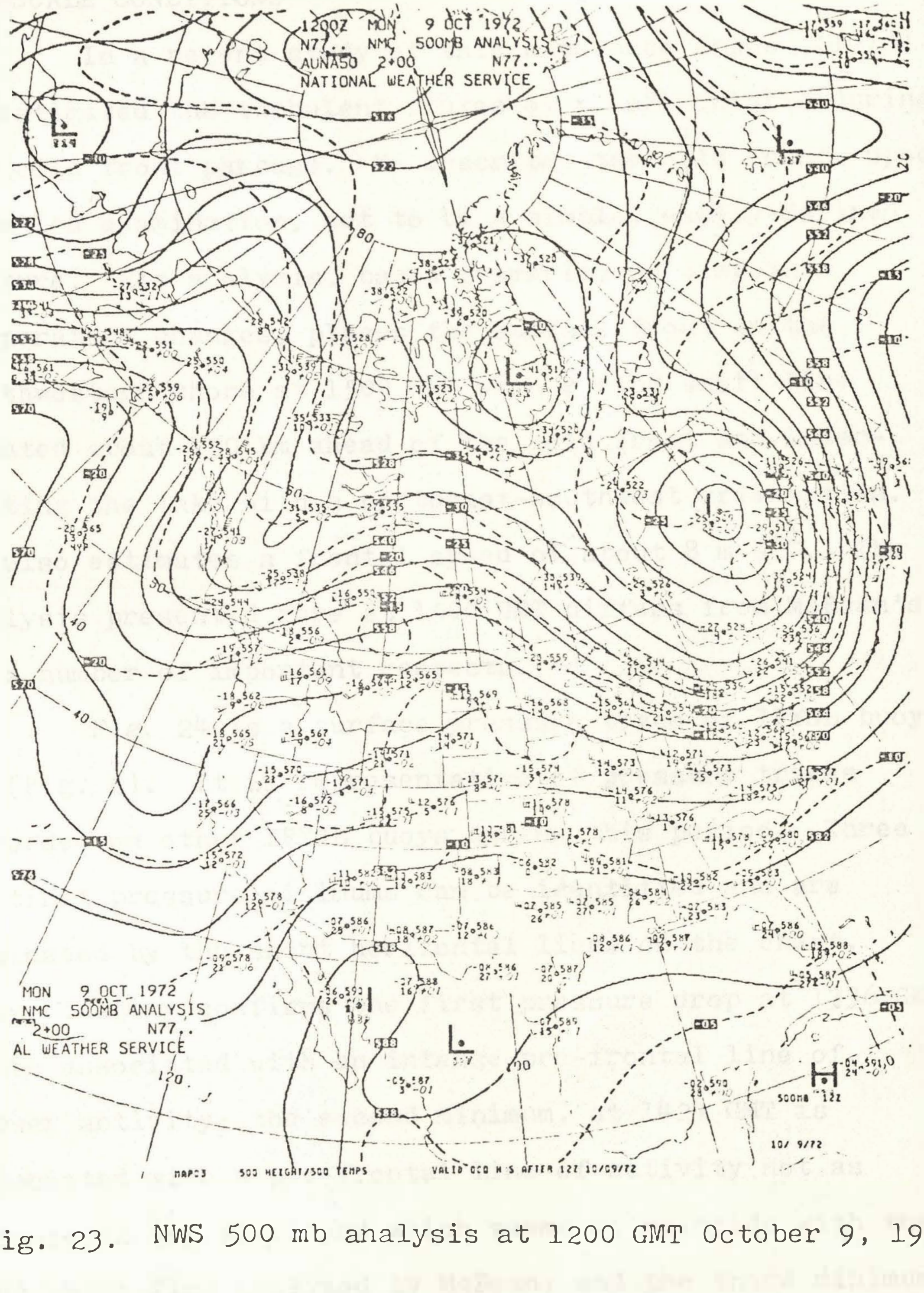

Fig. 23. NWS 500 mb analysis at 1200 GMT October 9, 1972.

MESOSCALE CONDITIONS

In a recent study of this same case McBean (1975) investigated the turbulent fluxes over Lake Ontario during the cold front passage. He describes the cold front, upon detailed examination, not to be a simple, easily-defined feature. His analysis, based primarily on dewpoint temperature changes, places the surface front on the northwestern shore at 1500 GMT with a wind shift line located about 130 km ahead of the cold front and intersecting the lake with a northeast-southwest orientation. He also estimates a frontal speed of about 8 m s^{-1}. The analysis presented here at 1500 GMT differs from McBean's in a number of important respects.

Fig. 24 is a surface pressure trace of IFYGL buoy 14 (Fig. 2). It is representative of pressure traces recorded on other IFYGL buoys during this period. Three distinct pressure minimums can be identified and are indicated by the short horizontal lines on the chart. Radar imagery confirms the first pressure drop at 1336 GMT to be associated with an intense pre-frontal line of shower activity; the second minimum, at 1424 GMT is associated with a pre-frontal line of activity not as intense as the first and which seems to coincide with the wind shift line analyzed by McBean; and the third minimum

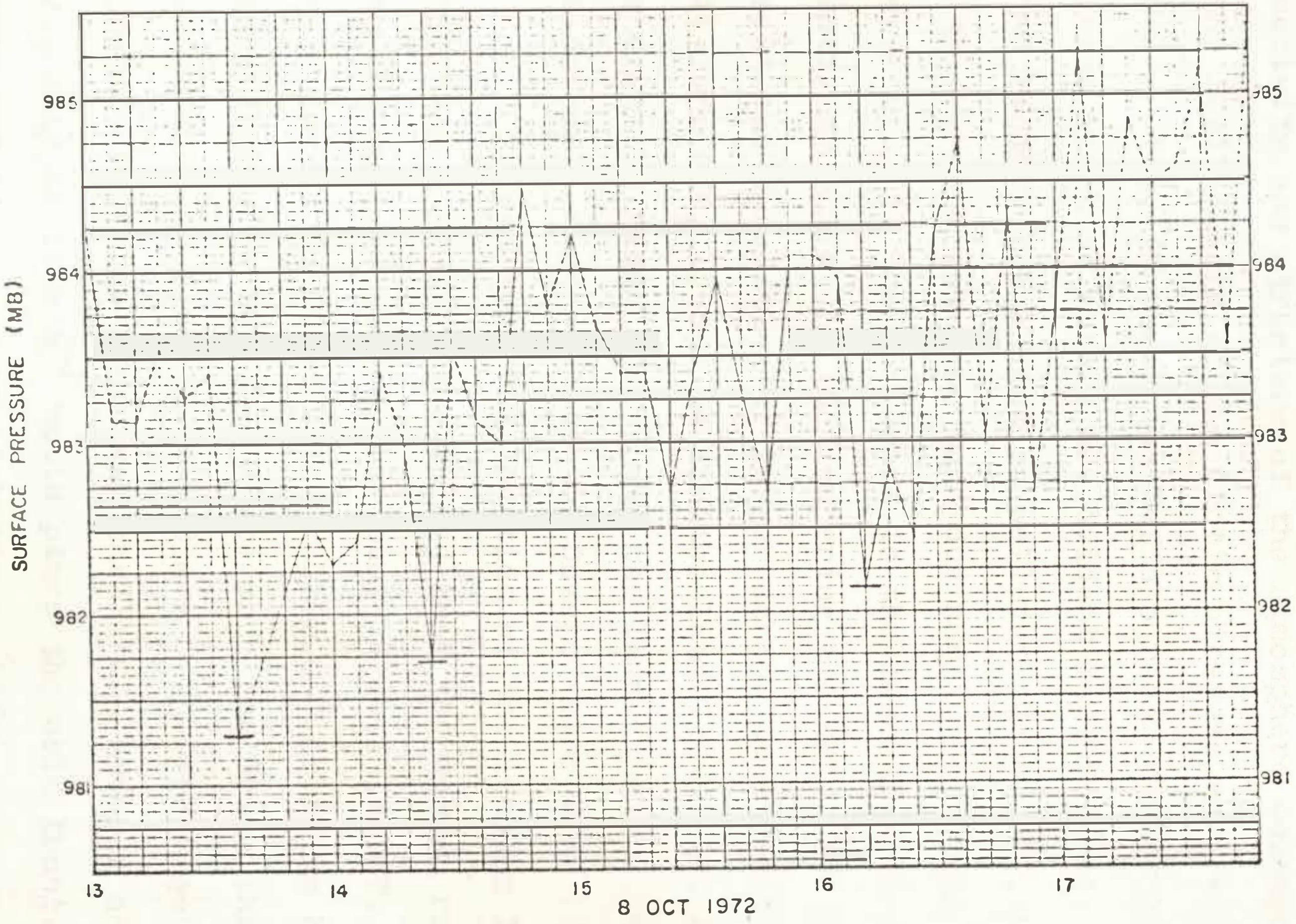

Fig. 24. Surface pressure trace at IFYGL buoy 14 (Fig. 2). Pressure minimums associated with organized frontal activity are indicated by horizontal lines.

at 1612 GMT is the echo activity associated with the surface cold front. Indeed, when viewed in detail, the activity and structure of the atmosphere accompanying the leading edge of the Arctic air-mass was very complex.

Fig. 25 shows the Buffalo radar PPI at 1332 GMT. Three lines of echoes are evident in this photo albeit the center line is not as well defined as the other two. The sharp narrow echo band due north of Buffalo and extending to the northeast is the leading line of activity while the band entering the PPI from the northwest and consisting of larger echoes is the cold front. At 1456 GMT, 1 hour 24 minutes later, Fig. 26, a photo of the Oswego radar PPI, shows the lead line now in a position north-northwest of the Oswego radar site (Fig. 1).

By plotting the location of the leading line of activity at 1456 GMT obtained from the Oswego radar and noting that it passed over buoy 14 at 1336 GMT, its phase velocity is calculated to be 17 m s^{-1} or 61 km hr^{-1}. This figure is believed to be more realistic than that of McBean's. Traveling at 8 m s^{-1} the front would take about 8 hours to pass over the lake. However a phase velocity of 17 m s^{-1} would place the cold front at 1900 GMT in agreement with the position estimated from the ESSA 9 satellite photo.

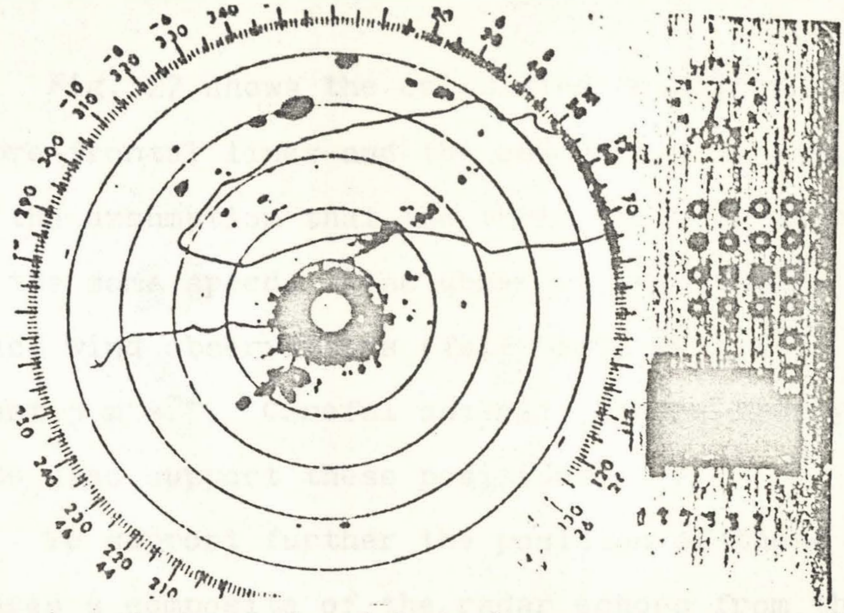

Fig. 25. Photograph of Buffalo PPI at 1332 GMT October 8, 1972. Three lines of activity are shown; the second line appears to have only one significant echo at this time.

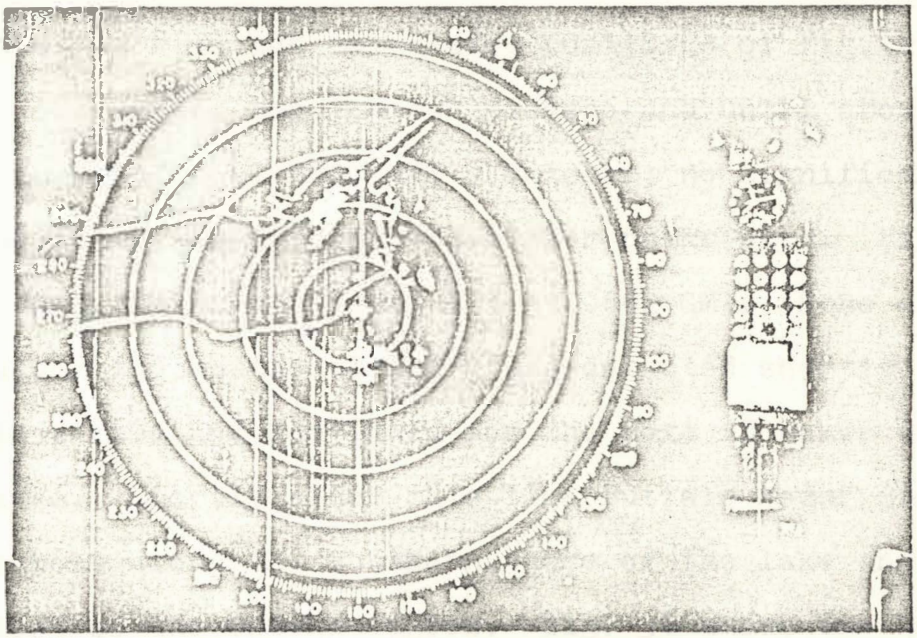

Fig. 26. Photograph of Oswego PPI at 1456 GMT October 8, 1972. Bright echo pattern is leading line of activity.

Fig. 27 shows the calculated positions of the two pre-frontal lines and the cold front at 1500 GMT, with the assumption that the three features translate with the same speed. Also shown on this figure are the surface wind observations (full barbs 10 m s^{-1}) to the nearest 5 m s^{-1}. Careful analysis of the hourly wind shifts also support these positions.

To support further the position of these three features a composite of the radar echoes from the 1438 GMT Buffalo PPI and 1456 GMT Oswego PPI was constructed and is shown in Fig. 28. Clearly, three distinct lines of activity exist over Lake Ontario and coincide very closely with the calculated positions of Fig. 27.

After the frontal passage and until about 15 hours later at 0600 GMT 9 October, no significant echo activity was recorded at either radar site. Fig. 29 shows the Oswego radar PPI at 0602 GMT. Echo activity along the southeast shore was detected shortly before this time and continued for the next 18 hours in this area. Shortly after this time Buffalo radar displayed echoes along the southern shore of the lake and to the west of the Oswego echoes. Fig. 30 shows the Buffalo radar at 0642 GMT. These echoes also persisted in varying degrees of intensity for the next 18 hours.

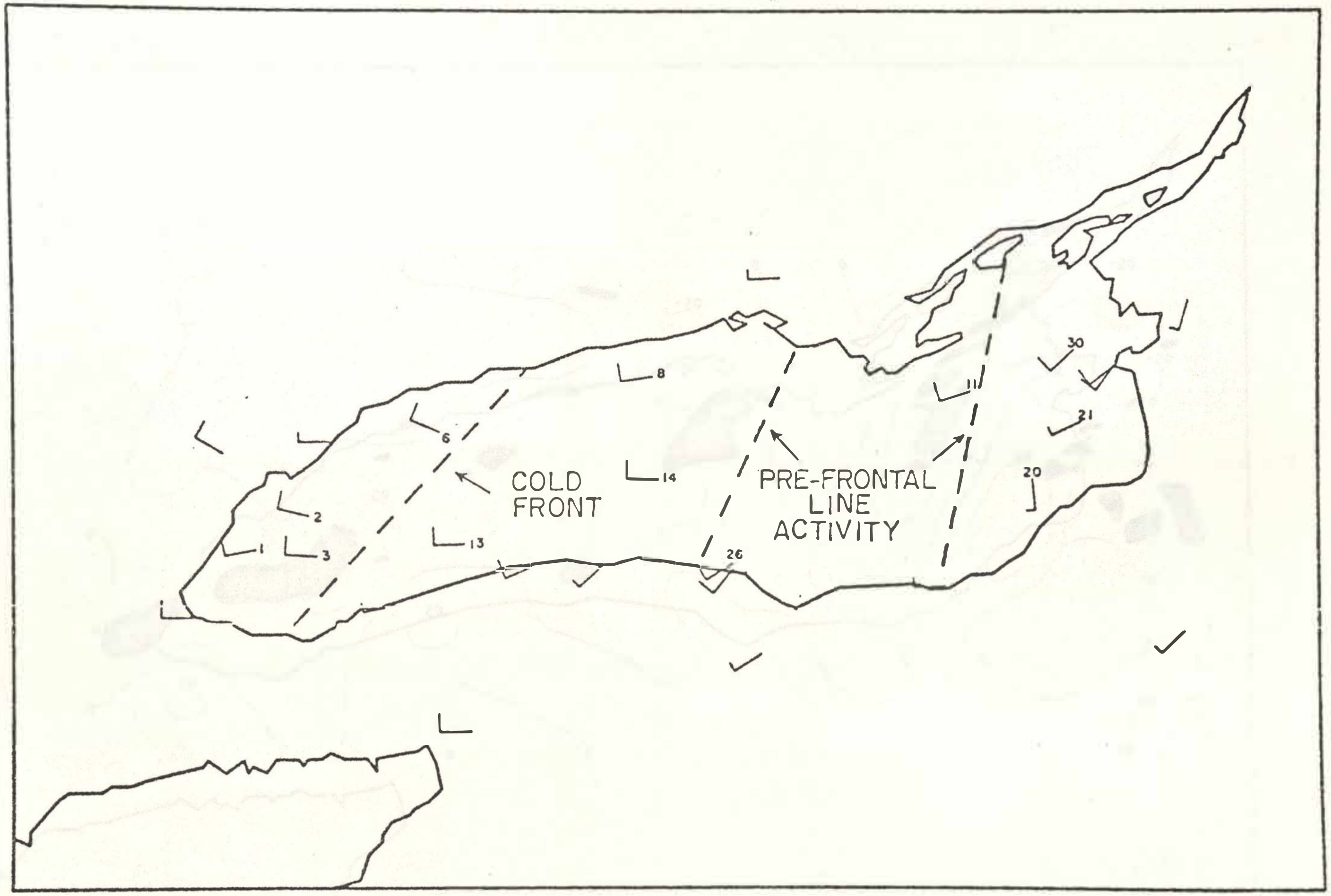

Fig. 27. Location of three lines of activity at 1500 GMT October 8, 1972 as deduced from surface pressure and wind observations. Wind observations at this time are superimposed.

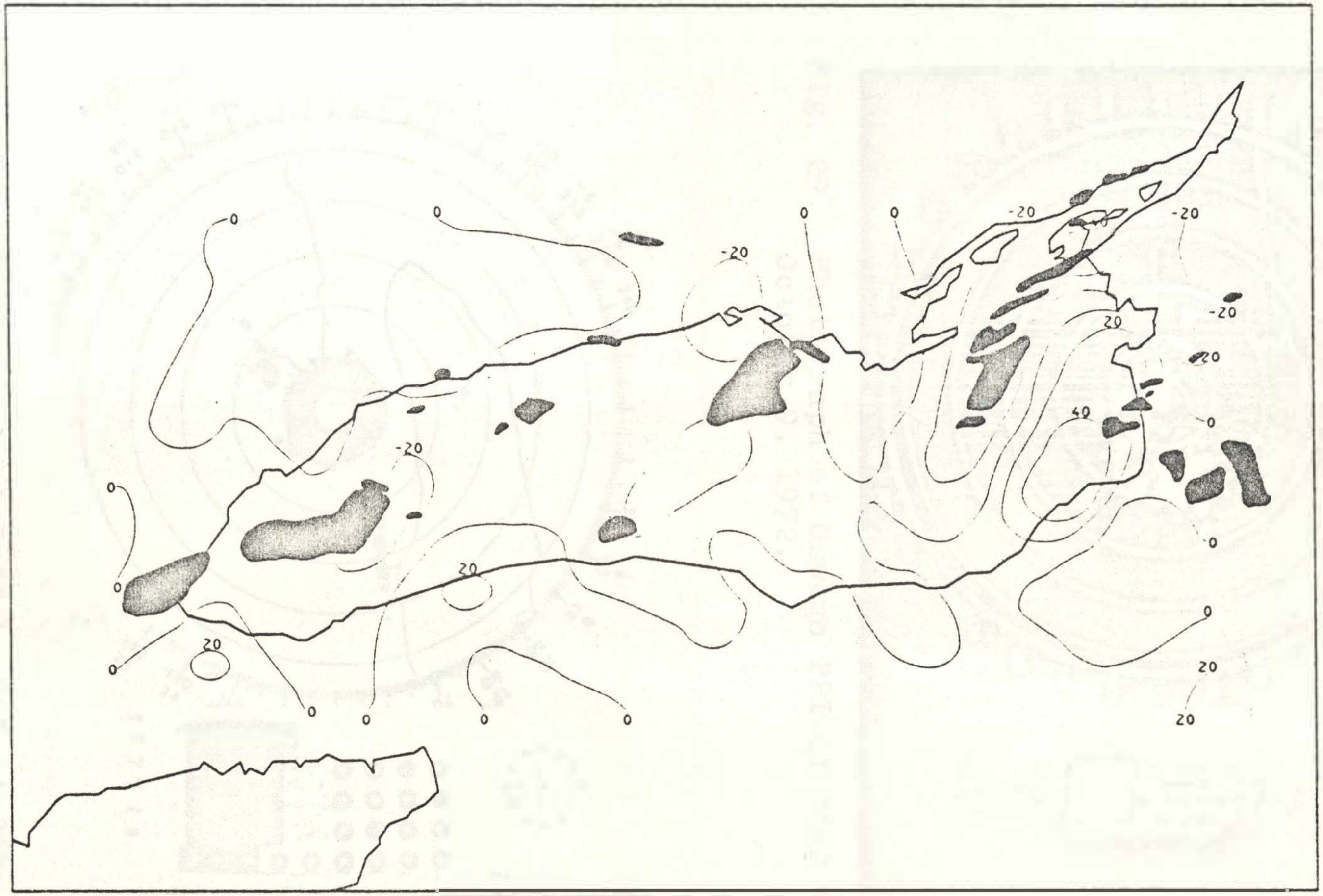

Fig. 28. Surface divergence (10^{-5} s^{-1}) calculated from NVA winds (1500 GMT October 8, 1972). Superimposed is composite of radar echoes from Buffalo PPI at 1438 GMT and Oswego PPI at 1456 GMT.

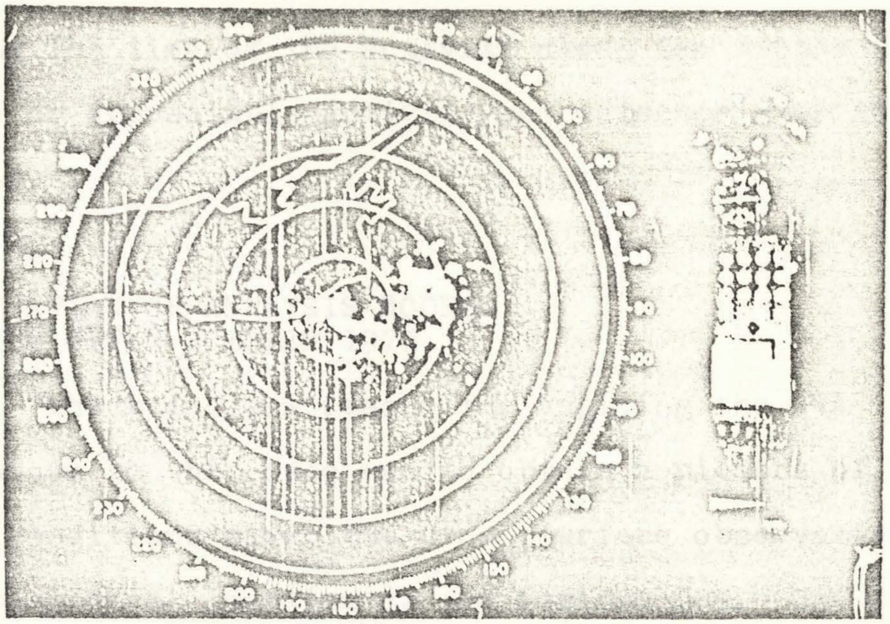

Fig. 29. Photograph of Oswego PPI at 0602 GMT October 9, 1972.

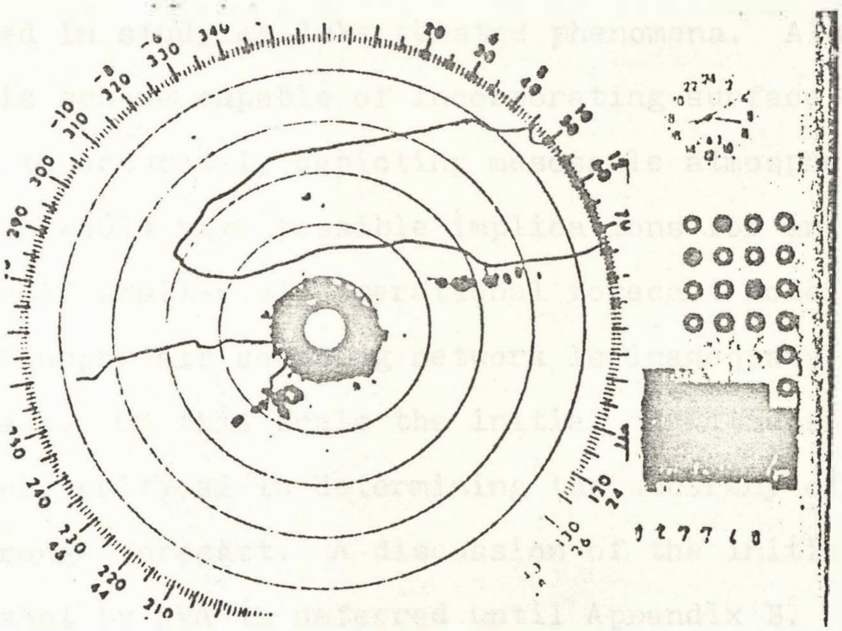

Fig. 30. Photograph of Buffalo PPI at 0642 GMT October 9, 1972.

During the time of the activity along the southern lake shore no appreciable activity was detected over the lake itself.

APPLICATION OF ANALYSIS MODEL AT 1500 GMT 8 OCTOBER 1972

The principal reason for applying the NVA technique to this case was to obtain a picture of over-lake conditions given the dense surface observations and the peripheral location of the rawinsondes. One objective was to attempt to extrapolate information from the dense surface observations into the upper-air; an analysis procedure first proposed by Sasaki but never utilized in studying lake related phenomena. Also, an analysis scheme capable of incorporating surface data as an aid to accurately depicting mesoscale atmospheric features would have possible implications for initialization of small-scale operational forecast models; the present upper-air sounding network is inadequate for this task. On this scale the initial conditions become extremely critical in determining the accuracy of the short-range forecast. A discussion of the initial field adjustment by NVA is deferred until Appendix B. In this and the following section mesoscale features that are detected over the lake as a result of applying the NVA model at the two times, 1500 GMT 8 October 1972 and 0600 GMT the following day are discussed.

Fig. 31 shows the NVA surface wind field at 1500 GMT resulting from the mutual adjustment of the surface wind and pressure observations. Careful comparison of this wind field with the locations of the echo line activity (Fig. 27) shows definite wind shifts in the vicinity of each line. The most intense change occurs at the leading edge of the lead squall line. Here the wind speed gradient was about 30 cm s^{-1} km^{-1} with wind shifts of 25 degrees or more. Two wind maximum areas just inland of the lake, one located on the extreme eastern edge, the other southwest of the lake are apparently caused in part by the larger terrain gradient in these areas (see Fig. 2). Both wind maximums were not present in the initial wind field (see Fig. 56 of Appendix B). The activity along each line corresponds closely to the convergence patterns calculated from the NVA surface wind field (Fig. 28). The lead line of echo activity lies in an area of surface convergence with maximum values of $4x10^{-4}$ s^{-1}. Just preceding the line is a large area encompassing the eastern portion of the lake of equally intense surface divergence. The second line and cold front lie in areas with values as high as $2x10^{-4}\ s^{-1}$. The coincidence of the areas of convergence, their shape and location, with the echo activity is clearly evident. This finding agrees with that of Matsumoto et al. (1967b) who found that the mesoscale disturbance is closely linked with the cumulus activity and that surface mesoscale convergence areas of the order of $10^{-4}\ s^{-1}$ are necessary for maintenance of the cumulus activity. Strong convergence of the moist air is necessary to maintain the cumulus. Peace and Sykes (1966) also calculated convergences of the order of $10^{-4}\ s^{-1}$ in snow squall situations over Lake Ontario.

Fig. 32 shows the surface relative vorticity field at 1500 GMT. A large pattern of negative vorticity dominates most of the lake with no readily apparent linkage with the echo line activity as did the divergence pattern. Although it would appear from Fig. 31 that the winds are undergoing cyclonic curvature over the lake and hence there should be an area of positive vorticity ahead of the cold front, the anticyclonic shear caused by stronger winds generally in the northern portions of the lake, acts to counteract the curvature effect resulting in mostly negative vorticity ahead of the cold front.

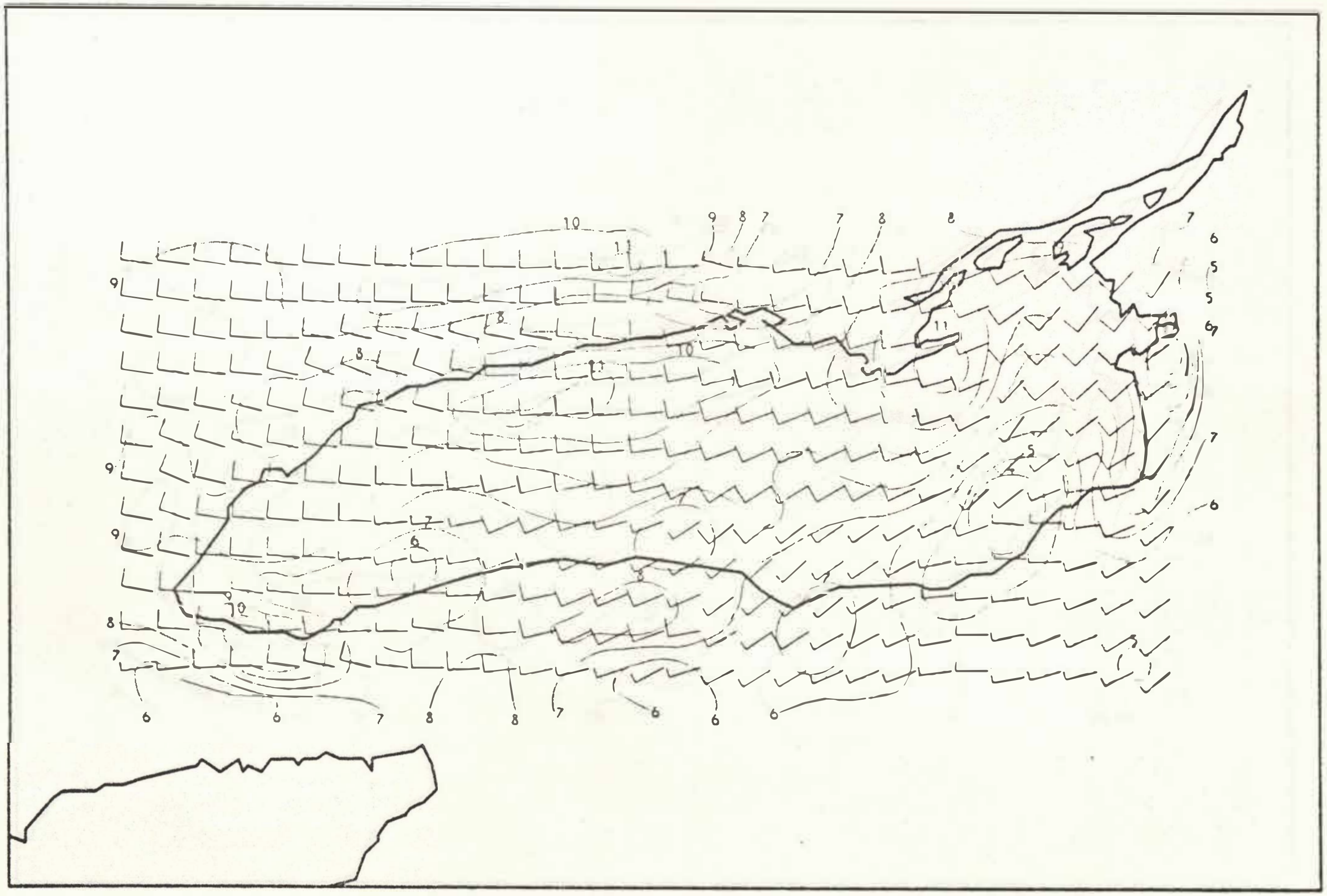

Fig. 31. NVA surface wind (m s^{-1}; 1500 GMT October 8, 1972).

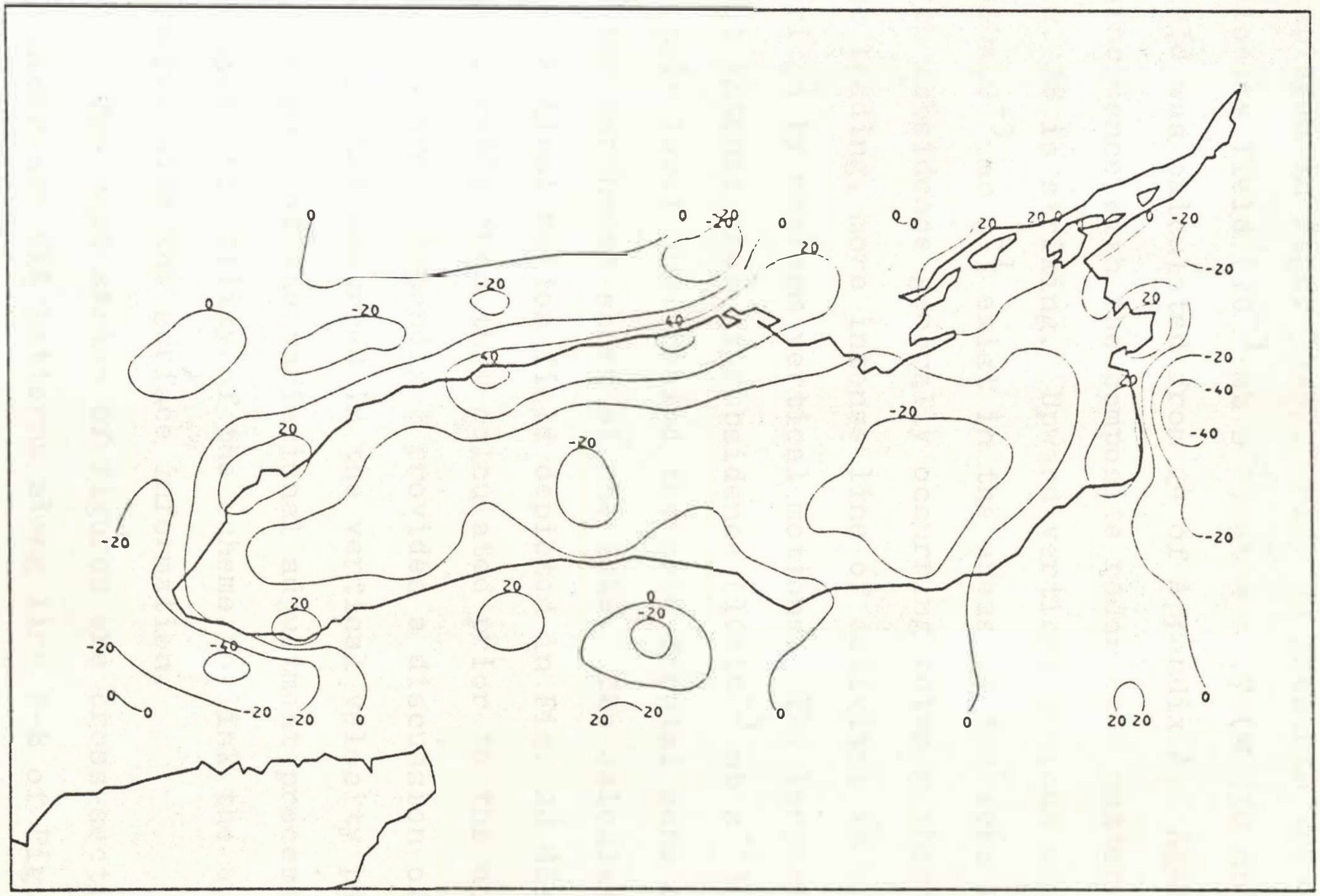

Fig. 32. Surface vorticity (10^{-5} s^{-1}) calculated from NVA winds (1500 GMT October 8, 1972).

The upper-air mesoscale patterns at 1500 GMT, reflecting the convective activity over the lake, are displayed in Figs. 33-37. Fig. 33 presents the ω vertical velocity field (10^{-3} mb s^{-1}) at $\sigma = .7$ (≈ 850 mb). This field was calculated from 24 of Appendix A. Again the coincidence with the composite radar echo pattern of Fig. 28 is striking. Upward vertical motions of $5\text{-}10\times10^{-3}$ mb s^{-1} exist in the areas of the echo activity, with subsidence generally occurring between these areas. The leading, more intense line of activity, is characterized by maximum vertical motions. The largest and most intense area of subsidence (10×10^{-3} mb s^{-1}) occurs at this level just behind the cold frontal echo activity on the northwest shore of the lake. The calculation of the vertical motion field depicted in Fig. 28 differs considerably from that calculated prior to the application of NVA. Appendix B provides a discussion of the changes that occurred in the vertical velocity pattern as a result of the variational adjustment process and the apparent ability of the scheme to link the upper-air patterns with the surface information.

The next series of figures are cross-sections of the upper-air NVA patterns along line B-B of Fig. 2. Fig. 34 depicts a complex isotach and wind direction

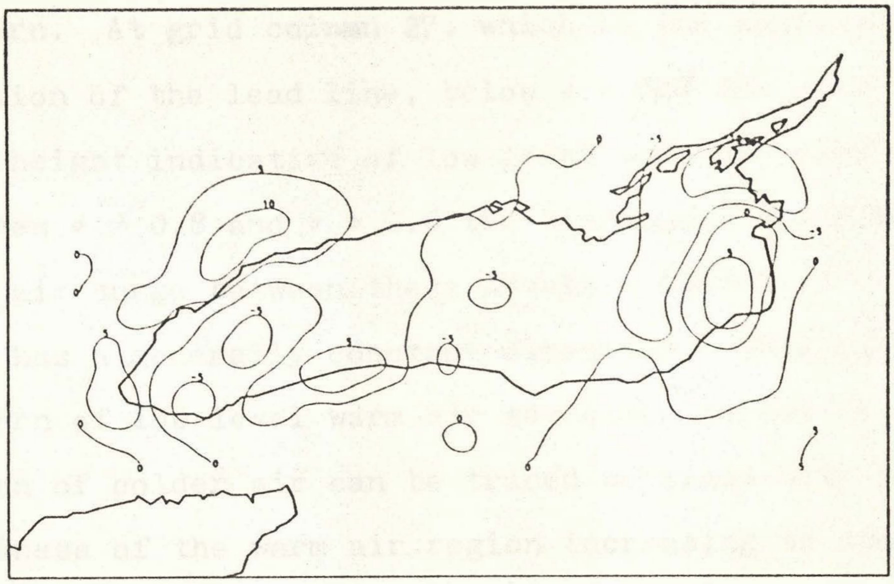

Fig. 33. NVA vertical velocity, ω (10^{-3} mb s^{-1}) at σ = .7 ($\simeq$ 850 mb; 1500 GMT October 8, 1972).

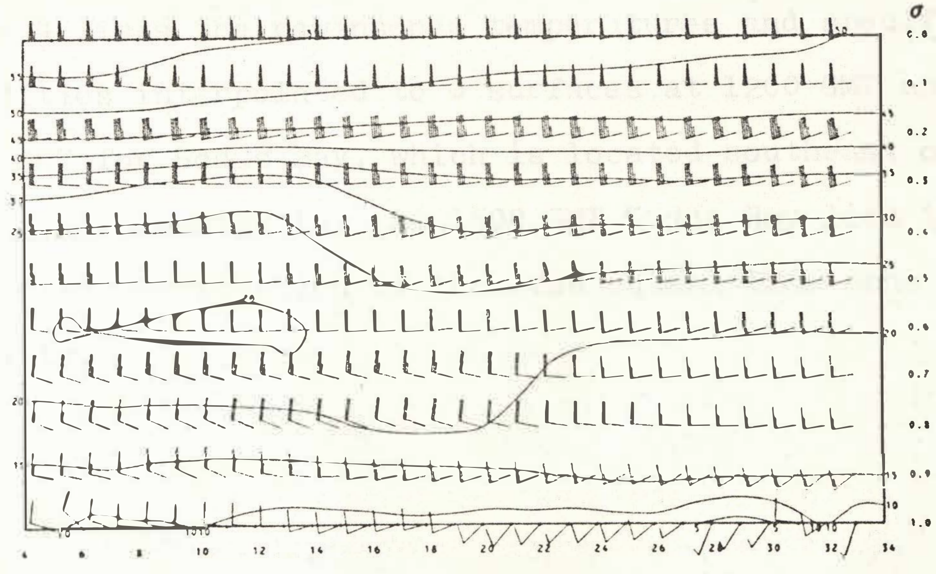

Fig. 34. Cross-section of NVA winds (m s^{-1}) along line B-B of Fig. 2 (1500 GMT October 8, 1972).

pattern. At grid column 27, which is the approximate location of the lead line, below $\sigma = 0.8$ the wind veers with height indicative of low level warm air advection. Between $\sigma = 0.8$ and $\sigma = 0.6$ the wind backs indicating a cold air surge between these levels. Above $\sigma = 0.6$ the wind has a generally constant direction. This same pattern of low level warm air advection capped by a region of colder air can be traced westward with the thickness of the warm air region increasing to about the $\sigma = 0.6$ level at grid column 12. Apparently the colder air in the upper levels has surged ahead of the leading edge of the Arctic air-mass and is responsible for the pre-frontal activity. Rawinsonde data support this view. Table 4 lists the rawinsonde temperatures and specific humidities interpolated to σ surfaces at 1200 GMT and 1500 GMT for Sodus Bay, which is located southeast of the lake (see Fig. 1). At 1500 GMT Sodus Bay lies in line with an extension of the lead squall line echo activity.

Table 4

Interpolated Rawinsonde Temperature and Specific Humidity for Sodus Bay at 1200 GMT and 1500 GMT 8 October 1972

	1200 GMT		1500 GMT	
σ	T(^{o}C)	q(g kg^{-1})	T(^{o}C)	q(g kg^{-1})
0.0	-13.2	0.4	-12.8	0.3
0.1	- 8.4	0.6	- 9.1	0.3
0.2	- 3.4	0.8	- 6.9	0.3
0.3	- 1.3	0.9	- 7.2	0.3
0.4	- 1.1	2.7	- 4.9	3.6
0.5	1.0	3.8	- 2.6	4.1
0.6	2.8	2.9	0.4	5.0
0.7	4.7	3.5	3.0	5.6
0.8	5.8	4.0	5.2	6.2
0.9	8.3	5.3	8.8	6.7
1.0	6.7	4.9	13.7	6.6

Below σ = 0.8 the temperature has increased during the 3-hour period in response to warm advection and insolation while simultaneously falling at all higher levels, except at 500 mb. Specific humidities have increased significantly at all levels up to and including σ = 0.4 ($\simeq$ 700 mb). The low level moisture convergence and upward transport by the vertical motion field and large scale eddies is believed responsible for the increased specific humidities at higher levels.

The vertical velocity pattern across the lake is depicted in Fig. 35. In this figure the pattern has been extrapolated to the surface ($\sigma = 1.0$) in order to prevent unreasonable-looking patterns near the surface. In actuality the vertical velocity is zero at $\sigma = 1.0$. Note the sharpness of the vertical velocity pattern in the vicinity of the more intense lead line of activity (grid column 27) and the three cells of upward vertical motion associated with the three lines of echo activity.

Fig. 36 shows the very complex pattern of potential temperature (solid lines) and specific humidity (dashed lines) associated with the activity over the lake. The specific humidity pattern shows a sharp rise in the area of the lead squall line, where the vertical velocity rapidly changes direction. This pattern differs significantly from that of the initial fields. In order to aid in interpreting the structure of the atmosphere represented by the moisture and temperature patterns of Fig. 36 the static energy was calculated and is depicted in Fig. 37.

Static energy is defined as the sum of the enthalpy, gravitational potential energy, and the latent heat potential energy. Kreitzberg and Brown (1970) analyzed this parameter in their study of

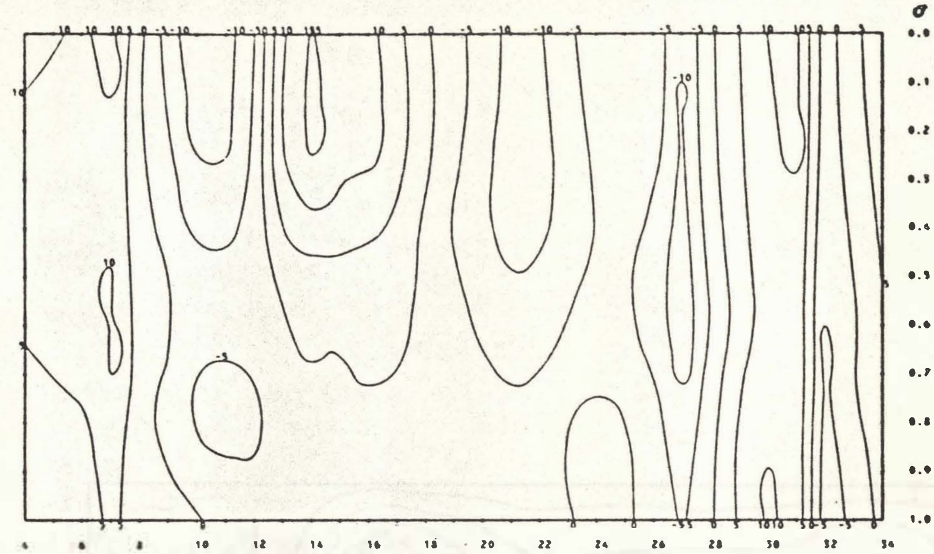

Fig. 35. Cross-section of NVA vertical velocity, ω (10^{-3} mb s^{-1}), along line B-B of Fig. 2 (1500 GMT October 8, 1972). Values at $\sigma = 1.$ are extrapolated from upper levels for clarity of display.

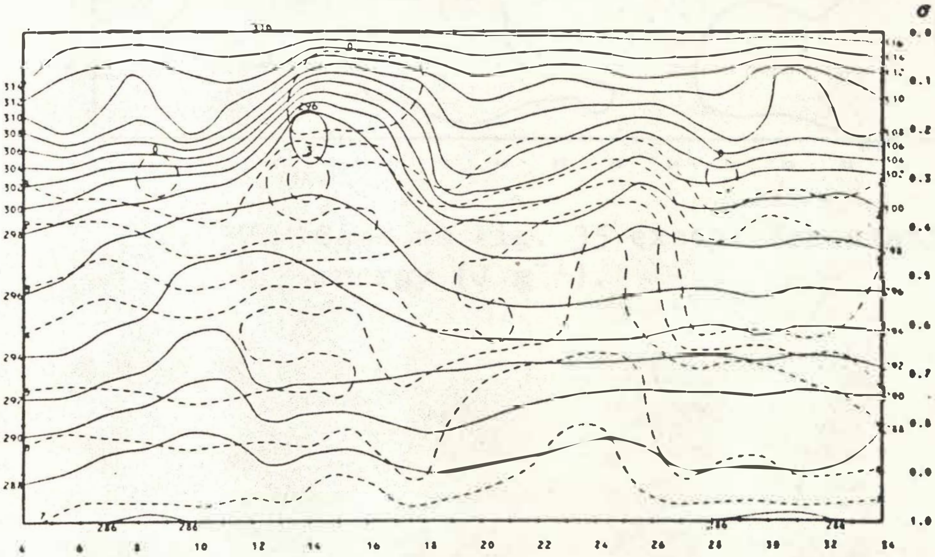

Fig. 36. Same as Fig. 35 except for potential temperature (^{o}K; solid lines) and specific humidity ($g\ kg^{-1}$; dashed lines).

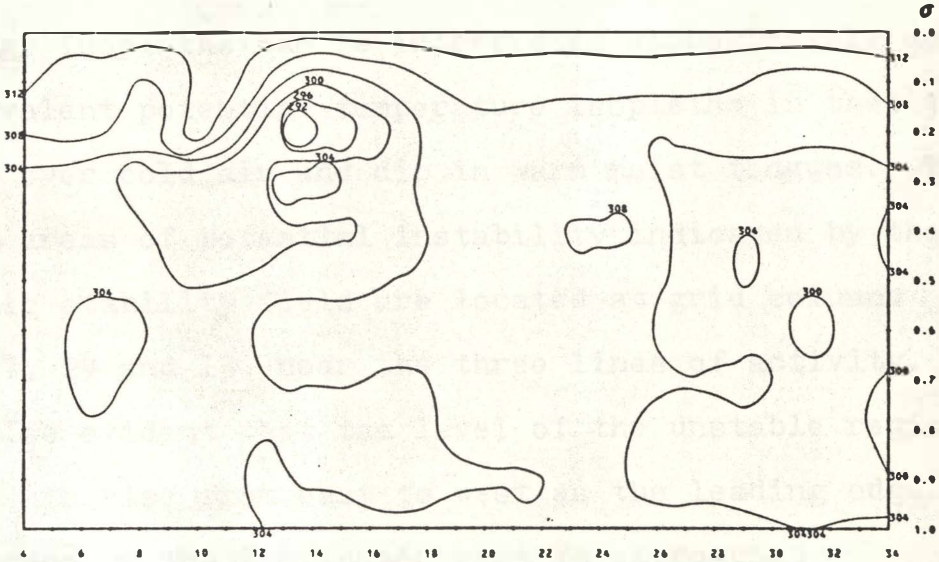

Fig. 37. Same as Fig. 35 except for static energy (J g^{-1}).

mesoscale weather systems within an occlusion. It also has been used extensively in studies of tropical energetics. As pointed out by Kreitzberg and Brown, static energy is conservative with respect to dry and moist adiabatic ascent and descent and can be simply interpreted in terms of energetics. A decrease of static energy with height indicates the existence of potential (convective) instability and generally static energy isopleths can be interpreted approximately as equivalent potential temperature isopleths in that they dome over cold air and dip in warm moist tongues. The main areas of potential instability indicated by the static stability field are located at grid columns 29-31, 24 and 13, near the three lines of activity. It is also evident that the level of the unstable regions tends to rise from east to west as the leading edge of the dome of the Arctic air-mass is approached.

From the available data it was not possible to determine whether activity along the pre-frontal lines and at the cold front itself increased significantly or changed in character when traversing the lake. Figs. 38 and 39 are 24-hour traces from 1200 GMT 8 October to 1100 GMT 9 October 1972 of (1) lake-surface temperature (dashed line) and 3-meter air temperature (solid line)

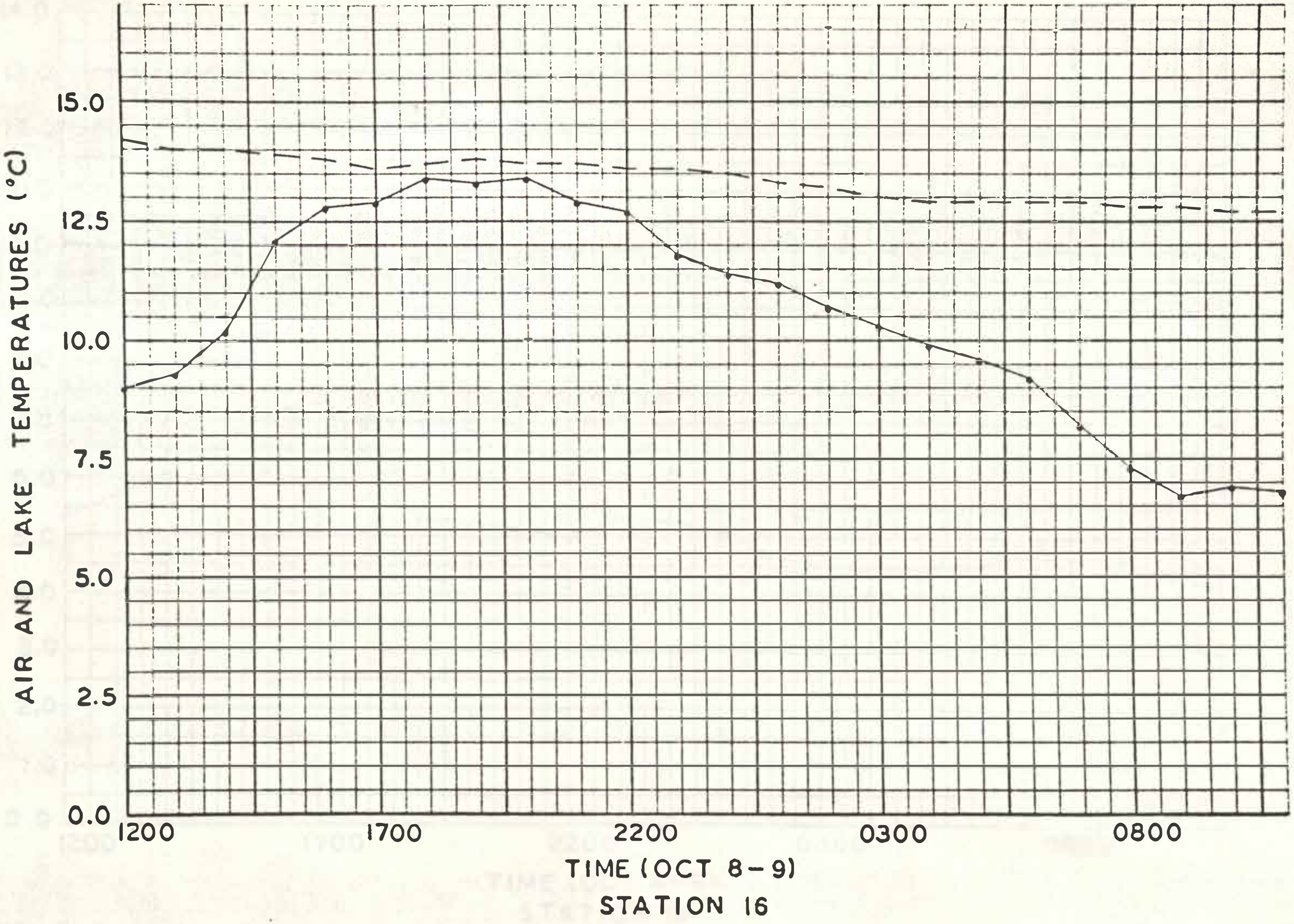

Fig. 38. Trace of lake surface temperature (dashed line) and air temperature at 3 meters (solid line) for 23-hour period 1200 GMT October 8 - 1100 GMT October 9, 1972 at IFYGL buoy 16 (Fig. 2).

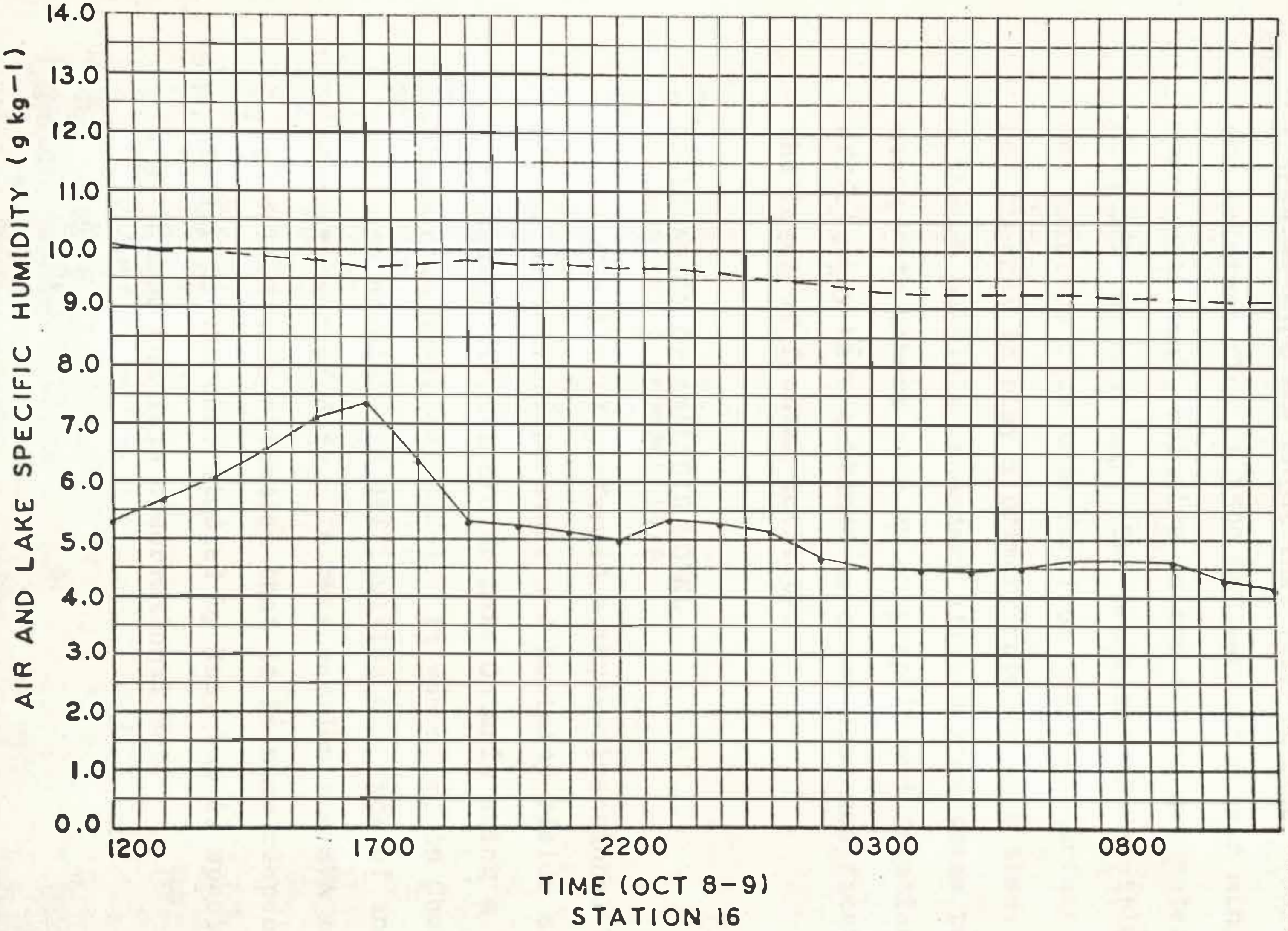

Fig. 39. Same as Fig. 38, except for saturated specific humidity corresponding to the surface water temperature (dashed line) and specific humidity of the air at 3 meters (solid line).

and (2) lake-surface specific humidity and 3-meter air specific humidity for IFYGL buoy 16 (Fig. 2). These traces support the point that lake-surface sensible heat and moisture flux at 1500 GMT were at a near minimum and were quite small relative to the fluxes generated at 0600 GMT the next day. The processes of sensible heat and moisture flux transfer from the lake-surface were not thought to play a primary role at this time, although possible secondary effects from these processes along with others such as orographic and frictional effects may have combined to cause some modification in the level of frontal activity.

APPLICATION OF ANALYSIS MODEL AT 0600 GMT 9 OCTOBER 1972

Rao (1971) performed a three-dimensional study of the motion, temperature and humidity fields of a snow-squall situation over Lake Ontario using a diagnostic numerical model. It was noted in Chapter I that one of his main difficulties was lack of an adequate set of data. In this section the NVA model is applied to a situation that is in many respects similar to the case studied by Rao, but is specified by a much more complete observational set.

Fig. 40 shows the NVA surface wind pattern at 0600 GMT 9 October 1972. In contrast to fifteen hours earlier surface winds at this time are generally from west-northwest throughout the basin, although lake and terrain related anomalies of wind direction and speed are very evident. Noteworthy features of the wind field are the cyclonic curvature that occurs over the lake and the wind maxima along its southern shore. Heating of the overlying air by the lake is theorized to be the cause of the cyclonic turning. Figs. 41 and 42 are the computed vorticity and divergence fields respectively. In contrast to 1500 GMT (Fig. 32) the vorticity at this time (Fig. 41) is positive over almost the entire lake with negative vorticity generally bordering the lake. The exception being an area of positive vorticity over-land southeast of the lake. This is also the area of major echo activity at this time. Petterssen (1956) provides a clear theoretical explanation for the production of positive vorticity by an underlying heat source.

Shown superimposed on the divergence field (Fig. 42) are the composite radar echoes from the Buffalo PPI at 0642 and from the Oswego PPI at 0602.

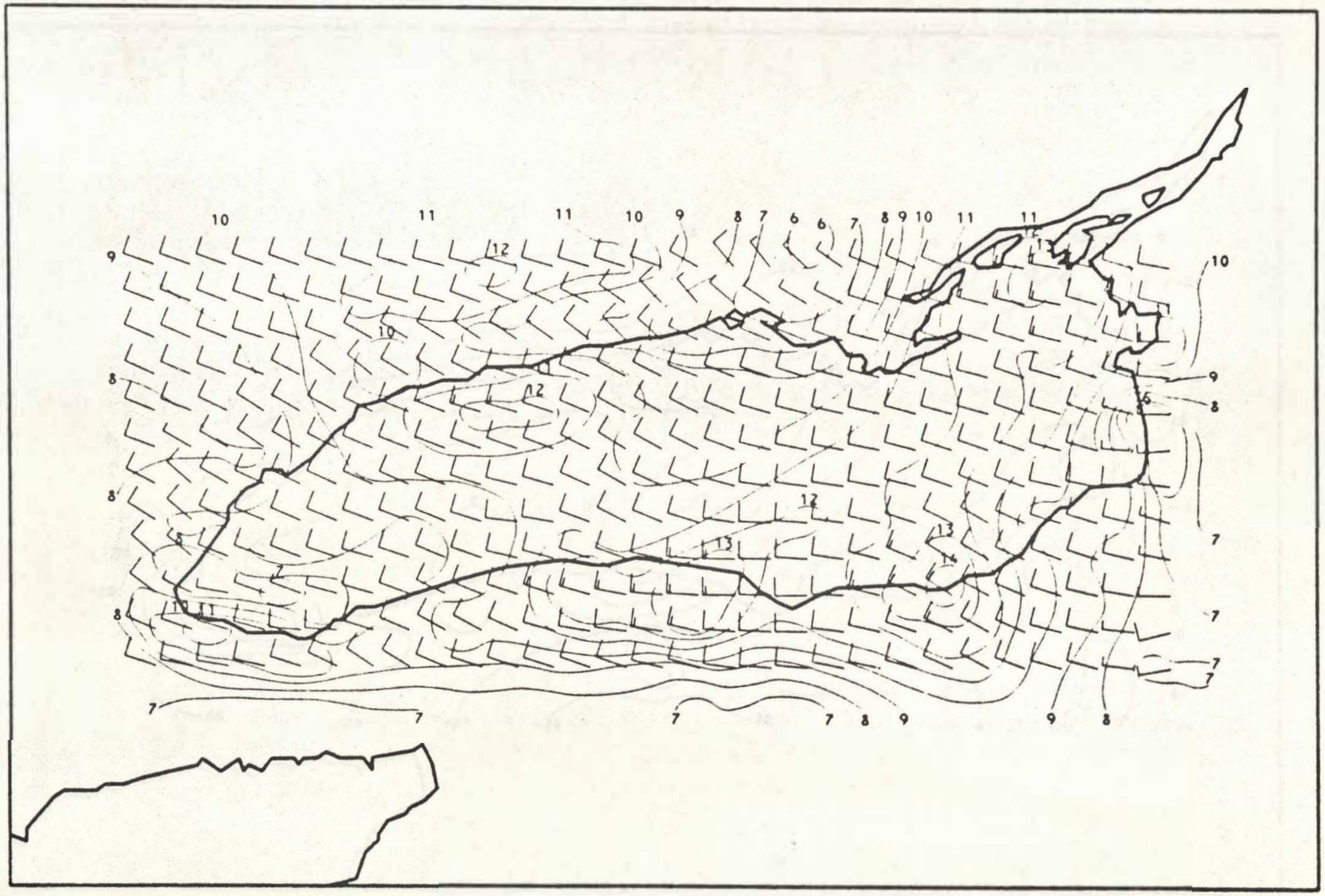

Fig. 40. NVA surface wind (m s^{-1}; 0600 GMT October 9, 1972).

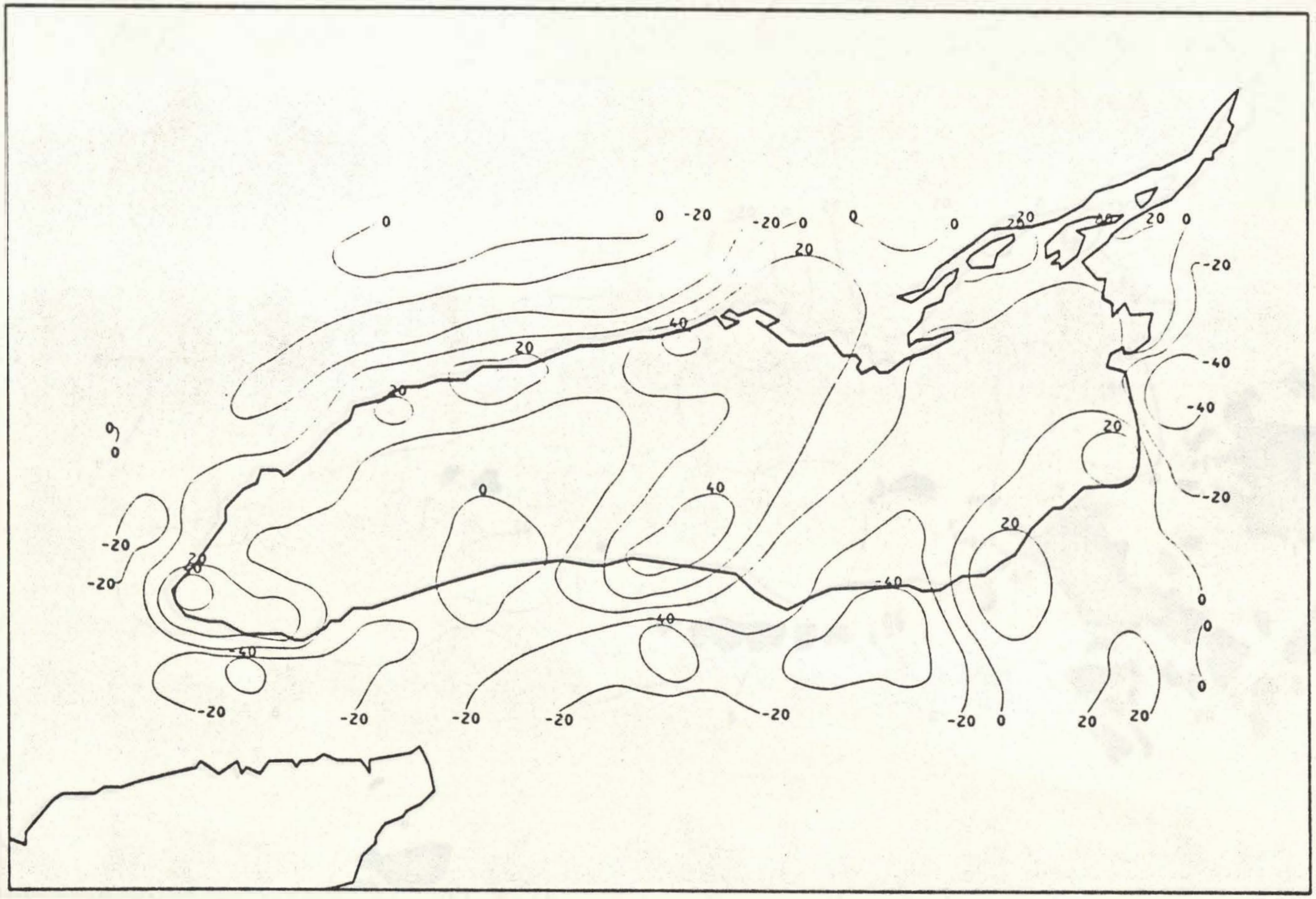

Fig. 41. Surface vorticity (10^{-5} s^{-1}) calculated from NVA winds (0600 GMT October 9, 1972).

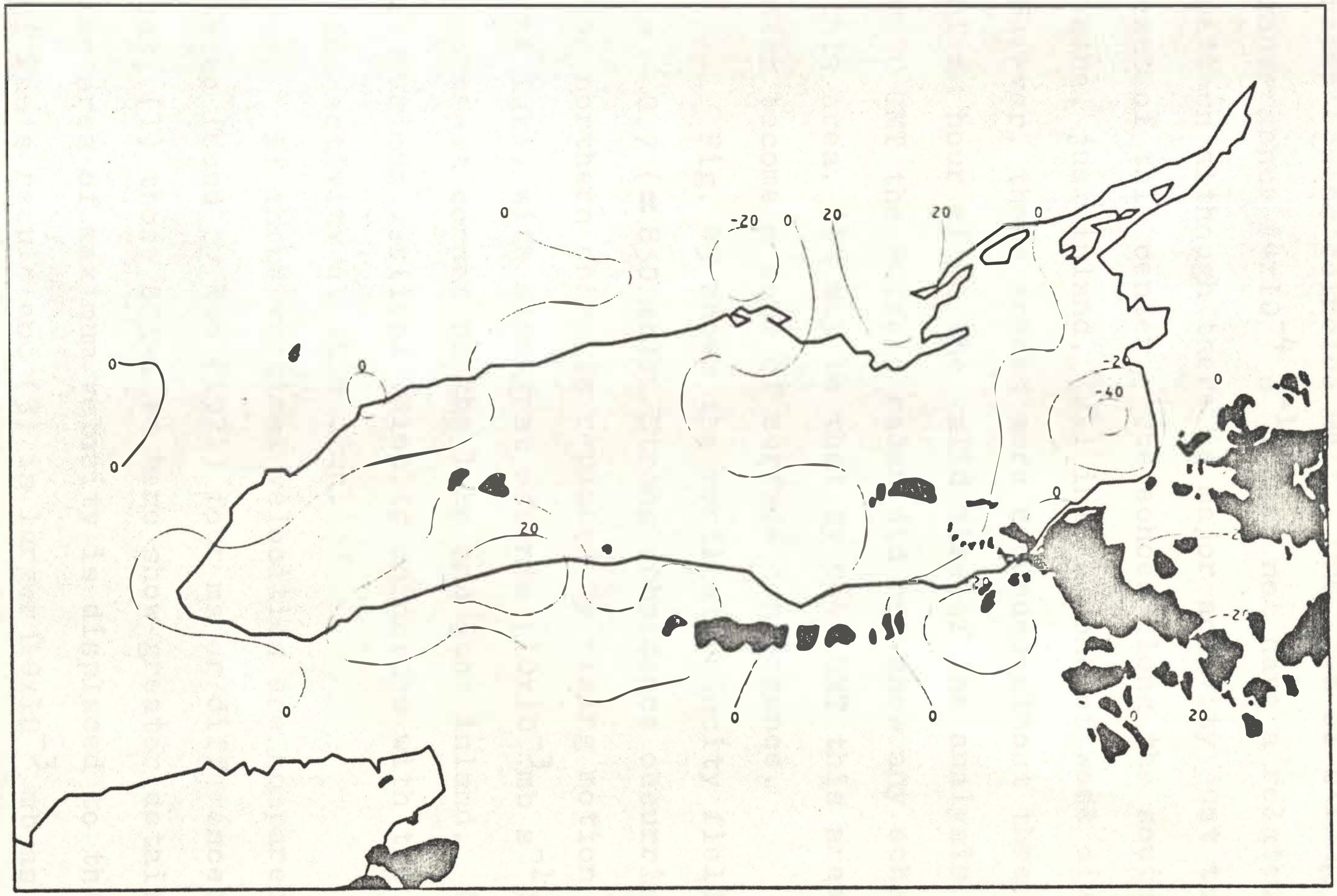

Fig. 42. Surface divergence (10^{-5} s^{-1}) calculated from NVA winds (0600 GMT October 9, 1972). Superimposed is composite of radar echoes from Buffalo PPI at 0715 GMT and Oswego PPI at 0602 GMT.

The major area of convergence on the southeast and the radar echoes coincide well. One area of strong convergence ($4\text{x}10^{-4}$ s^{-1}) does not have a related echo pattern although there is major activity just to the east of this center. The echoes along the southern shore, just inland, fall into a zone of weak divergence. However, these echoes were recorded almost three-quarters of an hour after the valid time of the analysis. At 0600 GMT the Buffalo radar did not show any echoes in this area. It may be that by 0642 GMT this area had also become a zone of surface convergence.

Fig. 43 shows the vertical velocity field at $\sigma = 0.7$ ($\simeq 850$ mb). Strong subsidence occurring along the northern shore is replaced by rising motion over the lake, with strongest ascents ($10\text{x}10^{-3}$mb s^{-1}) in the southeast corner of the lake and just inland. The area of maximum vertical velocity coincides with the major echo activity at this time.

If these vertical velocities are compared with those found by Rao (1971) four major differences stand out: (1) those obtained here show greater detail, (2) the area of maximum velocity is displaced to the east of Rao's result and (3) is larger ($10\text{x}10^{-3}$ mb as compared to $3\text{x}10^{-3}$ mb) and (4) subsidence along the northern shore is not obtained by Rao at this level. A number of possible reasons can be offered for these differences. Rao was forced to use very sparse upper-air information, which was subjectively analyzed, to initialize his diagnostic model. Also the vertical and horizontal resolution of his model was coarser than the NVA model used here. These effects would all tend to smooth the meteorological fields thus masking the finer mesoscale phenomena. Also as Rao noted, his study was of initial conditions that occur just prior to the onset of lake-effect storms. Hence the vertical velocities would be expected to be somewhat smaller than if convective activity had actually commenced as was the case here. Finally the result presented here tends to confirm the theoretical finding of Lavoie et al. (1970) who calculated a maximum upward velocity of 15 cm s^{-1} toward the lee side of Lake Erie for a typical snow-squall situation. However, it should be noted that caution must be exercised when making this comparison since there are a variety of differences that exist between the case presented here and the undisturbed flow characterizing the atmosphere for the Lavoie et al. study, e.g., their model had a constant lake-sea difference of 9^{o}C while here it varied over the lake from 4 to 7^{o}C.

Fig. 44 is a cross section of vertical velocity along line B-B of Fig. 2. The area of maximum ascent occurs between 900-800 mb. In general the influence of the lake extends to about 700 mb as evidenced by the rising motion over the lake. This result differs from Rao's in that his model showed rising motion up to 400 mb. He offered no explanation for his result. Rawinsonde data at 0600 GMT agree with the vertical motion field calculated in this study. Table 5 lists rawinsonde temperature and specific humidity for Scarboro, located on the northwest shore of the lake near Toronto (Fig. 1), and Sodus Bay located on the southeast shore. Specific humidity has increased at all levels from the surface to $\sigma = 0.4$ ($\simeq$700 mb) on the leeward side of the lake while a similar effect on temperature is observed up to about 800 mb ($\sigma = 0.6$).

Table 5

Interpolated Rawinsonde Temperature and Specific Humidity for Scarboro and Sodus Bay at 0600 GMT 9 October 1972

	Scarboro		Sodus Bay	
σ	T(^{0}C)	q(g kg^{-1})	T(^{0}C)	q(g kg^{-1})
0.0	-28.1	0.1	-29.0	0.1
0.1	-22.9	0.1	-24.8	0.1
0.2	-18.6	0.1	-20.8	0.1
0.3	-15.8	0.2	-19.1	0.1
0.4	-13.2	0.6	-14.4	1.1
0.5	-10.4	1.4	-10.8	2.0
0.6	- 7.8	2.0	- 7.8	3.4
0.7	- 4.4	2.2	- 3.0	3.5
0.8	- 0.2	2.4	- 0.1	4.2
0.9	1.7	3.8	4.1	4.3
1.0	5.3	3.7	9.9	6.0

It is of interest to attempt to explain the motion field in light of recent theoretical findings. Estoque and Bhumralkar (1969) designed a general theoretical model to analyze the properties of perturbations induced when air flows over an isolated warm portion of the earth's surface. They made computations for two cases: (1) prevailing flow normal to a narrow (10 km) heat source of infinite length and (2) prevailing flow parallel to the heat source. In the first

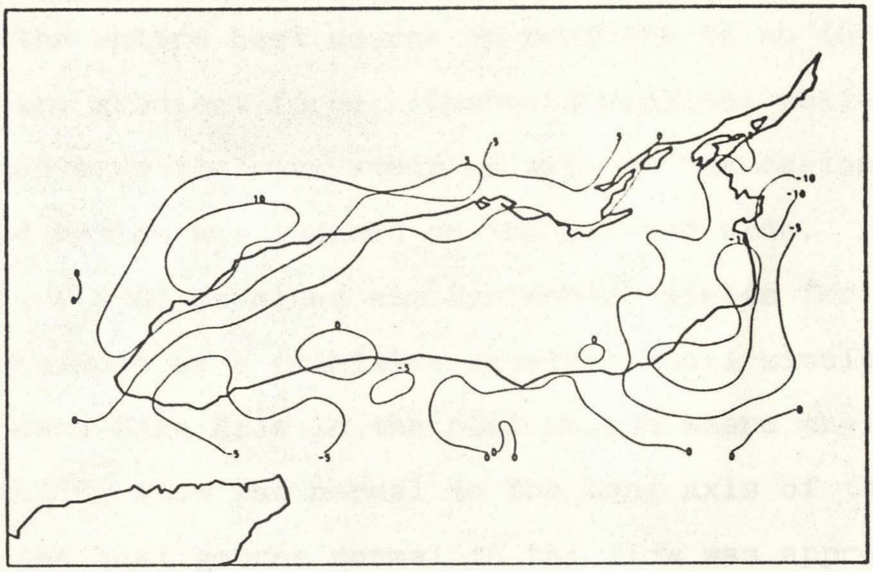

Fig. 43. NVA vertical velocity, ω (10^{-3} mb s^{-1}) at σ = .7 (≃850 mb; 0600 GMT October 9, 1972).

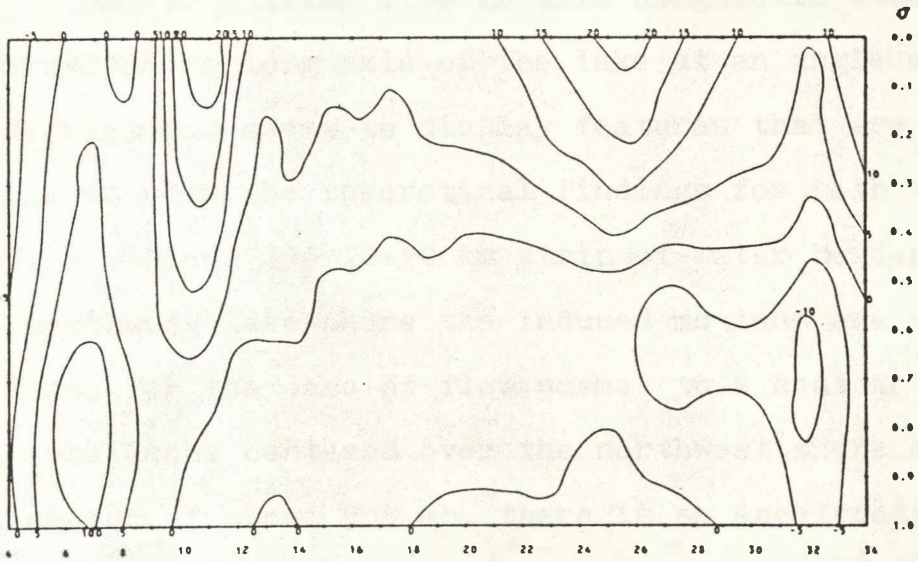

Fig. 44. Cross-section of NVA vertical velocity, ω (10-3 mb s^{-1}), along line B-B of Fig. 2 (0600 GMT October 9, 1972).

case strong winds were induced in the surface layers over the entire heat source in response to an increased pressure gradient force. Downward vertical motions were induced over the warm strip as well as the region upwind; upward motion was induced on the leeward side. Lavoie et al. (1970) obtained similar motion fields for integrations of a primitive equation model simulating flow over Lake Erie in the cool season where the prevailing flow was normal to the long axis of the lake. Thus the heat source normal to the flow was approximately 60 km wide. In the second case convergence is induced over the center of the heat source resulting in upward vertical motion over the strip.

The prevailing flow in this diagnostic study intersects the long axis of the lake at an angle of 30 degrees and seems to display features that are in agreement with the theoretical findings for both types of flow. Along the 10-20 km strip of water bordering the northwest lake-shore the induced motions are similar to those for the case of flow normal to a heat source. The subsidence centered over the northwest shore has its center at about 900 mb, there is an acceleration of the wind at low levels along the shore and upward vertical motion exists leeward of this strip.

Grid points 7-9 at $\sigma = 0.9$ of Fig. 45 depict this increase of wind speed, as does the NVA surface wind field (Fig. 40). The low level wind thereafter decelerates (see Figs. 40 and 45), presumably in response to the decreased pressure gradient force over the lake, giving rise to horizontal convergence over and to the lee of the lake, which is characteristic of flow parallel to the heat source. A plausible mechanism for the local maxima observed along the leeward shore is strong vertical momentum transfer associated with the organized convective activity. Matsumoto et al. (1967) concluded from their study of the dynamics of heavy snowfall over the Japan Sea that strong wind in the lower layers was formed by convective mixing. Furthermore, the strong winds were favorable in maintaining the convergence of the low level system.

The winds at all levels are primarily northwest at 0600 GMT (Fig. 45). In contrast to 1500 GMT, there is now a general backing of the winds with height, except locally in the lower levels.

Fig. 46 is the same as Fig. 36 except the time is for 0600 GMT. The moisture and potential temperature isopleths slope upward from west to east with the largest increase located in the area of greatest

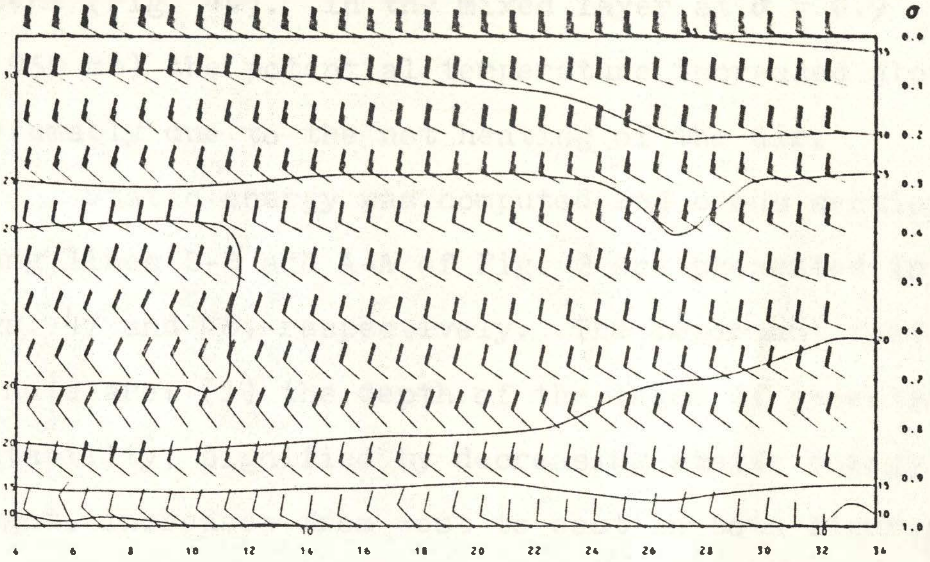

Fig. 45. Same as Fig. 44, except for NVA winds (m s^{-1}).

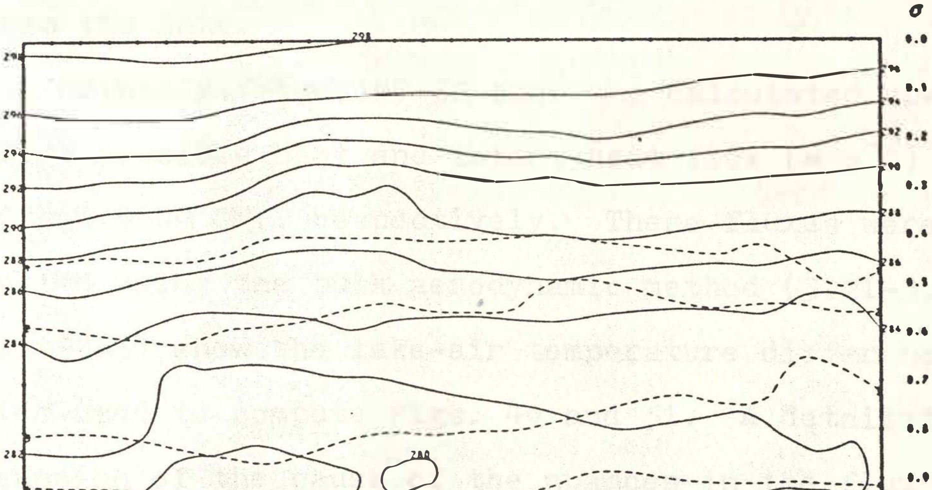

Fig. 46. Same as Fig. 44, except for potential temperature (°K; solid lines) and specific humidity (g kg^{-1}; dashed lines).

ascent (Fig. 44). In the mixed layer at $\sigma = 0.9$ ($\simeq 950$ mb) the potential temperature increased about 2°C presumably due to the net heating of the air.

Static energy was computed and cross sections along lines B-B and A-A of Fig. 2 are presented in Figs. 47 and 48, respectively. The important features to note are: (1) the depth of the layer of potential instability, signified by decreasing static energy with height, increases from west to east in both figures, and (2) along the southern shore of the lake the layer of potential instability is larger than over the center of the lake; both features reflecting the net heating of the low-level air parcels as they follow a trajectory across the lake.

Finally, Figs. 49-52 show the calculated upward surface sensible heat and latent heat flux (w m^{-2}) for 1500 and 0600 GMT, respectively. These fluxes were computed using the bulk aerodynamic method (3.21-3.22). Figs. 53-54 show the lake-air temperature difference fields used to compute Figs. 49 and 51. A detailed discussion of the cause of the nuances in the flux patterns is beyond the scope of this work. As McBean (1975) points out, the complicated flux patterns probably result from local topographical features and other

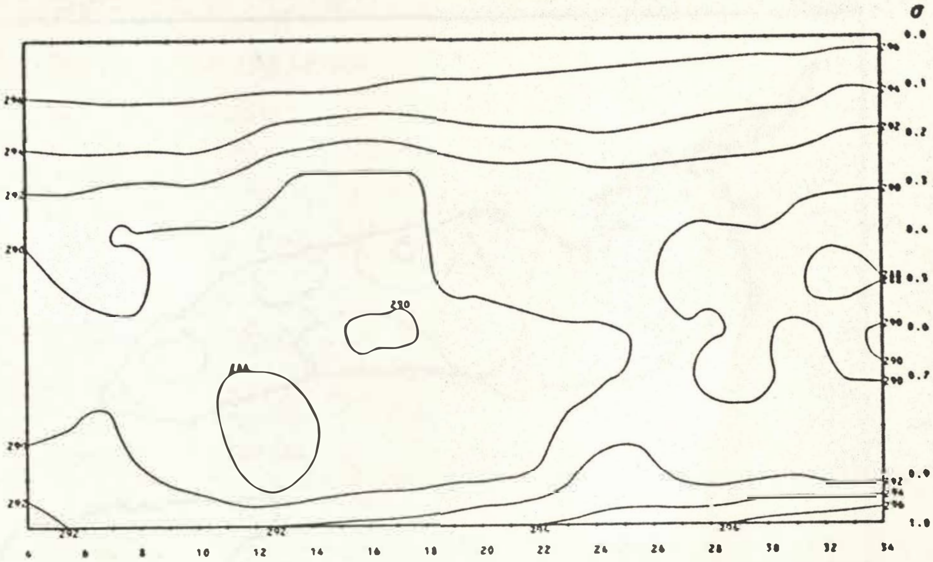

Fig. 47. Same as Fig. 44, except for static energy (J g-1).

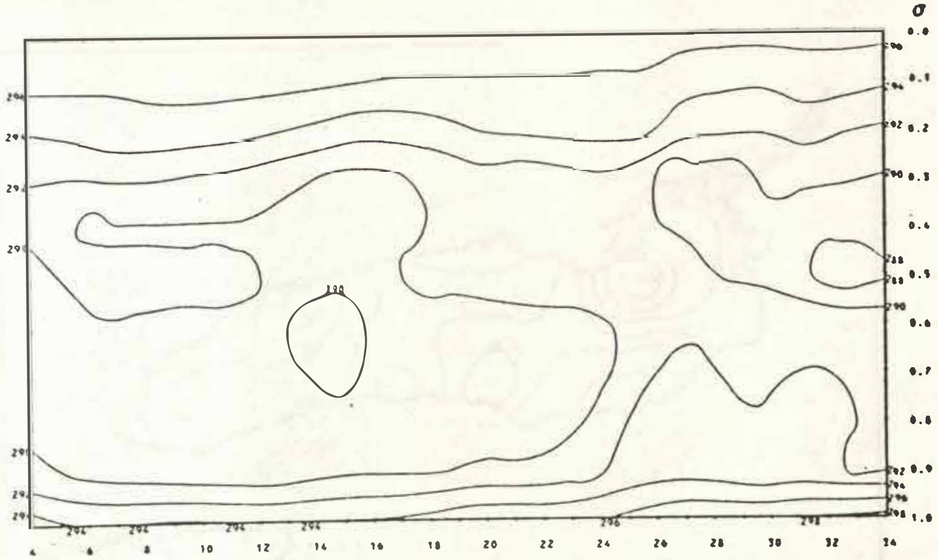

Fig. 48. Same as Fig. 47, except along line A-A of Fig. 2.

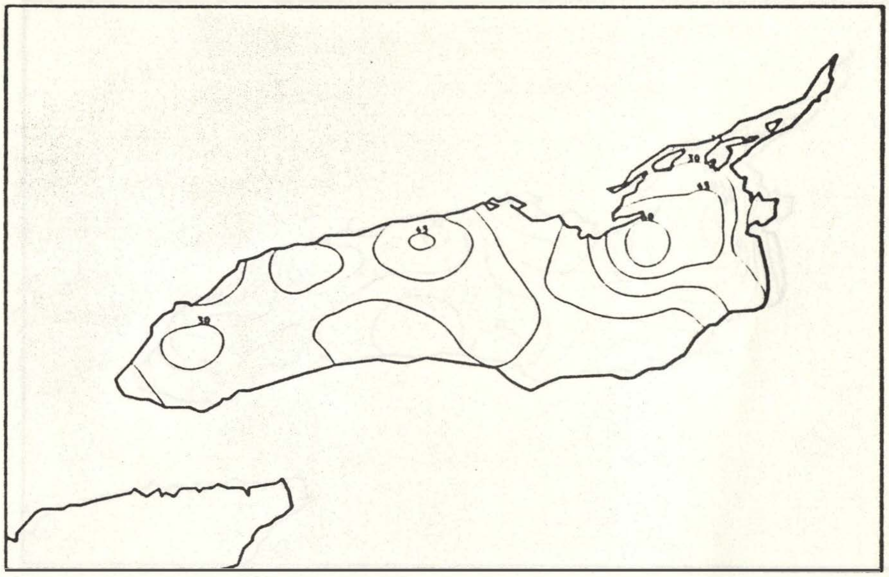

Fig. 49. Surface sensible heat flux (w m^{-2}) at 1500 GMT October 8, 1972.

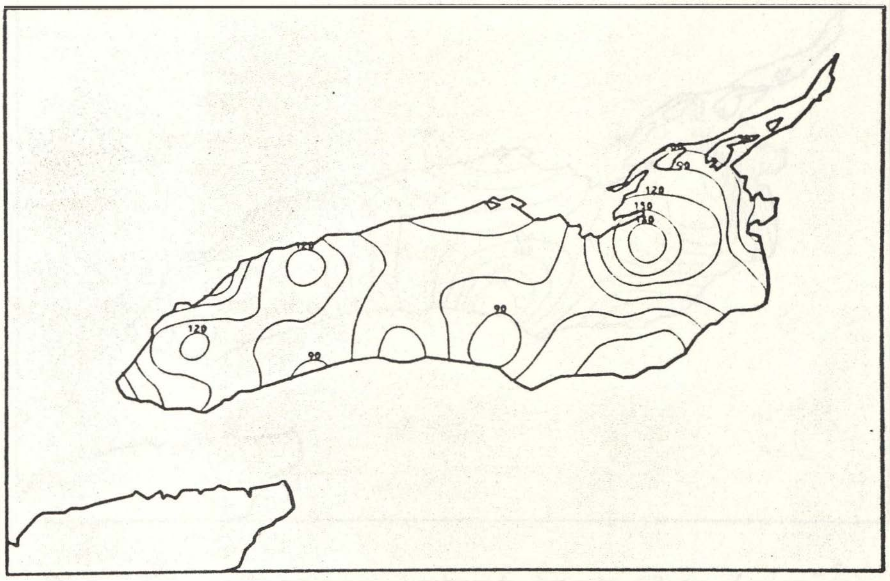

Fig. 50. Surface latent heat flux (w m^{-2}) at 1500 GMT October 8, 1972.

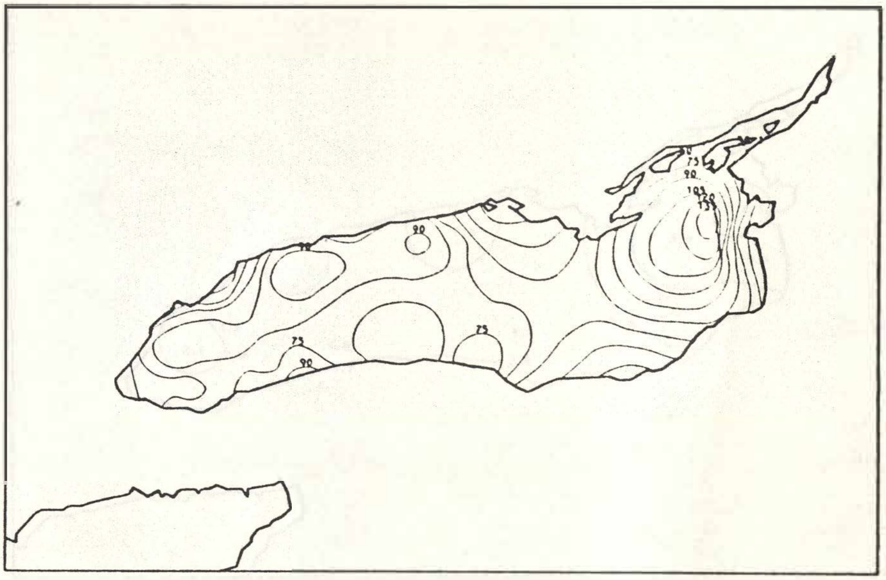

Fig. 51. Surface sensible heat flux (w m^{-2}) at 0600 GMT October 9, 1972.

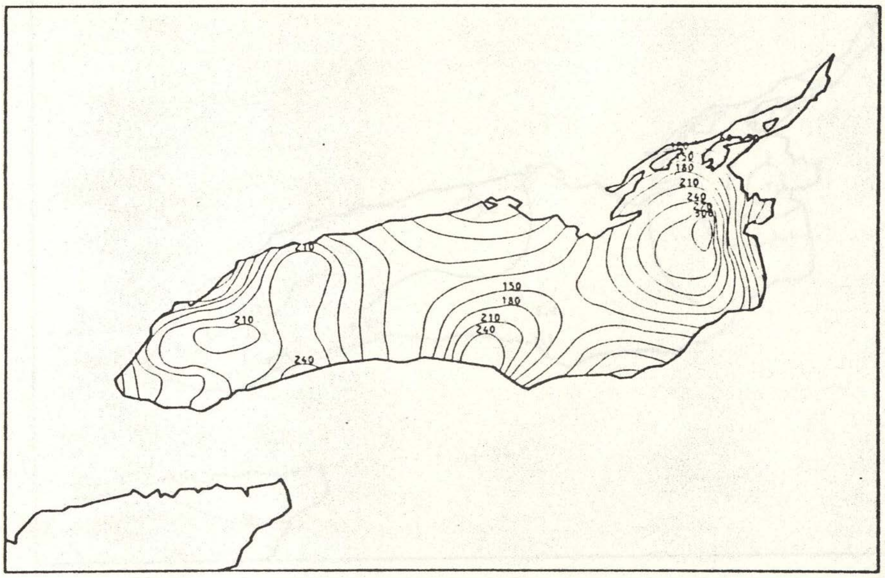

Fig. 52. Surface latent heat flux (w m^{-2}) at 0600 GMT October 9, 1972.

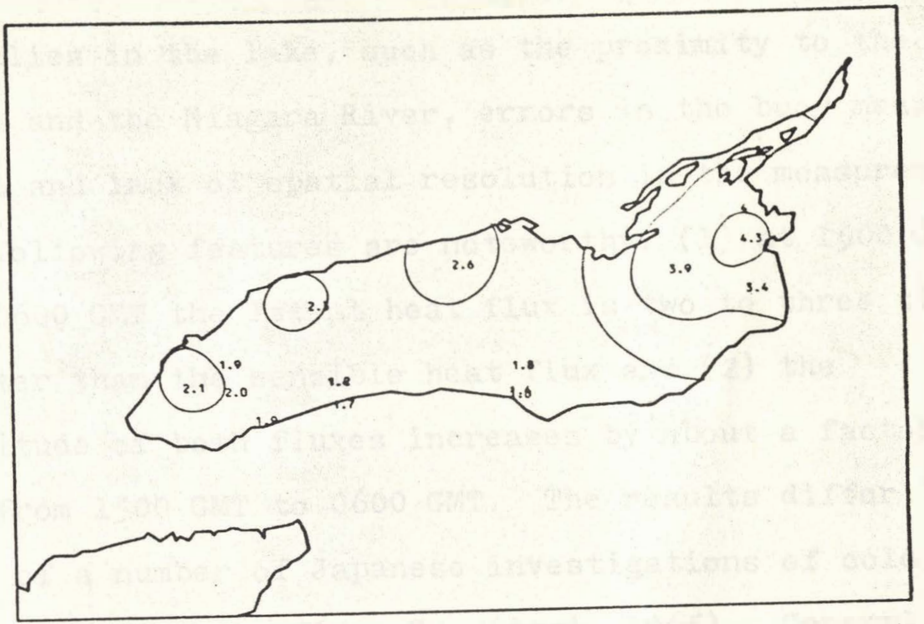

Fig. 53. Lake-air temperature difference (^{o}K) at 1500 GMT October 8, 1972.

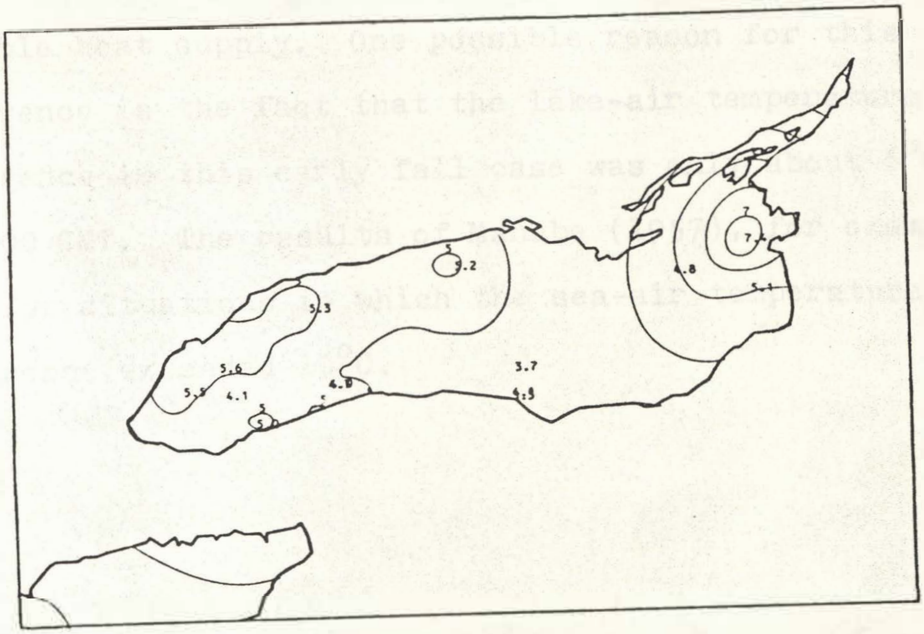

Fig. 54. Lake-air temperature difference (^{o}K) at 0600 GMT October 9, 1972.

anomalies in the lake, such as the proximity to the shore and the Niagara River, errors in the buoy measurements and lack of spatial resolution in the measurements. The following features are noteworthy: (1) at 1500 GMT and 0600 GMT the latent heat flux is two to three times greater than the sensible heat flux and (2) the magnitude of both fluxes increases by about a factor of two from 1500 GMT to 0600 GMT. The results differ from that of a number of Japanese investigations of cold air outbursts over the Japan Sea (Asai, 1965). Generally they found the amount of latent heat supplied through evaporation from the sea reached about half that of the sensible heat supply. One possible reason for this difference is the fact that the lake-air temperature difference in this early fall case was only about 6^{o}C at 0600 GMT. The results of Manabe (1957), for example, were for situations in which the sea-air temperature difference exceeded 10^{o}C.

CHAPTER V

SUMMARY AND CONCLUSIONS

INTRODUCTION

Previous studies of lake related mesoscale phenomena that occur during the fall and early winter have all been hampered by a lack of sufficient data. Thus studies to date have been either of a qualitative nature, in which the effects of the lake are investigated in terms of observable weather or they have been theoretical, in which the behavior of a model designed to simulate the atmosphere is studied for response to variations of the forcing terms that are presumed important in lake related motions.

In this work a new source of observational data, of a spatial and temporal density heretofore not available, have been carefully analyzed for the purpose of studying the over-lake mesoscale structure of the atmosphere. The data were collected over and around Lake Ontario in conjunction with the International Field Year for the Great Lakes. Two times were chosen: (1) when the leading edge of an Arctic air mass accompanied by a complex convective regime was over the lake and (2) fifteen hours later, when the Arctic air mass completely encompassed the region of the lake. As an aid in performing the objective analyses, a variational analysis model was designed and applied at the two times.

RESULTS

From this study it appears that the advance of the Arctic outbreak of 8 October 1972 is preceded by a complex frontal structure that is not evident on the synoptic scale. Over Lake Ontario, accompanying the cold front are three distinct lines of activity, with the lead line about 150 km ahead of the surface front. This is supported by surface pressure traces, wind shift data, and satellite and radar imagery. Analysis of the motion, temperature and moisture structure over the lake reveals the following features:

1. The phase velocity of the frontal structure is calculated to be 17 m s^{-1} or 61 km $hr.^{-1}$.

2. The cumulus activity and the mesoscale surface convergence field are closely interrelated. Convergences averaging $2x10^{-4}$ s^{-1} are associated with the line activity. The leading more intense line of activity has surface convergence values

over 4×10^{-4} s^{-1} and is preceded by a large area encompassing the eastern portion of the lake of equally intense surface divergence.

3. The upper-air structure reflects the line activity. The lead squall line is characterized by a sharp area of subsidence immediately followed by an intense area of upward vertical motion, with values greater than 10×10^{-3} mb sec^{-1} between about 850 mb and 550 mb. Vertical motions associated with the two following lines are equally intense but occur at higher levels. The specific humidity increases rapidly at upper levels across a narrow band coincident with the vertical velocity maximum of the lead squall line.

4. The line activity is caused by a surge of cold air above 900 mb that has advanced ahead of the main Arctic cold air dome. Static stability calculations indicate the main areas of potential instability to be at the location of each line.

5. Because of the small lake-to-air fluxes at this time the effect of the lake upon the mesoscale disturbances as they crossed the lake appear to be minimal. Study of the progression of the line

activity across the lake and information relating to the history of the front prior to its reaching the northwest lake-shore, however, would be necessary to confirm this point. The upper-air data unfortunately were not of a sufficient spatial or temporal density to permit such an investigation. Surface sensible heat flux varied from 30 to 60 w m^{-2} over the lake while latent heat flux was larger and varied from 90 to 160 w m^{-2}.

At 0600 GMT the following day a typical fall-winter lake-effect phenomenon has set up. Cumulus activity resulting in rain showers develops along the southern and southeast shore of the lake at this time and continues with variations of intensity for the next eighteen hours. The mesoscale features found to be characteristic of this situation are:

1. The low-level air over the lake is generally undergoing cyclonic vorticity presumably caused by the large sensible heat flux from lake to air.

2. Areas of surface convergence are primarily located in the southeast section of the lake. Values range from $2\text{-}4 \times 10^{-4}$ s^{-1}. This agrees with values calculated by McVehil et al. (1967) but are nearly

an order of magnitude greater than model predictions made by Lavoie (1968). Peace and Sykes (1966) found convergences somewhat higher ($5\text{-}9\times10^{-4}$ s^{-1}) but their calculations were for a very narrow snow-band wind-shift line over the lake.

3. The vertical velocity pattern reveals ascending motion from $1\text{-}10\times10^{-3}$ mb s^{-1} over almost the entire lake from the surface to 700 mb. Above this level the air is generally subsiding. Maximum upward vertical velocity occurs between 900-800 mb along and just inland of the southeast shore. Synoptic scale subsidence is evidently affected by the lake resulting in a large area northwest of the lake of more intense low level downward vertical motion. This appears in-line with the theoretical calculations for flow over a narrow heat source.

4. A layer of potential instability with base at the surface is found to increase both from west to east and north to south across the lake in response to the net heating effect of the lake as the air follows a trajectory from northwest to southeast.

5. Surface sensible heat flux varied from 75 to 135 $w\ m^{-2}$ over the lake; latent heat flux from 210 to 300 $w\ m^{-2}$.

CONCLUSIONS

It is believed that the value of this work lies in the detailed analyses that have been obtained of mesoscale features accompanying an Arctic outbreak over a warm lake during the cool season. Of primary interest is the vertical velocities in the lower atmosphere associated with the mesoscale phenomena. This is the first diagnostic study presented with such detail to be made of the over-lake atmospheric state. Although no attempt is made to generalize the results of this case study, the case is typical of many situations occurring over the Great Lakes region in the fall and early winter. Thus, results presented here will hopefully serve as a basis for comparison for other diagnostic and theoretical modelling studies of these phenomena.

These results also indicate that the NVA technique can be a very useful tool in studies of complex atmospheric motion. Although the procedure involves the solution of complex systems of equations the application of the method is straightforward and can be readily programmed for solution by standard methods on large electronic computers. It has been shown that when sufficient data are available NVA can be successfully used to extrapolate this information. Finally, this study further demonstrates the possible beneficial use of this technique for mesoscale model initialization where initial conditions play a prime role in the short-range forecast.

APPENDIX A

DERIVATION OF CONSTRAINT EQUATIONS IN σ COORDINATES

The equations of constraint are developed for a generalization of Phillips (1957) σ or terrain following coordinate system. The vertical transformation is given by

$$\sigma = \frac{P - P^*}{P_s - P^*} \tag{1}$$

P_s represents the pressure at the terrain surface and P^* the pressure at an upper surface. A variation of the coordinate system is used at the National Meteorological Center for two operational primitive equation models (1968). This discussion is similar to that presented by Hovermale (1965) but differs in that here P^* is not considered a material surface. We begin with the hydrostatic equation in the p-coordinate system.

$$\frac{\partial \phi}{\partial P} = -\frac{1}{\rho} = -\frac{RT}{P} = -\frac{R\Theta}{P}\left[\frac{P}{P_0}\right]^{R/c_p} \tag{2}$$

where θ, the potential temperature of a gas at temperature T and pressure p, is defined to be the temperature obtained by adiabatic expansion or compression to 1000 mb. From calculus and using 2

$$\frac{\partial \phi}{\partial \sigma} = \frac{\partial \phi}{\partial P}\frac{\partial P}{\partial \sigma} = \frac{R\Theta}{P}\left[\frac{P}{P_0}\right]^{R/c_p}\frac{\partial P}{\partial \sigma} \tag{3}$$

letting

$$\pi = \left[\frac{P}{P_0}\right]^{R/c_p} \tag{4}$$

and thus

$$\frac{\partial \pi}{\partial \sigma} = \frac{R}{c_p P}\left[\frac{P}{P_0}\right]^{R/c_p} \frac{\partial P}{\partial \sigma} \tag{5}$$

and comparing 3 and 5 we arrive at a form of the hydrostatic equation in the σ system.

$$\frac{\partial \phi}{\partial \sigma} = - c_p \theta \frac{\partial \pi}{\partial \sigma} \tag{6}$$

To transform the horizontal momentum equations we note that the rate of change of any variable ϕ with respect to x along a P surface may be given by

$$\left.\frac{\partial \phi}{\partial x}\right)_P = \left.\frac{\partial \phi}{\partial x}\right)_\sigma - \left.\frac{\partial \phi}{\partial P}\right)_x \left.\frac{\partial P}{\partial x}\right)_\sigma \tag{7}$$

If we now let ϕ be the geopotential, from 2

$$\left.\frac{\partial \phi}{\partial P}\right)_x = - \frac{R\theta\pi}{P} \tag{8}$$

and from 4

$$\left.\frac{\partial P}{\partial x}\right)_\sigma = \frac{P_0 C_p}{R}\left[\frac{P}{P_0}\right]^{1-R/c_p} \left.\frac{\partial \pi}{\partial x}\right)_\sigma \tag{9}$$

Substituting 8 and 9 in 7 gives

$$\left.\frac{\partial \phi}{\partial x}\right)_p = \left.\frac{\partial \phi}{\partial x}\right)_\sigma + \left. c_p \theta \frac{\partial \pi}{\partial x}\right)_\sigma \tag{10}$$

Using the expansion of the total derivative in the σ system and 10, the horizontal momentum equations may be written

$$\frac{\partial u}{\partial t} + u\frac{\partial u}{\partial x} + v\frac{\partial u}{\partial y} + \dot{\sigma}\frac{\partial u}{\partial \sigma} = -\frac{\partial \phi}{\partial x} - c_p \theta \frac{\partial \pi}{\partial x} + fv + F_x \tag{11}$$

$$\frac{\partial v}{\partial t} + u\frac{\partial v}{\partial x} + v\frac{\partial v}{\partial y} + \dot{\sigma}\frac{\partial v}{\partial \sigma} = -\frac{\partial \phi}{\partial y} - c_p \theta \frac{\partial \pi}{\partial y} - fu + F_y \tag{12}$$

where $\dot{\sigma} = d\sigma/dt$, f is the coriolis parameter and F_x and F_y are frictional forces.

The energy and moisture conservation equations transform directly to

$$\frac{\partial \theta}{\partial t} + u\frac{\partial \theta}{\partial x} + v\frac{\partial \theta}{\partial y} + \dot{\sigma}\frac{\partial \theta}{\partial \sigma} = \frac{Q}{c_p \pi} \tag{13}$$

where Q includes sensible and latent heating ratio.

$$\frac{\partial q}{\partial t} + u\frac{\partial q}{\partial x} + v\frac{\partial q}{\partial y} + \dot{\sigma}\frac{\partial q}{\partial \sigma} = S \tag{14}$$

where S is specific humidity generation.

The mass continuity equation in the P system may be written

$$\left.\frac{\partial u}{\partial x}\right)_p + \left.\frac{\partial v}{\partial y}\right)_p + \left.\frac{\partial \omega}{\partial P}\right)_{x,y} = 0 \qquad (15)$$

where $\omega = dP/dt$

Similarly to 7 we may write

$$\left.\frac{\partial u}{\partial x}\right)_p = \left.\frac{\partial u}{\partial x}\right)_\sigma - \frac{(\partial u/\partial \sigma)_x (\partial P/\partial x)_\sigma}{(\partial P/\partial \sigma)_x} \qquad (16)$$

and

$$\left.\frac{\partial v}{\partial y}\right)_p = \left.\frac{\partial v}{\partial y}\right)_\sigma - \frac{(\partial v/\partial \sigma)_v (\partial P/\partial y)_\sigma}{(\partial P/\partial \sigma)_y} \qquad (17)$$

But noting that

$$\frac{\partial P}{\partial \sigma} = P_s - P^* = \Delta P \qquad (18)$$

and if P* = constant

$$\frac{\partial P}{\partial x} = \sigma \frac{\partial P_s}{\partial x} \qquad (19)$$

then 16 and 17 become

$$\left.\frac{\partial u}{\partial x}\right)_p = \left.\frac{\partial u}{\partial x}\right)_\sigma - \frac{\sigma}{\Delta P}\frac{\partial P_s}{\partial x}\frac{\partial u}{\partial \sigma} \qquad (20)$$

$$\left.\frac{\partial v}{\partial y}\right)_p = \left.\frac{\partial v}{\partial y}\right)_\sigma - \frac{\sigma}{\Delta P}\frac{\partial P_s}{\partial y}\frac{\partial v}{\partial \sigma} \qquad (21)$$

Expanding the total derivative we may write

$$\omega = \frac{\partial P}{\partial t} + u\frac{\partial P}{\partial x} + v\frac{\partial P}{\partial y} + \dot{\sigma}\frac{\partial P}{\partial \sigma} \qquad (22)$$

From 1

$$\frac{\partial P}{\partial t} = \sigma\frac{\partial P_s}{\partial t}\ ;\ \frac{\partial P}{\partial x} = \sigma\frac{\partial P_s}{\partial x}\ ;\ \frac{\partial P}{\partial y} = \sigma\frac{\partial P_s}{\partial y}\ ;\ \frac{\partial P}{\partial \sigma} = \Delta P \qquad (23)$$

Using 23 in 22

$$\omega = \sigma\left(\frac{\partial P_s}{\partial t} + u\frac{\partial P_s}{\partial x} + v\frac{\partial P_s}{\partial y}\right) + \dot{\sigma}\,\Delta P \qquad (24)$$

but we note

$$\frac{\partial \omega}{\partial P} = \frac{\partial \sigma}{\partial P}\frac{\partial \omega}{\partial \sigma} = \frac{1}{\Delta P}\frac{\partial \omega}{\partial \sigma} \qquad (25)$$

Thus differentiating 24 with respect to **σ** and substituting in 25 yields

$$\frac{\partial \omega}{\partial P} = \frac{1}{\Delta P}\Bigg(\frac{\partial P_s}{\partial t} + u\frac{\partial P_s}{\partial x} + v\frac{\partial P_s}{\partial y} + \sigma\left[\frac{\partial u}{\partial \sigma}\frac{\partial P_s}{\partial x} + \frac{\partial v}{\partial \sigma}\frac{\partial P_s}{\partial y}\right] + \Delta P\frac{\partial \dot{\sigma}}{\partial \sigma} \qquad (26)$$

Using 20, 21 and 26 in 15 yields the mass continuity equation in the σ system.

$$\frac{\partial u}{\partial x} + \frac{\partial v}{\partial y} + \frac{\partial \dot{\sigma}}{\partial \sigma} + \frac{1}{\Delta P}\left(\frac{\partial P_s}{\partial t} + u\frac{\partial P_s}{\partial x} + v\frac{\partial P_s}{\partial y}\right) = 0 \qquad (27)$$

Equation 27 may be integrated to obtain $\dot{\sigma}$ at any level above the surface.

$$\dot{\sigma} = -\int_1^{\sigma}\left(\frac{\partial u}{\partial x} + \frac{\partial v}{\partial y}\right)d\sigma - \frac{1}{\Delta P}\left\{\frac{\partial P_s}{\partial x}\int_1^{\sigma} u\,d\sigma + \frac{\partial P_s}{\partial y}\int_1^{\sigma} v\,d\sigma\right\} + \frac{(1-\sigma)}{\Delta P}\frac{\partial P_s}{\partial t} \qquad (28)$$

Since we did not require P* to be a material surface particles are not constrained to remain at this surface. Thus while the kinematic boundary condition requires $\dot{\sigma}$ = o at σ = 1; $\dot{\sigma}$ is not necessarily o at P*.

APPENDIX B

DISCUSSION OF NVA ADJUSTMENT

In this section some comparisons between the interpolated fields and the final adjusted NVA fields are briefly discussed.

Fig. 55, the vertical velocity at $\sigma = .7$ computed from interpolated fields at 1500 GMT, when compared to Fig. 33 clearly demonstrates the importance of using the NVA model. In the eastern part of Lake Ontario in the vicinity of the lead line of activity, which was marked by strong surface convergence preceded by an area of strong divergence (Fig. 28), the vertical velocities computed by NVA are in much better agreement with the surface features. The weak ascending motion over the area of surface divergence has been transformed to subsiding motion and the weak ascending air in the vicinity of the squall line has been intensified as have the motions over the other two lines of activity.

The interpolated surface wind fields at 1500 GMT and 0600 GMT (Figs. 56 and 57) have been substantially modified (see Figs. 31 and 40). The nearly circular patterns of the interpolated fields reflect the use of a decreasing radius of influence in the successive

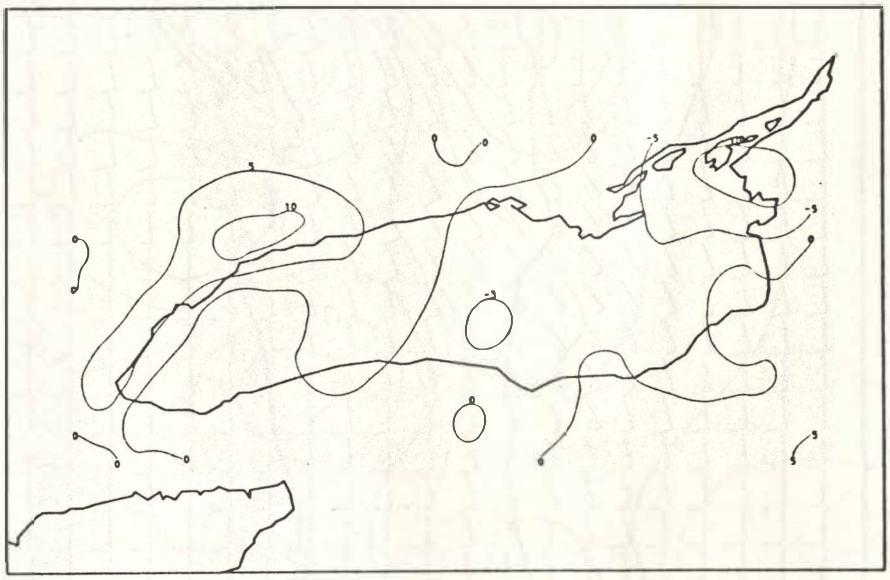

Fig. 55. Vertical velocity, ω (10^{-3} mb s^{-1}) at σ = .7 ($\approx$ 850 mb; 0600 GMT October 9, 1972) calculated from initial interpolated fields.

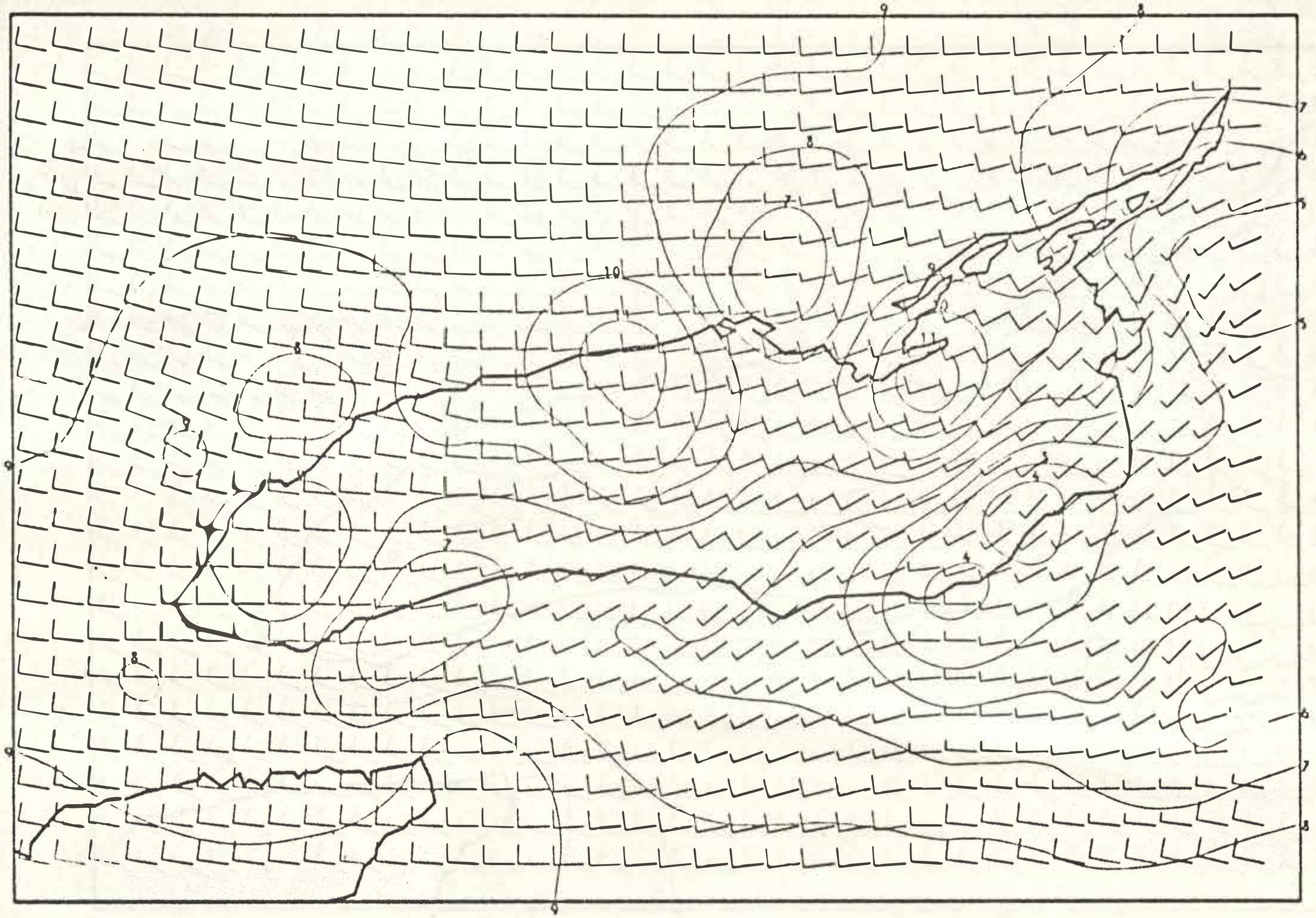

Fig. 56. Initial interpolated surface winds (1500 GMT October 8, 1972).

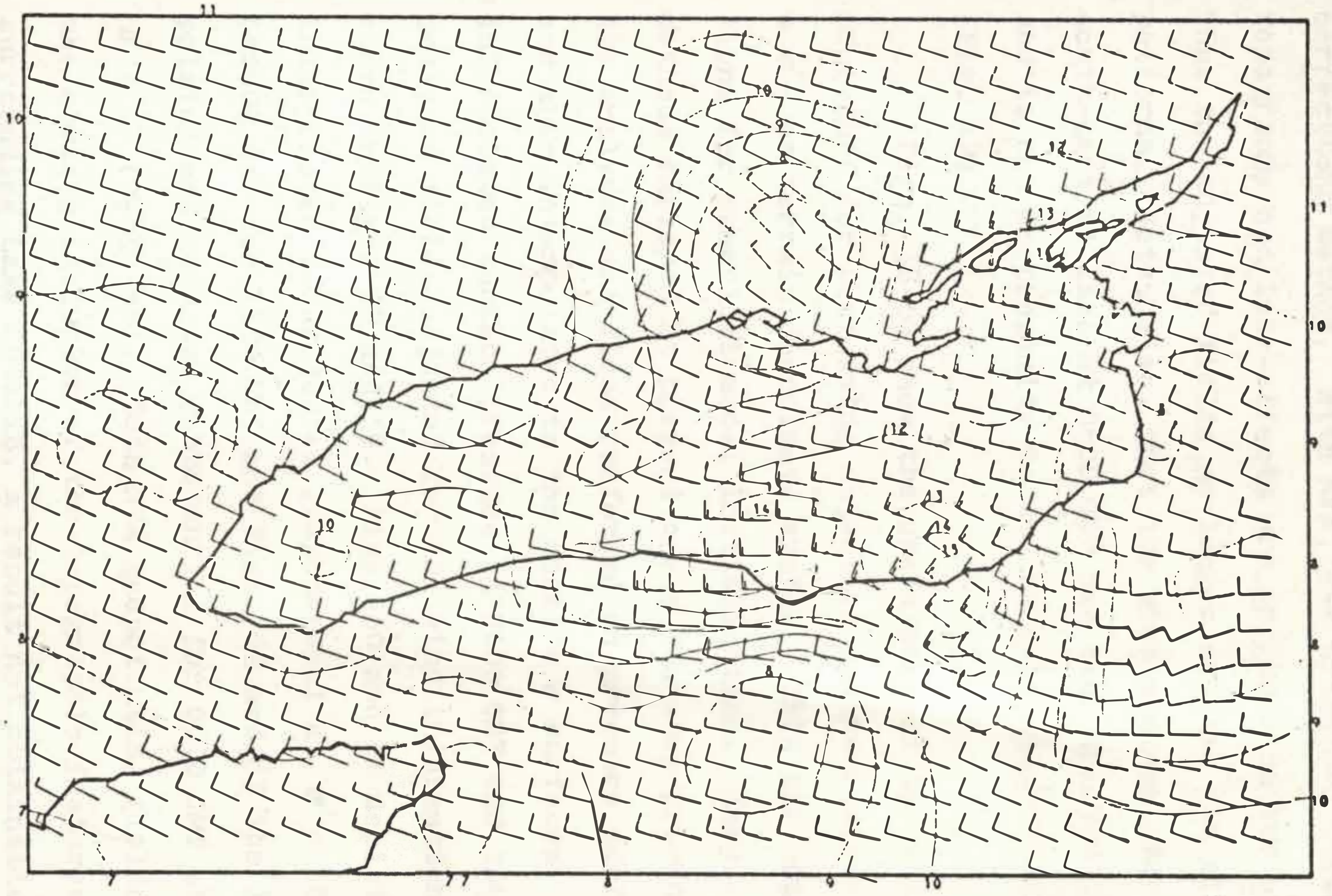

Fig. 57. Initial interpolated surface winds (0600 GMT October 9, 1972).

corrections method. With NVA, the dynamics, including topography and lake-effects are included in the analysis. Thus the adjusted fields no longer contain the circular patterns. Note, also, that the wind maximum over the south-central lake at 0600 GMT has been shifted inland and is now in proximity to the band of radar echos (Fig. 42).

Figs. 58-63 show the usefulness of the NVA procedure for performing objective analyses directly on a σ - or terrain coordinate system. This has implications for numerical model initialization. Many of the methods employed at present use a two step procedure; the analyses are first performed on pressure surfaces and then interpolated to the model's σ surfaces. The interpolated surface pressure at 0600 GMT and the final analyzed field, adjusted for the wind information is shown in Figs. 58 and 59. Figs. 60 and 61 depict the interpolated and adjusted geopotential at $\sigma = .8$ ($\simeq$900 mb) for 1500 GMT and Figs. 62 and 63 the interpolated and adjusted geopotential for 0600 GMT at $\sigma = .3$ ($\simeq$ 650 mb). Both NVA geopotential fields show the obvious inclusion of the topographic features surrounding Lake Ontario, a result not obtainable by most objective analysis techniques.

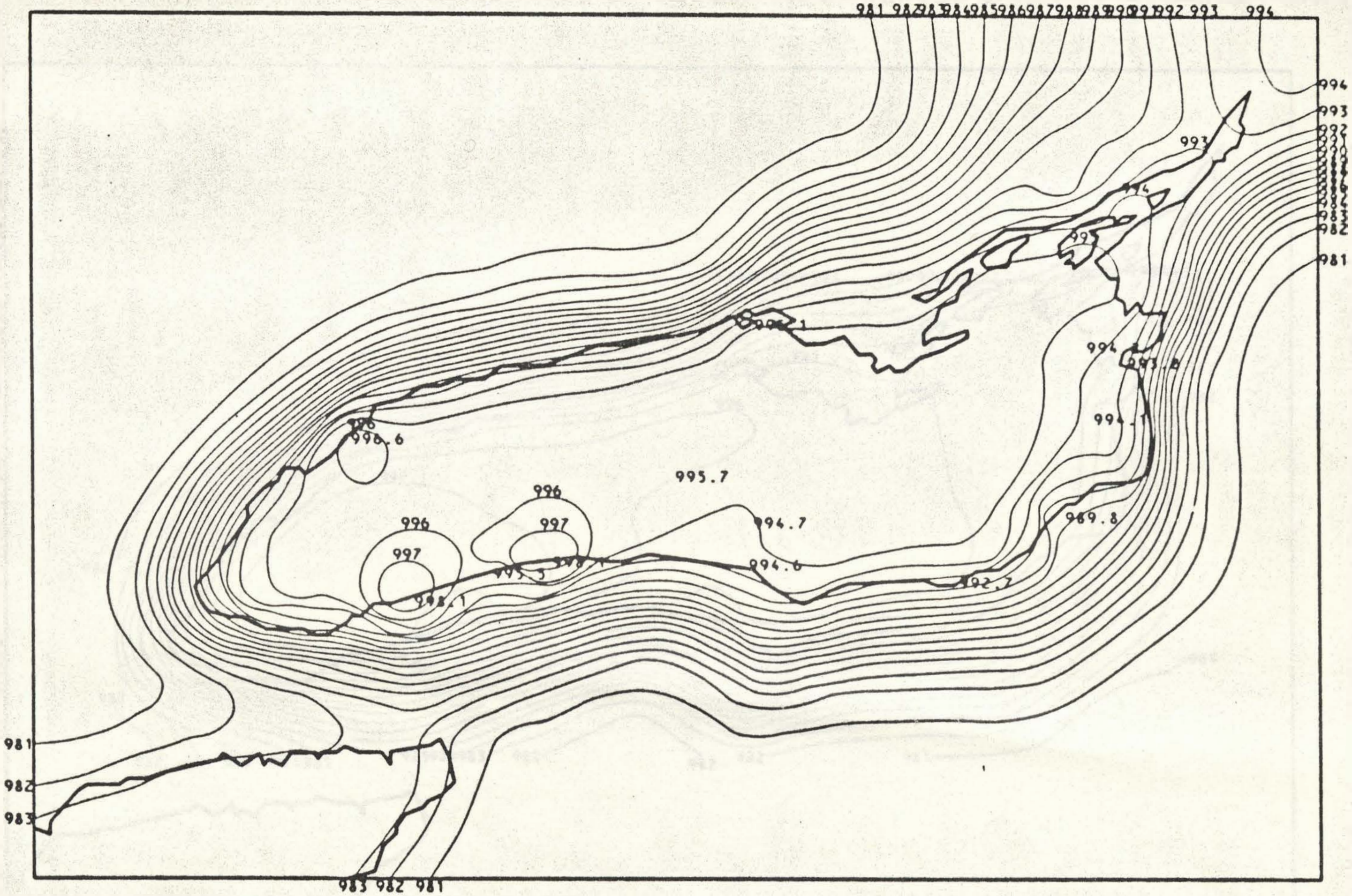

Fig. 58. Initial interpolated surface pressure (0600 GMT October 9, 1972).

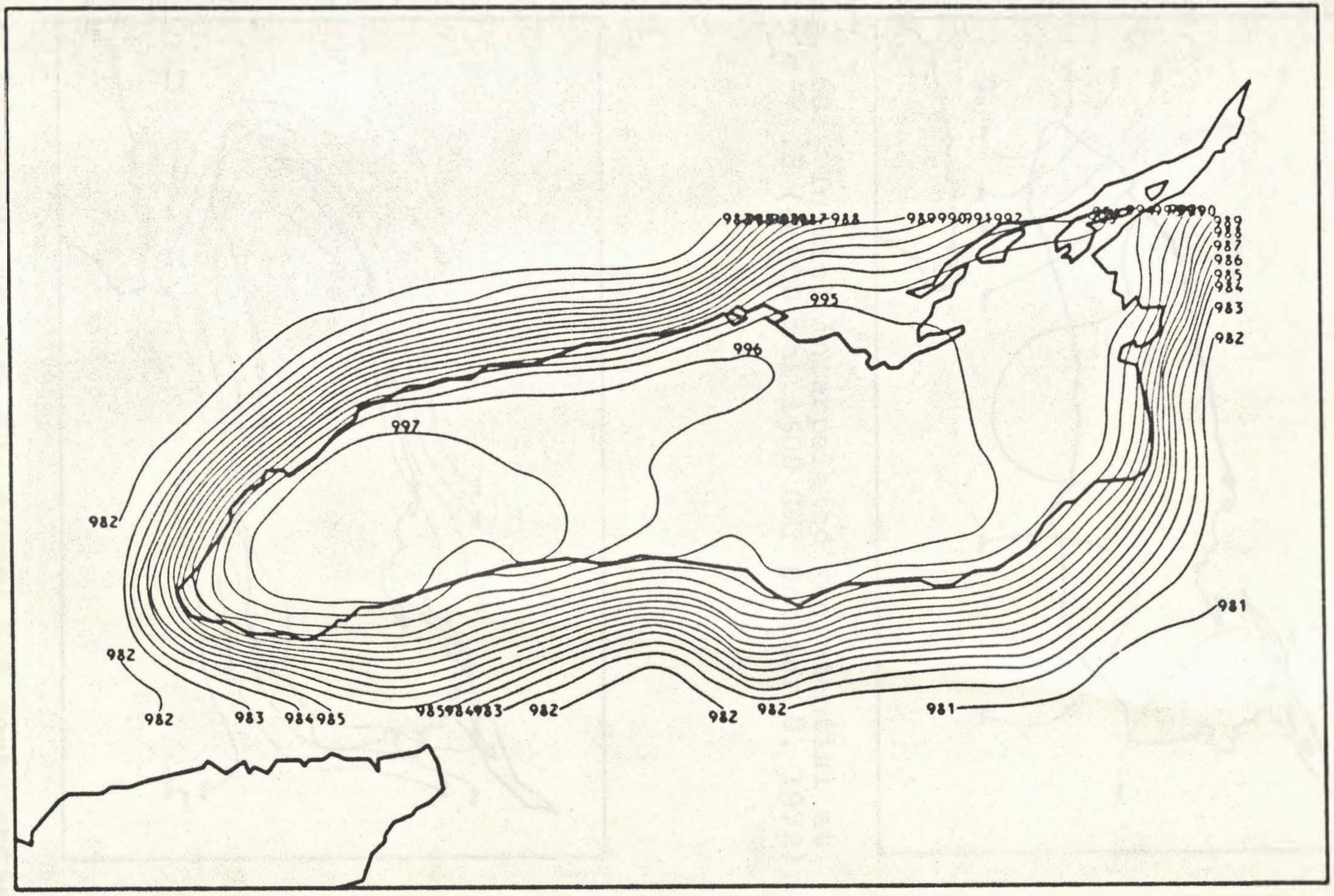

Fig. 59. NVA surface pressure (0600 GMT October 9, 1972).

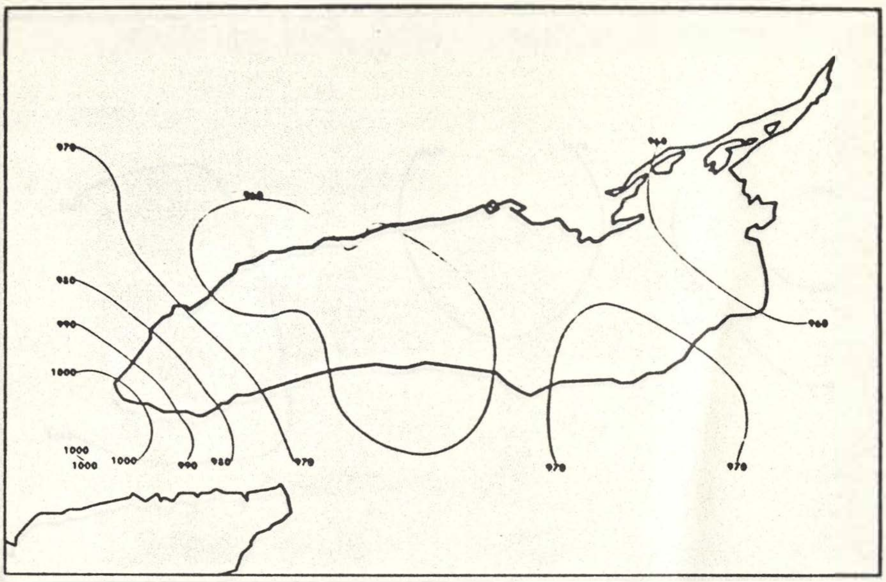

Fig. 60. Initial interpolated geopotential at σ = .8 ($\simeq$900 mb; 1500 GMT October 8, 1972).

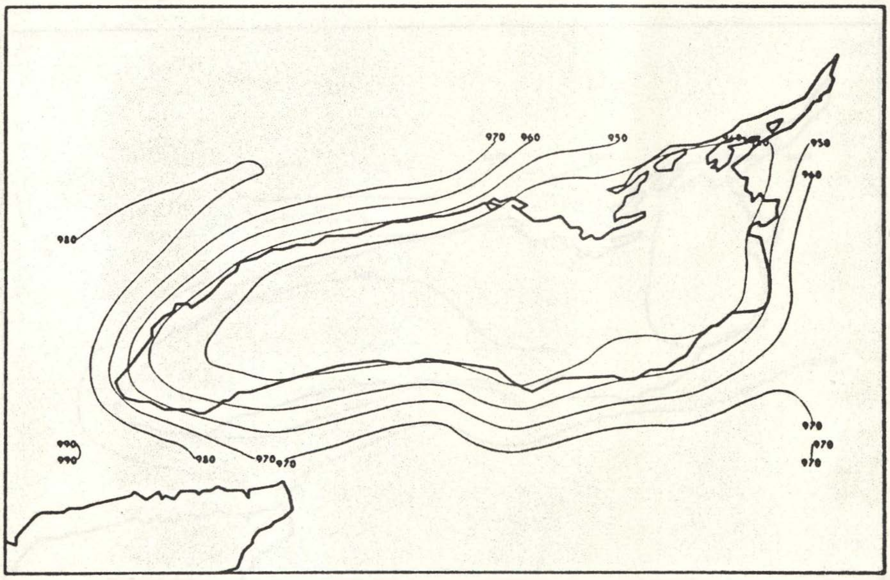

Fig. 61. Same as Fig. 60, except NVA geopotential.

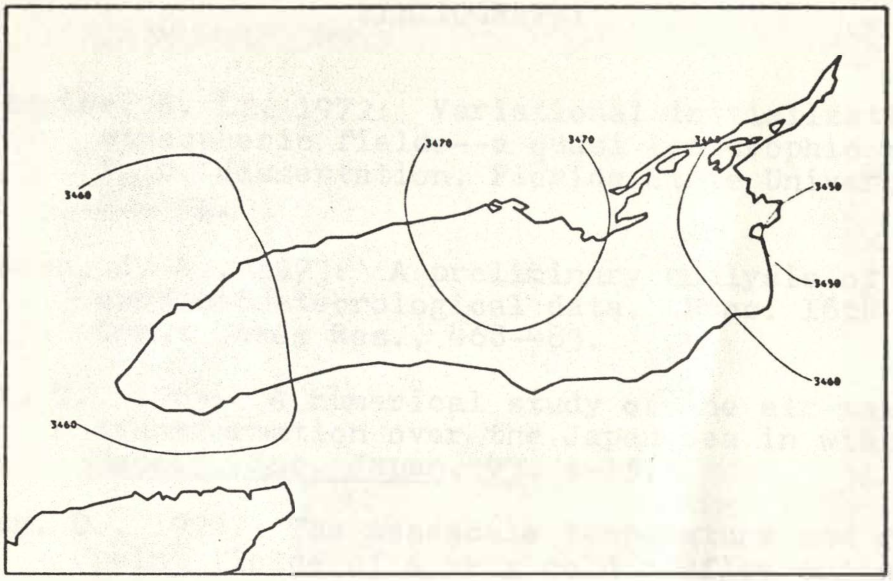

Fig. 62. Initial interpolated geopotential at σ = .3 ($\simeq$ 650 mb; 0600 GMT October 9, 1972).

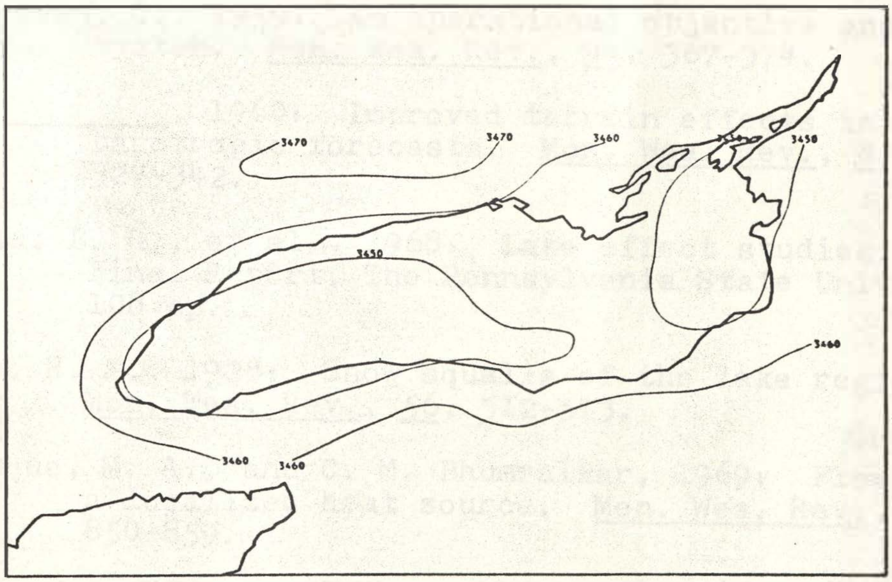

Fig. 63. Same as Fig. 62, except NVA geopotential.

BIBLIOGRAPHY

Achtemier, G. L., 1972: Variational initialization of atmospheric fields--a quasi geostrophic model. Ph.D. dissertation, Florida State University, 211 pp.

Almazan, J. A., 1973: A preliminary analysis of IFYGL surface meteorological data. Proc. 16th Conf. Great Lakes Res., 468-483.

Asai, T., 1965: A numerical study of the air-mass transformation over the Japan Sea in winter. *Meteor. Soc. Japan, 43,* 1-15.

Baker, D., 1976: The mesoscale temperature and dew point fields of a very cold airflow across the Great Lakes. To be published in *Mon. Wea. Rev.*

Bergthórsson, P. and B. Döös, 1955: Numerical weather map analysis. *Tellus,* *7*, 329-340.

Burke, C. J., 1945: Transformation of polar continental air to polar maritime air. *J. Meteor., 2,* 94-112.

Cressman, G., 1959: An operational objective analysis system. *Mon. Wea. Rev.,* *94*, 367-374.

__________, 1960: Improved terrain effects in barotropic forecasts. *Mon. Wea. Rev., 8,* 327-342.

Davis, L. G., et al., 1968: Lake effect studies. Final Report, The Pennsylvania State University, 108 pp.

Dole, R. M., 1928: Snow squalls of the lake region. *Mon. Wea. Rev.,* *56*, 512-513.

Estoque, M. A., and C. M. Bhumralkar, 1969: Flow over a localized heat source. *Mon. Wea. Rev., 97,* 850-859.

Haltiner, G. J., and F. Martin, 1957: Dynamical and physical meteorology. New York, McGraw-Hill, 470 pp.

BIBLIOGRAPHY (continued)

Haltiner, G. J., 1971: Numerical weather prediction. New York, Wiley and Sons, 317 pp. (see p. 263).

Harrison, H. T., 1939: Terminal weather on the Chicago-New York Airway. United Airlines Transport Corporation, 35 pp.

Hart, H. B., 1967: Meteorological scaling theory, energetic consistency constraints, and their application to numerical models under development at Hq Third Weather Wing. Aerospace Sciences Technical Note 15, 55 pp.

Hess, S., 1959: Introduction to theoretical meteorology. New York, Holt, 362 pp. (see p. 179).

Hovermale, J., 1965: A non-linear treatment of the problem of airflow over mountains. Ph.D. dissertation, The Pennsylvania State University, 88 pp.

Kaplan, M. L., and D. A. Paine, 1972: A macroscale-mesoscale numerical model of intense baroclinic development. J. Appl. Meteor., 1224-1235.

Klein, W. H., 1946: Modification of polar air over water. J. Meteor., 3, 100-101.

Kondo, J., 1975: Air-sea bulk transfer coefficients in diabatic conditions. Boundary Layer Met., 9, 91-112.

Kreitzberg, C., and A. Brown, 1970: Mesoscale weather systems within an occlusion. J. Appl. Meteor., 9, 417-432.

Lanczos, C., 1970: The variational principles of mechanics. 4th ed. University of Toronto Press, 418 pp. (see p. 68).

Lansing, L., 1965: Air mass modification by Lake Ontario during the April-November period. Great Lakes Research Division, The University of Michigan, Pub. No. 13, 257-261.

BIBLIOGRAPHY (continued)

Lavoie, R. L., 1968: A mesoscale numerical model and lake-effect storms. Ph.D. dissertation, The Pennsylvania State University, 102 pp.

__________, et al., 1970: Investigations of lake effect storms. Final Report, The Pennsylvania State University, 127 pp.

__________, 1972: A mesoscale numerical model of lake-effect storms. J. Atmos. Sci., 29, 1025-1040.

Lenschow, D. H., 1973: Two examples of planetary boundary layer modification over the Great Lakes. J. Atmos. Sci., 30, 568-581.

Lewis, J. M., and T. H. Grayson, 1972: The adjustment of surface wind and pressure by Sasaki's variational matching technique. J. Appl. Meteor., 11, 586-597.

__________, 1972: An operational upper air analysis using the variational method. Tellus, 24, 514-530.

Lumley, J. L., and H. A. Panofsky, 1964: The structure of atmospheric turbulence. New York, Wiley and Sons, 239 pp.

Manabe, S., 1957: On the modification of air-mass over the Japan Sea when the outburst of cold air predominates. J. Meteor. Soc. Japan, 35, 1-16.

Matsumoto, S., et al., 1967a: A synoptic and dynamic study on the three dimensional structure of mesoscale disturbances observed in the vicinity of a cold vortex center. Meteor. Soc. Japan, 45, 64-82.

__________, et al., 1967b: Cumulus activities in relation to the mesoscale convergence field. Meteor. Soc. Japan, 45, 292-305.

BIBLIOGRAPHY (continued)

McBean, G., 1975: Turbulent fluxes over Lake Ontario during a cold frontal passage. Can. Meteor. Soc., 13, 37-48.

McVehil, G. E., and R. L. Peace, 1965: Project lake effect: a study of interactions between the Great Lakes and the atmosphere. Cornell Aeronautical Laboratory, Inc., Final Report, 50 pp.

______________, and R. L. Peace, 1966: Project lake effect: a study of lake effect snowstorms. Cornell Aeronautical Laboratory, Inc. Final Report, 52 pp.

______________, et al., 1967: Project lake effect: a study of lake effect snowstorms. Cornell Aeronautical Laboratory, Inc., Final Report, 80 pp.

______________, et al., 1968: The structure and dynamics of lake-effect snowstorms. Cornell Aeronautical Laboratory, Inc., Final Report, 49 pp.

Miyakoda, K., 1961: Contribution to numerical weather prediction - computation with finite difference. Geophysical Institute, Tokyo University, 190 pp.

Peace, Jr., R. L., and R. B. Sykes Jr., 1966: Mesoscale study of a lake effect snow storm. Mon. Wea. Rev., 94, 495-507.

Petterssen, S., 1956: Weather analysis and forecasting. New York, McGraw-Hill, 1, 428 pp. (see p. 325).

Phillips, D. W., and J. W. McCulloch, 1972: The climate of the Great Lakes basin. Environment Canada, Climatological Studies, 20, 40 pp.

Phillips, N., 1957: A coordinate system having some special advantages for numerical forecasting. J. Meteor., 14, 184-185.

BIBLIOGRAPHY (continued)

Pond, S., et al., 1971: Measurements of the turbulent fluxes of momentum, moisture and sensible heat over the ocean. J. Atmos. Sci., 28, 901-917.

Rao, G. B., 1971: Some mesoscale features of the initial fields of motion and temperature for a lake-induced winter disturbance. J. Appl. Meteor., 10, 694-702.

Rasmusson, E. M., and J. A. McCulloch, 1974: The IFYGL lake meteorology program. Unpublished manuscript, National Oceanic and Atmospheric Administration, 10 pp.

Remick, J. T., 1942a: The effect of Lake Erie on the local distribution of precipitation in winter (I). Bull. Amer. Meteor. Soc., 23, 1-4.

____________, 1942b: The effect of Lake Erie on the local distribution of precipitation in winter (II). Bull. Amer. Meteor. Soc., 23, No. 3, 111-117.

Remson, et al., 1971: Numerical methods in subsurface hydrology. New York, Wiley and Sons.

Roll, H., 1965: Physics of the marine atmosphere. Academic Press, 426 pp.

Sasaki, Y., 1958: An objective analysis based on the variational method. J. Meteor. Soc. Japan, 36, 77-88.

__________, 1968: Numerical variational method of objective analysis: principle of initialization. Report No. 10, The University of Oklahoma, 21 pp.

__________, and J. M. Lewis, 1970: Numerical variational objective analysis of the planetary boundary layer in conjunction with squall line formation. Meteor. Soc. Japan, 48, 381-399.

__________, 1970a: Some basic formalisms in numerical variational analysis. Mon. Wea. Rev., 98, 875-883.

BIBLIOGRAPHY (continued)

Sasaki, Y., 1970b: Numerical variational analysis formulated under the constraints as determined by longwave equations and a low-pass filter. Mon. Wea. Rev., 98, 884-898.

__________, 1970c: Numerical variational analysis with weak constraint and application to surface analysis of severe storm gust. Mon. Wea. Rev., 98, 899-910.

Shuman, F. G., and J. B. Hovermale, 1968: An operational six-layer primitive equation model. J. Appl. Meteor., 7, 525-547.

Smith, S. D., 1974: Eddy flux measurements over Lake Ontario. Boundary Layer Met., 6, 235-255.

Sykes, R. B., 1966: The blizzard of '66 in Central New York--legend in its time. Weatherwise, 19, 241-247.

Wiggin, B. L., 1950: Great Snows of the Great Lakes. Weatherwise, 3, 123-126.

Wilson, B. W., 1960: Note on surface wind stress over water at low and high wind speeds. J. Geophys. Res., 65, 3377-3382.